Effects of GFRP Reinforcement on the Compressive Behaviour of Square SPF Timber Columns

by

Robert Benjamin O'Callaghan

A thesis
presented to the University of Waterloo
in fulfillment of the
thesis requirement for the degree of
Master of Applied Science
in
Civil Engineering

Waterloo, Ontario, Canada, 2021

AUTHOR'S DECLARATION

I hereby declare that I am the sole author of this thesis. This is a true copy of the thesis, including any required final revisions, as accepted by my examiners.

I understand that my thesis may be made electronically available to the public.

Abstract

Wood structural elements are gaining popularity of use through greater availability of engineered wood products and a more sustainability focused construction industry. Stringent modern codes and extreme load cases (e.g., blast, impact) have prompted efforts to improve the performance of wood structural elements through rehabilitation and retrofit using fibre-reinforced polymer (FRP) composites. Previous research has primarily focused on improving the flexural performance leading to the investigation of reinforcement arrangements where elements are wrapped by transverse composites, which also reinforces the compression zone. On the other hand, research into the material behaviour of wood under parallel-to-grain compression as reinforced by transverse FRP composites is sparse.

Therefore this study is undertaken in order to test unreinforced and reinforced wood specimens under static compression loading parallel-to-grain up to large strains, to establish the material behaviour. Varying orientations and thicknesses of glass FRP (GFRP) composites were applied to investigate the effects of fibre angle and reinforcement quantity on the behaviour of the timber specimens. An experimental program investigating the behaviour of thirty-six 140 × 140 × 685 mm Spruce-Pine-Fir (SPF) No. 2 column specimens was developed where thirty specimens were reinforced with transverse-oriented GFRP composites on the full length of the specimen.

The results found reinforcement provided by GFRP composites improved the peak strength, and stiffness. Major improvements were seen in post-peak behaviour where reinforced specimens retained greater strength to higher strains. Failure modes involving longitudinal splitting were eliminated amongst reinforced specimens, and the damage was localized to a small area of wood characterized by wood fibre crushing. The thinnest reinforcement arrangements provided least improvement; samples with other arrangements performed similarly on average despite increasing thickness, regardless of glass fibre orientation. The ability of the GFRP composites to remain relatively intact and bonded to the wood specimen appears to be critical in strength retention and superior post-peak behaviour as well as in localizing damage. Effectively reinforced specimens behave as though comprised of clear wood rather than wood with defects present.

Acknowledgements

The totality of this degree would have been impossible without help from a large number of individuals who mentored and encouraged me, and in some cases gently critiqued my work or procedures. First and foremost, I must make particular mention of my supervisors Professors Daniel Lacroix and Eugene Kim, who have been my test audience for all my work and ideas, and who made this body of work come together despite every major setback the pandemic et al. could throw at us.

I'd like to personally thank my family and my fiancée for putting up with me during this period of my life, it couldn't have been easy because it wasn't easy for me. Their vigilant support was extremely welcome.

In the process of data collection, a huge number of hands were involved and at times on a tight schedule. Richard Morrison, Peter Volcic, and Douglas Hirst are all owed my extreme gratitude for their friendship, their supervision, their efforts, and keeping all of us safe in the lab. To Tyler Hull, Patrick Aquino, Herry Chen, Maria Stakheiko, Avneet Kaur, and Ella Smith, thank you for hours and hours put into preparing specimens, tearing off FRP, processing data, generating figures, and in one unfortunate instance driving me to the hospital. I hope each of you got something out of the experience as much as I did working with you.

Lastly, a posthumous thank you to my maternal grandparents. Each of you encouraged me in turn and your unending love and support will never be forgotten by me. Rest in Peace.

Table of Contents

List of Figures

List of Tables

CHAPTER 1
Introduction

1.1 Research Needs

Concerns related to the impact of climate change on the environment has increased the need for sustainable practices in construction. Also, the larger availability of engineered wood products has prompted greater interest for incorporating wood in larger structures (e.g., Brock Commons, Vancouver, John W. Olver Design Building, Amherst, Origine, Québec City). Stringent requirements of modern codes and standards along with extreme loading (e.g., blast, impact) have prompted efforts to improve the performance of both existing and new wood structures through rehabilitation or retrofitting using fibre-reinforced polymer (FRP) composites. FRP composites are one possible reinforcement solution due to their high tensile strength, low weight, and very simple application methods. They are a desirable retrofit alternative for both in-situ application and member design for a wide range of structures including concrete and wood.

In terms of application to wood structures, FRPs have traditionally been used to rehabilitate timber bridges due to existing damage or increased frequency and higher value loads of modern vehicles. In addition, building taller wood structures has led researchers to investigate the use of FRP as a means to improve the performance of wood structural elements against extreme loading (e.g., seismic, blast, impact). As codes allow for larger wood structures the actual loads to be resisted by wood structural elements increase accordingly, leading to the need for reinforced members. Although the Canadian blast design standard (CSA, 2012) includes guidelines for the use of FRP composites as a retrofit for reinforced concrete and masonry elements, design guidelines for wood structural elements are not included. Recent research efforts have shown that the addition of glass FRP (GFRP) contributes to significant performance enhancements for wood light-frame walls (Battelli et al. 2021), cross-laminated-timber (Lopez-Molina and Doudak, 2019), and glulam (Lacroix and Doudak 2018a, 2018b and 2020). Although there is a lack of experimental research into the behaviour of FRP reinforced glulam subjected to extreme dynamic loads, an extensive body of knowledge pertaining to strengthening wood beams using FRPs under static loading does exist.

Researchers have focused on increasing the flexural and shear strength, stiffness, and overall ductility of wood members. For glulam structural elements, significant work has been done to establish material properties (Fox, 1978, Moody et al., 1983, Xiong, 1985, Plevris & Triantafillou, 1992 and 1995, Lee & Kim, 2000, Davids et al., 2008, Raftery & Harte, 2013, Yang et al., 2016, Lacroix & Doudak, 2018c) as well as their behaviour under environmental loads such as wind and earthquake (Buchanan and

Fairweather, 1993; Bjertnaes and Malo, 2014). Plevris and Triantafillou (1992) investigated the behaviour of clear wood reinforced with carbon FRP (CFRP) bonded sheets and reported improved performance up to reinforcement ratios of 3%, while further reinforcement did not provide any significant increases in flexural strength capacity. Lindyberg and Dagher (2012) developed a non-linear probabilistic model using moment-curvature analysis and Monte Carlo simulation to analyze glulam beams in bending reinforced by FRP tension elements. The authors showed a reinforcement ratio of 3% using simple tension reinforcement increased bending strength more than 100%. Raftery and Harte (2013) developed non-linear finite element modeling that adequately captured the flexural behaviour of GFRP reinforced glulam members. The major drawback in using simple tension reinforcement for wood in flexure is partial- or full-length debonding when the extreme tension fibre of the wood fails, as shown by several studies (Dorey and Cheng, 1996; Sonti et al., 1996; Hernandez et al., 1997). Johns and Lacroix (2000) investigated the effects of a U-shaped unidirectional GFRP and CFRP tension reinforcement on sawn lumber and found that using the simple transformed sectional analysis underpredicted the performance. Furthermore, the improvements due to FRP were reported to be the greatest for the weakest wood specimens which was attributed to the phenomenon of FRP bridging defects in the wood. The latter finding was also corroborated by other researchers (Gentile et al., 2002; Lacroix and Doudak 2018a, 2018b & 2020). Buell and Saadatmanesh (2005) investigated the effects of wrapping timber bridge girders with bidirectional CFRP. They found flexural performance was improved and in addition significant increases in the horizontal shear strength were observed. Lacroix and Doudak (2020) demonstrated that the use of bidirectional FRPs resulted in ductility ratios ranging from 2.3 – 3.6 and proposed a two-step approach to predict the resistance curves of the FRP reinforced beams. Although their material model can predict up to peak resistance, it is unable to predict the post-peak resistance due to a lack of a material model for the compressive behaviour of wood when wrapped with FRP (i.e., confined behaviour).

Despite the numerous studies investigating the flexural behaviour of wood members reinforced with FRP, little research has been conducted on the compressive behaviour of FRP-reinforced members to be used as input for flexural moment-curvature analysis. Applications are limited largely by the lack of research into the mechanics of the behaviour and reliable material models. Thus, the investigation of the effects of FRP composites on the compressive behaviour of wood structural products has become of interest within the research community to develop an FRP-reinforced compressive material model, which is required as one of the primary inputs of moment-curvature analysis, to predict the flexural response of FRP-reinforced members. The current study contributes to this field of knowledge by testing FRP composites applied as transverse wrap to short square timber columns under parallel-to-

grain loading. The effects of different FRP fabric fibre orientations and wrap volumes on the compressive stress-strain behaviour are investigated.

1.2 Research Objectives

The overarching aim of this research program is to assess the effects of GFRP transverse wraps on the parallel-to-grain compressive resistance of short timber columns. The purpose of the study is to determine whether the standard parallel-to-grain compressive modelling of unreinforced wood is a reasonable baseline for wood reinforced with GFRP transverse wraps. Determining the extent of the effects of the transverse reinforcement on qualitative behaviour (i.e., failure modes and damage sustained) as well as quantitative behaviour (i.e., stress-strain) will provide a basis for further, more specific investigation and possibly identify shortcomings of wood modelling for other applications such as flexural reinforcement with transverse or bidirectional GFRP.

More specifically, the research specific objectives are to:

1. Investigate the parallel-to-grain compressive behaviour of short timber columns when reinforced with externally bonded GFRP wraps consisting of different fabric orientation and quantity of reinforcement.
2. Evaluate the observed failure modes of the control and reinforced specimens and to document the various levels of damage.
3. Compare the research findings and suggest behavioural enhancements where necessary.

1.3 Scope

These research goals are met through the following steps:

1. A detailed literature review on the behaviour of wood material under parallel-to-grain compression and the state of research into FRP reinforcement and retrofit of wood structural elements;
2. Determine the base properties of short column specimens without GFRP wrap by testing six unreinforced specimens;
3. Wrap full-size short column specimens, varying number of layers provided and orientation of GFRP provided;
4. Test a total of 30 reinforced short columns under standard compression load methods;
5. Analysis of the results of the control and wrapped specimen tests.

1.4 Structure of Thesis

This chapter provides an overview of the topic, and establishes the need for research, objectives of the research program, and the scope of the work. Within chapter 2, a detailed literature review focusing on existing research into FRP as reinforcement for wood structural elements is presented, also covering general information pertinent to the two materials of wood and FRP. Chapter 3 describes the experimental methodology employed in this research, as well as a summary of the specimens and materials tested. The results of the experimental program, both quantitative and qualitative, are presented in Chapter 4. Chapter 5 then discusses the experimental results highlighting the most significant observations and the overall impact of GFRP reinforcement on properties and behaviour of the short columns. Finally chapter 6 provides the conclusions, a summary of the most significant findings of the research work and proposes future work that this study could lead to.

In the appendices detailed results of testing for each individual specimen are found. Appendix A provides detailed test results for the control specimens (i.e., unreinforced) including the individual stress-strain curve versus the average of the group and the progression of failure. Appendix B provides detailed test results for the reinforced specimens including the individual stress-strain curve versus the average of the group and the progression of failure.

CHAPTER 2
Background and Literature Review

2.1 General

The increasing use of timber and engineered wood products for larger structures, the decay and damage of existing wood structures, and the stringency of modern design requirements led to great interest in the potential of reinforcement alternatives to improve the mechanical properties and behaviour of wood. Fibre-reinforced polymer (FRP) composites have recently become an interesting alternative for retrofitting and strengthening applications due to their workability and ease of installation, versatility of form, durability, light weight, and high strength.

2.2 Wood as a Construction Material

2.2.1 Wood Properties

Wood is an orthotropic material with distinct mechanical properties in the longitudinal, radial, and tangential directions relative to the fibres and their arrangement in annual growth rings (Ross, 2010). As a viscoelastic material, the mechanical properties of wood are also affected by load duration and load rate, and subject to the effects of creep and fatigue (i.e., time-dependent). Figure 2.1 shows the relative bending strength of wood as a function of maximum load duration, where the time of a standard duration test is indicated. It is clear in the figure that for loads of short duration (i.e., less than 5 minutes), the material has significantly increased strength compared to when loaded in standard static testing duration (i.e., approximately 10 minutes). Studies have demonstrated that creep effects play a significant role for long duration loads (e.g., years) where the strength capacity of the material approaches only 50-60% of its standard duration test strength (Breyer et al., 2007; Ross, 2010).

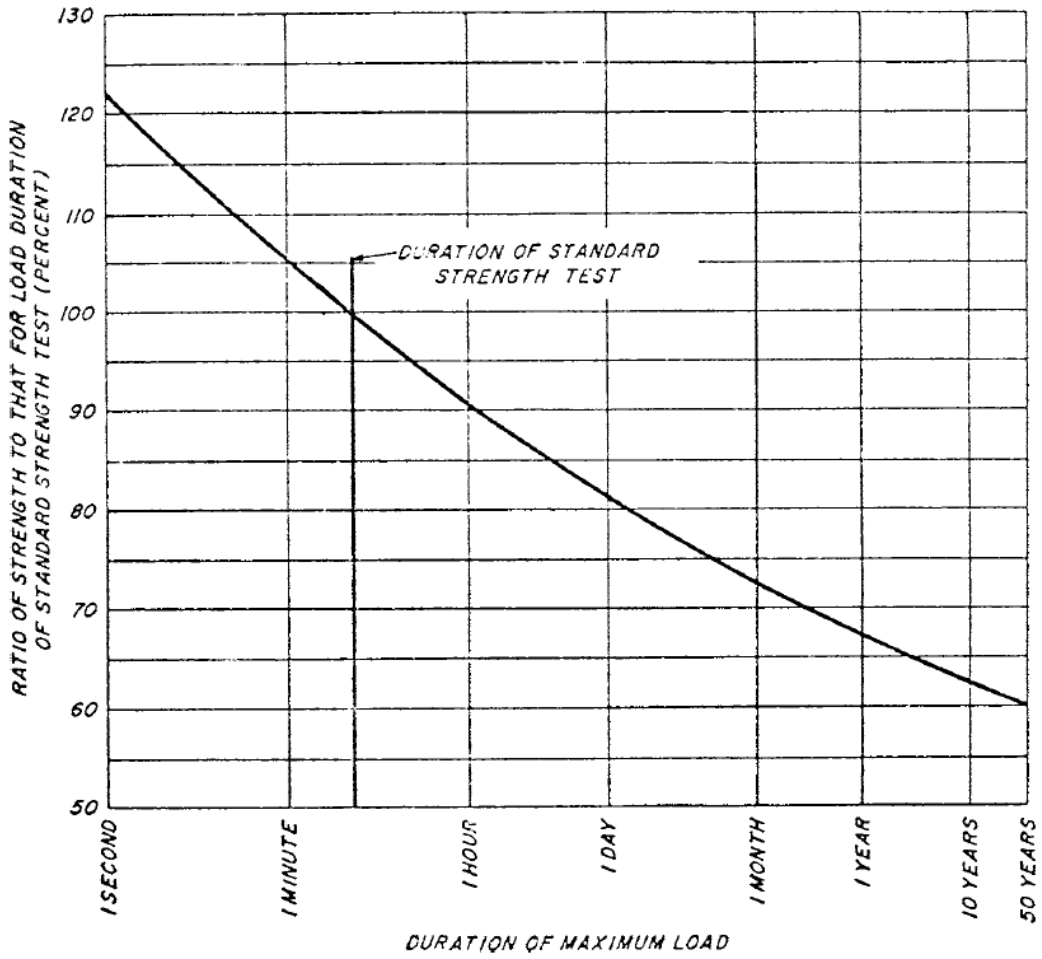

Figure 2.1: Effect of Load Duration on Maximum Bending Stress

*Reproduced from ASTM (2011)

The behaviour of clear wood (i.e., wood with no defects) is significantly different from the behaviour of lumber and timber member sizes typically used in construction (i.e., containing defects), and generally exhibits higher properties due to the absence of defects. The inclusion of unknown defects adds to the complexity of determining wood mechanical properties (Barrett and Lau, 1994; Breyer et al., 2007; Ross, 2010). In fact, the presence of knots due to the growth of branches is accounted for in the design of structural members with large volumes by a capacity reduction factor that corresponds to the statistical likelihood of a controlling defect being present (CSA O86, 2019). Flexural failure of clear wood members is commonly governed by wrinkling of the fibres on the compression side (i.e., compressive failure), whereas tension failure is typical for lumber or timber members in flexure as shown in Figures 2.2a to 2.2d (ASTM, 2014). Other less common types of failure for lumber and timber include compression (Fig. 2.2e) and horizontal shear (Fig. 2.2f) (ASTM, 2014).

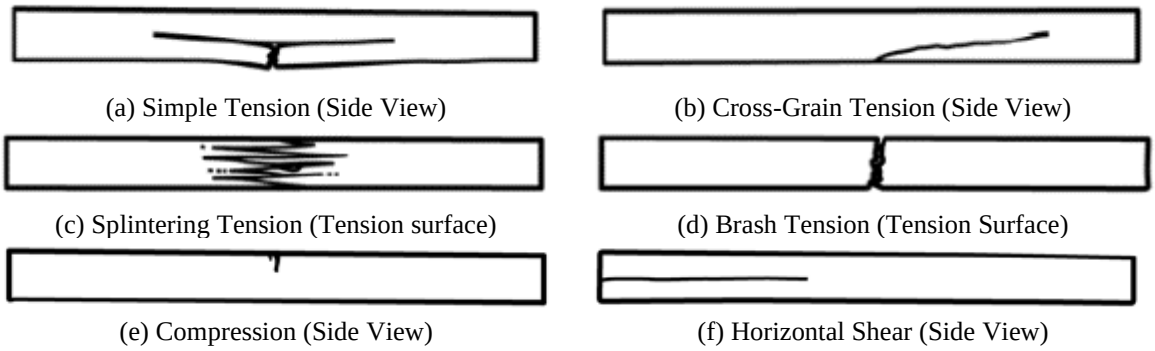

(a) Simple Tension (Side View) (b) Cross-Grain Tension (Side View)

(c) Splintering Tension (Tension surface) (d) Brash Tension (Tension Surface)

(e) Compression (Side View) (f) Horizontal Shear (Side View)

Figure 2.2: Types of Failure in Static Bending

*Reproduced from ASTM (2014)

Compared to steel or even concrete, the properties of wood material are highly variable due to circumstances of the natural environment and sylviculture. Factors during growth including temperature, length of growing seasons, and water availability will alter the material properties such as density, grain angle, and arrangement and frequency of branches. All of these are critical aspects that affect mechanical properties of lumber. The location of the wood within the cross-section of the tree also has an effect; wood nearest the centre or pith of the tree, also known as juvenile wood, has significantly different properties from mature wood at the perimeter of the tree.

Lumber is therefore sorted by ratings or grades based on visual inspection or by non-destructive testing methods (i.e., machine stress-rated, machine evaluated). These represent a minimum standard the specific lumber product has achieved based on its intended use, size, quality, and species. The grades of lumber are assigned at lumber mills by certified inspectors and are tied to design properties within the *Engineering design in wood* (CSA O86, 2019) based on extensive test data (Barret and Lau 1994). Machine stress-rated (MSR) lumber is often used where a tighter tolerance on the variation of properties is desired. For example, MSR lumber lamellae are employed in the creation of glulam beams.

2.2.2 Flexural Resistance of Wood

The moment-curvature relationship of a wooden member can be described using the tensile and compressive constitutive material relationship. The model for flexural behaviour of wood proposed by Buchanan is shown in Figure 2.3.

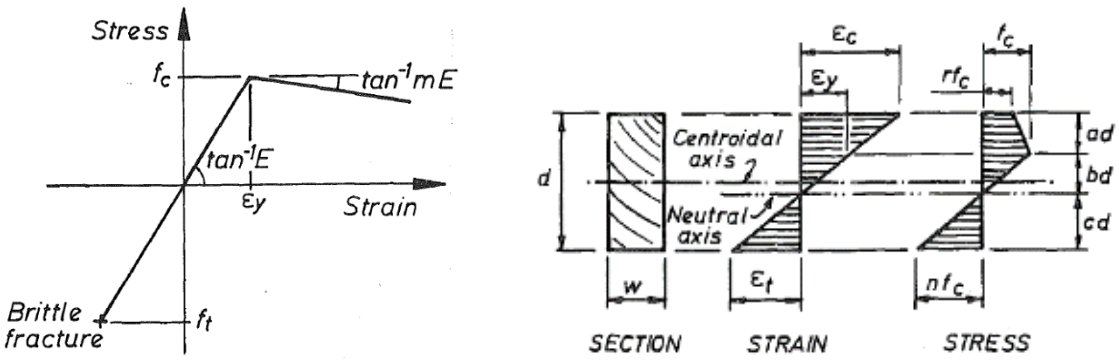

(a) Linear Stress-strain relationship (b) Distribution of Flexural Stress and Strain

Figure 2.3: Model Proposed by Buchanan (1990)

*Reproduced from Buchanan (1990)

The behaviour of wood in tension parallel-to-grain is linear elastic as shown in the lower half of Figure 2.3a, as opposed to the non-linear behaviour of the material in compression parallel-to-grain in the upper half. The parallel-to-grain compression behaviour of wood as modelled in Figure 2.3a is linear to a proportional maximum stress limit (ε_y, f_c), with a linear descending branch thereafter. Above the point of yield strain, crushing or buckling of fibres takes place with residual capacity, as shown in the compression stress block in the upper half of Figure 2.3b.

While the model of tension parallel-to-grain is straightforward and well-established, separate models for the behaviour of wood under parallel-to-grain compression have been suggested and a given model is not necessarily universally applicable.

2.2.3 Wood Compression Parallel-to-Grain

The stress-strain behaviour of wood under parallel-to-grain compression loads is non-linear for which models describing this behaviour have evolved over more than a hundred years. Without performing and presenting an exhaustive review of all models suggested, a subset is covered here which provide context to observations and results of this study. Figure 2.4 shows graphical representations of the stress-strain relationships for these models.

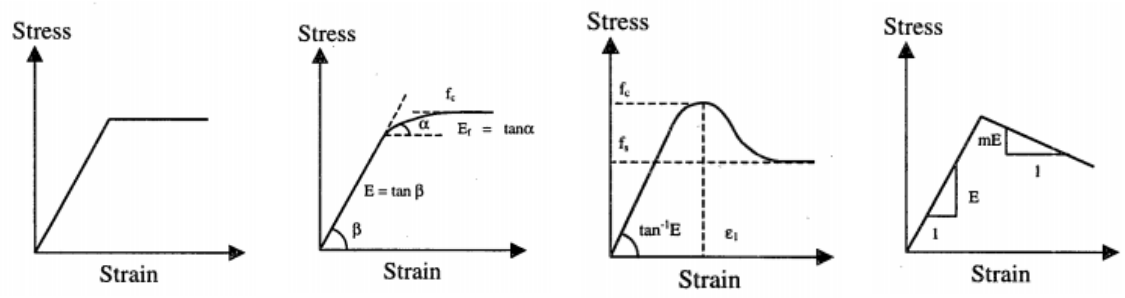

(a) Neely (1898) (b) Malhotra (1970) (c) Glos (1978) (d) Buchanan (1990)

Figure 2.4: Models for Parallel-to-Grain Compression Stress-Strain Behaviour of Wood

*Reproduced from Lau (2000)

The earliest and arguably simplest model is Neely's elastoplastic behaviour from 1898, which captures the initially linear elastic behaviour and suggests a plateau of maximum capacity at the point of plastic behaviour. Malhotra and Mazur (1970) investigated two by four specimens of eastern spruce both clear and including defects for compressive buckling strength, proposing the stress-strain relationship as given in Equation 2.1.

$$\varepsilon = \frac{1}{E} \cdot \left[c \cdot \sigma - (1 - c) \cdot f_c \cdot \ln\left(1 - \frac{\sigma}{f_c}\right) \right] \qquad 2.1$$

where ε is strain, σ is stress, f_c is maximum compression stress, E is the Young's modulus or modulus of elasticity (MOE), and c is a shape parameter.

Unlike the previous two researchers, Glos' model (1978) was derived using an extensive set of test data of timber with measured defects; and is unique to all models presented here in defining multiple critical strengths of the peak and asymptotic plateau. Equation 2.2 describes Glos' proposed relationship using a polynomial of seventh power, the four parameters thereof are given in Equations 2.3 to 2.6.

$$\sigma = \frac{\varepsilon/\varepsilon_1 + G_1 \cdot (\varepsilon/\varepsilon_1)^7}{G_2 + G_3 \cdot (\varepsilon/\varepsilon_1) + G_4 \cdot (\varepsilon/\varepsilon_1)^7} \quad 2.2$$

$$G_1 = \frac{f_s}{6E \cdot (1 - f_s/f_c)} \quad 2.3$$

$$G_2 = 1/E \quad 2.4$$

$$G_3 = 1/f_c - 7/6E \quad 2.5$$

$$G_4 = G_1/f_s \quad 2.6$$

where σ is the stress, ε is the strain, E is the modulus of elasticity, f_c is the maximum compressive stress as before for Mazur and Malhotra, ε_1 is the strain at maximum stress and f_s is an asymptotic compression stress for large strain. Glos' parameters were defined using multicurvilinear regression techniques to fit his experimental data. The advantage of Glos' model is that it is more representative of the real behaviour of their specimens including at large strains; however, the material dependent parameters need to be calibrated for every data set.

Bazan (1980) suggested refinements to the bilinear approach of Neely's model to adapt the plastic behaviour from perfect elastoplastic to a linear falling branch. Bazan assumed the slope of the falling branch as an arbitrary variable. Bazan's work was further refined by Buchanan (1984, 1990) to describe the slope of the softening branch as both a constant of the material throughout a cross-section in flexure and a ratio, m, of the material's elastic modulus. Buchanan's model is the most widely accepted and has been implemented in ASTM standards for predicting the flexural strength of glulam reinforced with FRP on the tension side (ASTM D7199, 2020). For large strain a given slope of the falling branch might imply negative or zero stresses which aren't correct, but in practice such large strains have rarely been of interest to designers. The majority of research investigates up to the maximum strength point and ignores post-peak behaviour.

ASTM D143 (2014) identifies six primary failure modes for defect-free clear wood under compression parallel-to-grain loading which are crushing, wedge splitting, shearing, splitting, combined crushing and parallel-to-grain shear, and brooming. Figures 2.5a to 2.5f illustrate these failure modes (ASTM D143, 2014).

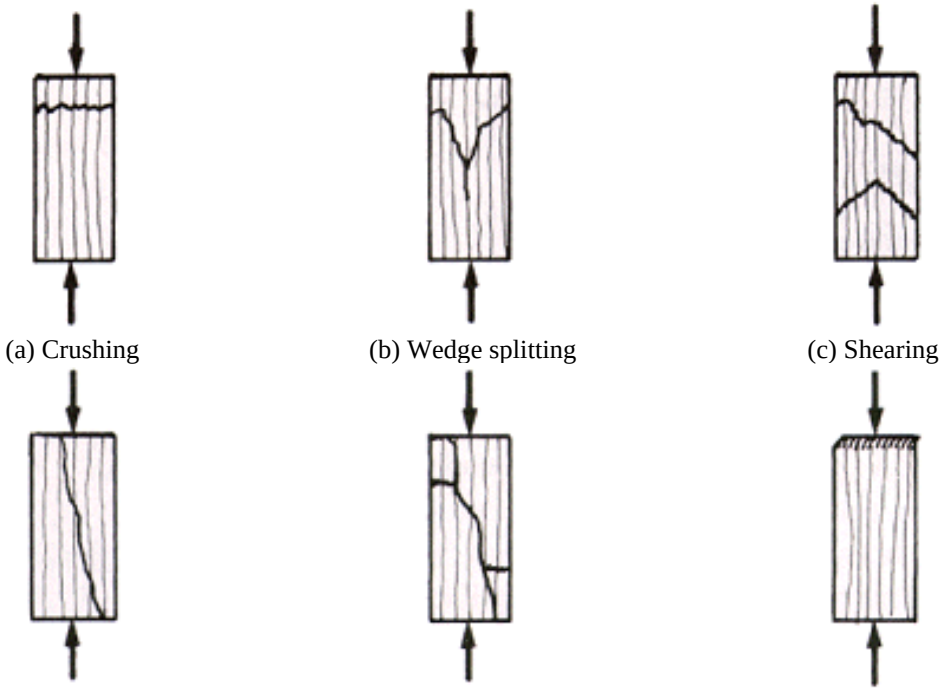

Figure 2.5: Material Failure Modes of Wood in Compression

* Reproduced from ASTM D143 2014

The crushing failure mode is characterized by a plane of failure that is approximately horizontal. In the case of the wedge splitting failure mode, wedge-shaped rupture planes form with a longitudinal crack at their intersection. Shearing failure is similar to crushing but with a rupture plane more than 45 degrees relative to the axial load or grain orientation. Splitting failure mode defines the formation of a continuous longitudinal crack generally parallel to the fibres connecting the end grains. Combined crushing and shearing parallel-to-grain commonly occur in wood with a severe angle between the wood fibre grain and the load and is characterized by separate zones of partial crushing connected by a longitudinal crack. Finally, brooming failure represents the condition where fibres near the end of the loaded material bend and buckle without rupture and typically occurs when there is higher moisture content at the end grain of the specimen. Pure splitting, brooming, and combined crushing and shearing are failure modes typically caused by defects in the wood for structural size specimens. When establishing the pure compression strength of the material for small specimens, failures of this kind would be omitted (ASTM D143, 2014). Wood failure, in particular splitting and shearing, can occur suddenly with little residual load carrying capacity. Therefore, if the influence of defects could be mitigated in full-size sawn lumber, more consistent and desirable behaviour as in clear wood might result. The common use of FRP as tension reinforcement for flexure has been shown to bridge the defects present in the tension zone, this study will go on to discuss how transverse reinforcement may

do the same for defects in compression (Johns & Lacroix 2000, Gentile et al., 2002; Lacroix and Doudak 2018a, 2018b & 2020).

2.3 FRP Composites

2.3.1 Overview

FRP composites are comprised of fibres which are the strong, load-carrying component and a polymer matrix which acts as both protection for the fibres and a means of distributing forces. The materials that comprise these components (i.e., the polymer matrix, fibres, and any additives) as well as the ratios of components are what determine the properties of the FRP composite in the principal orientation of the fibres employed. Alignment of fibres in one direction creates a composite system with a single strong axis but maximizes strength and stiffness and is generally known as unidirectional fabric. If fibres are interwoven or laminated at angles to one another, a multiaxial system can be created with strength and stiffness in more than one direction. Fibres are provided either as yarns or as fabrics. When fabrics have bidirectionality, the longitudinal fibres are referred to as the "warp", and the perpendicular fibres as the "fill" or "weft". The quantity of fibres in the warp and fill directions enumerate which orientations of the bidirectional fabric should be expected to have superior mechanical properties.

FRPs are very light weight and have both high strength and stiffness, thus they have been a popular material for mechanical applications including aerospace engineering, vehicles, sporting equipment, and so on. The construction industry is now gaining interest and practice in its use as a rehabilitation and strengthening material for existing materials where small cross-sections or higher load requirements demand greater performance of new or existing structures. One of the leading advantages of FRP is the adaptability of form and the ease of application. Extreme variation is possible in the material, form, shape, and properties of FRP composites. Fabric sheets comprised of fibres can be used to strengthen existing structural elements by surface application and bonding, or bars and plates can be manufactured and used in new structural elements as reinforcement. This study focuses on the former, the application of FRP composite sheets to the external surface of wood members.

2.3.2 Fibre Materials

The fibres which reinforce FRP typically used in the construction industry can be man-made or natural, with man-made being more commonly employed due to higher tensile strength and stiffness properties and tighter tolerances thereof. Man-made fibres include materials such as glass, carbon, and aramid. Natural fibres such as basalt or plant-based fibres are used less often.

GFRP is the most commonly employed due to its commercial viability and low cost. Fabrication of GFRP is performed by mixing colemanite, limestone, kaolin, and sand; the proportions of the provided

constituents create varying grades of glass fibres. Common grades for fibreglass include E(electrical-grade)-glass which is low cost and S(strength)-glass (R-glass in Europe) which provides higher tensile strength and stiffness. Further grades include C(corrosion)-glass more resistant to chemicals or ions, T(thermal insulator)-glass (a North American variant of C-glass), A(alkaline)-glass with little to no boron oxide, and D(dielectric)-glass also known as borosilicate glass with a low dielectric constant (Fitzer et al. 2000). The weaknesses of glass fibre include poor abrasion resistance such that they require protective coatings during manufacturing, and relatively low stiffness compared to steel or other fibres.

Carbon fibre-reinforced polymers (CFRPs) have greater stiffness, strength, and fatigue resistance but are expensive to produce. The fibre material is thermally and electrically conductive and has low thermal expansion, which allows CFRP composites to be used for applications that exceed the limits of other fibres. Polyacrylonitrile is the most widely used carbon fibre and is classified based on its modulus of elasticity with classifications of standard (SM) intermediate (IM) and high modulus (HM) as well as high strength (HS). For some applications including seismic retrofit of concrete columns by FRP confinement, carbon is more popular and cost-effective than glass based on its superior properties (Estrada and Lee, 2014)

Aramid and basalt fibres are more rarely used or researched but are employed for concrete reinforcement on occasion. Aramid FRP (AFRP) has very low density and high specific tensile strength in comparison to other reinforcing fibres. AFRP is light weight and has a high impact damage tolerance, hence its best-known usage is in bullet-proof vests. However, it is extremely sensitive to environmental conditions and is not always suitable for structural applications.

Figure 2.6 shows the stress-strain behaviour of GFRP, CFRP, and AFRP along with that of mild steel. What is immediately obvious is that FRP composites are not elastoplastic as mild steel, but linear elastic to the point of rupture although the ultimate strength is higher than for mild steel. The modulus and strength used for the FRP were the average typical values provided by the American Concrete Institute's *Guide for the design and construction of externally bonded FRP systems for strengthening concrete structures* (ACI PRC-440.2, 2017).

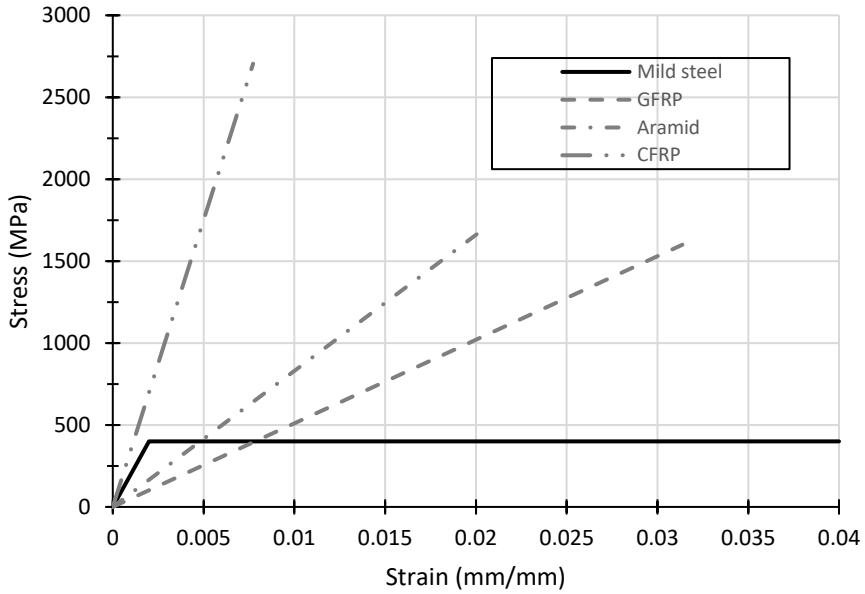

Figure 2.6: Typical Stress-Strain Curves for Common FRP and Mild Steel

*Reproduced from American Concrete Institute (2008)

2.3.3 Fibre Orientation

It is the fibres anchored in the polymer matrix which bear the applied loads on the composite, and therefore the orientation of the fibres' tensile axis has a distinct impact on the mechanical properties of the composite as a whole. Typically, fibres are arranged to be uniaxial, biaxial, or multiaxial. Uniaxial fabric is the most efficient for carrying a single load parallel to the fabric. Biaxial fabrics arrange a percentage of the present fibres in two directions, typically perpendicular to one another (e.g., 0° & 90° or ±45° relative to the fabric dimensions). Multiaxial fabric can have even further fibre directions included in the fabric as a whole (e.g., triaxial or quadraxial), which allows for multiple principal orientations in which fibre layers directly carry the load.

2.3.4 Polymeric Matrices

The polymer matrix, also known as resin, accounts for anywhere from 30 to 80 % of the composite material by weight. The primary function of the matrix is distribution of the load between fibres, and protection of the fibres from exposure to the surrounding environment. Once set, the matrix provides lateral support against fibre buckling and transfers shear stresses through the composite. Adhesive bonding of the polymer matrix is the most effective technique for transferring stress between FRP reinforcement and wood as it prevents stress concentrations associated with mechanical fasteners (Custidio et al., 2009). Depending on the response of the matrix to heat, it is either classified as a thermoset or thermoplastic resin.

Thermoset resins undergo permanent chemical reactions between polymeric chains (i.e., cross-linking) when exposed to heat. They are typically produced in a liquid state before undergoing a reaction to harden through a curing process. Although there are multiple products of this type (e.g., polyester, vinyl ester), epoxy resins are frequently employed due to their excellent properties at the higher end of the expected temperature range for structures. Epoxies are versatile in their application due to high resistance to corrosion, chemical attack, and fatigue; they settle at a slower rate than other resins and are brittle when cured. Epoxies show strong adhesion to dissimilar materials making them a good generic choice for the adhesive bond between wood and FRP (Custidio et al., 2009). A two-part epoxy resin is employed in this study. Thermoset matrices tend to have better interfacial bonds between polymeric chains and outperform in terms of mechanical properties when compared to thermoplastics. In addition, their workability at room temperature and starting liquid state make them more flexible to the configuration of the structural fibres (Yan et al., 2012).

Thermoplastic resins (e.g., polypropylene, polyethylene, polystyrene) become soft when exposed to heat to become a viscous liquid, then resolidify at service temperatures. Unlike thermoset resins no cross-inking or chemical reactions occur, and the process is completely reversible even after curing. There are certain advantages to the thermoplastic system including short fabrication time, greater ductility, ease of handling and repair, recyclability, and storage life. However, it is difficult to reinforce thermoplastics with fibres due to the high viscosity (Mallick, 1993). Typically, thermoplastics are rarely used in construction due to poor chemical resistance, high shrinkage, and durability concerns in addition to lower stiffness and strength than thermosets.

2.4 Previous Research

2.4.1 FRP Reinforcement for Flexural Behaviour

The major body of existing research on reinforcing wood structural elements with FRP is for flexural reinforcement. Within that realm of the research, most studies have focused on improving the global performance including peak strength, stiffness, and overall ductility of wooden beams. FRP as a flexural retrofit is applied as a means of increasing the beam's tensile capacity such that failure is of a compression yielding mode rather than a brittle tensile failure. The material properties of glulam in various grades have been established by a very large body of work (Fox, 1978, Moody et al., 1983, Xiong, 1985, Plevris & Triantafillou, 1992 and 1995, Lee & Kim, 2000, Davids et al., 2008, Raftery & Harte, 2013, Yang et al., 2016, Lacroix & Doudak, 2020, etc.).

Plevris and Triantafillou (1992) used very thin FRP sheets applied as simple reinforcement to the tension face of clear wood in bending. The addition of reinforcement resulted in a compression yielding

behaviour with higher reinforcement ratios experiencing extensive yielding, thereby creating a plastic hinge behaviour which correlates to an upper limit of bending strength increases achievable with simple tension reinforcement. Reinforcement ratios above 3% did not provide any further significant increases in flexural strength capacity. Lindyberg and Dagher (2012) investigated glulam beams in bending reinforced by simple FRP tension elements and found reinforcement ratios of 3% could increase the bending strength by more than 100%. The authors developed a non-linear probabilistic model using moment-curvature analysis that was accurate in predicting the strength and stiffness of the specimens in the test program. Raftery and Harte (2013) reinforced low-grade glulam beams with FRP plates and successfully developed non-linear finite element modelling (FEM) capable of predicting the flexural response. Furthermore, the researchers reported that the level of plasticity experienced in the top wood lamination (i.e., compression) is a function of the strength of the bottom lamination (i.e., higher strength tension reinforcement leads to more plasticity).

The major drawback in using simple tension reinforcement for wood in flexure is the potential partial- or full-length debonding when the tension surface of the wood fails, as shown by several studies. Dorey and Cheng (1996) reinforced glulam with GFRP on either the tension face or both tension and compression faces and noted that the application of tension FRP reinforcement lowered the beam's neutral axis while also increasing the allowable wood tensile failure strain by 10%; however, failure of the extreme tension surface of the wood often caused sudden delamination of the GFRP by shearing off the extreme wood fibres. Sonti et al. (1996) investigated glulam beams wrapped with varying FRP quantities and fabric orientations and showed that arrangements including transverse fibres were less prone to debonding and created greater apparent increases to flexural stiffness. Hernandez et al. (1997) tested yellow-poplar glulam with GFRP panels affixed as simple tension reinforcement up to reinforcement ratios of 3% by volume. The authors found that increases in stiffness and strength were promising, but observations of delamination indicated an improved bonding strength of the interface was necessary for practical use.

Triantafillou (1997) applied FRP material sheets to the sides of glulam beams as shear reinforcement and found simple mechanics were satisfactory for predicting resulting improvement, and further that the most efficient fibre orientation for shear capacity improvement was longitudinal. Johns and Lacroix (2000) reinforced commonly available "two-by-four" (38 mm × 89 mm, width × depth) sections in flexure with a U-shaped wrap of CFRP or GFRP unidirectional composite to improve both shear and bending capacity. The authors specifically provided increased FRP length for anchorage to prevent shear delamination failure at the interface of wood and FRP materials, and matched reinforced and unreinforced specimens to mitigate systemic error due to variability in defect volume and placement. Their results found simple transformed sectional analysis was accurate to calculate stiffness and

deflection in bending, but underpredicted strength increases. Further, improvements due to FRP were greatest for lower percentile wood specimens which is attributable to FRP bridging defects in the tension zone of the wood. The higher strength and stiffness of the FRP reinforcement in tension arrested crack opening of the extreme wood lamination, confining local rupture, and bridging over weak defects. It was reported that the wood material could support higher nominal stresses before failing. Buell and Saadatmanesh (2005) investigated the effects of bidirectional CFRP wrap and simple tension laminates on flexural and shear performance of large solid sawn timber bridge stringers. The authors' observations include: the horizontal shear strength was significantly improved by wrap in addition to bending strength and stiffness, the provision of only carbon laminate strips in simple tension allowed for shear failure below expected strength for the composite section, reinforcement by a single continuous piece of CFRP wrap along the length of the stringer performed better than reinforcement of overlapped strips wrapped transverse to the stringer in both flexure and shear. Lacroix & Doudak (2018a) investigated glulam beams reinforced with FRP for blast loading strain rates. They showed U-shaped tension reinforcement or tension reinforcement combined with transverse wrap significantly altered the failure mode to compression (Fig 2.2e) and brash tension (Fig 2.2d) rather than splintering tension (Fig 2.2c), while also limiting damage to a very small region. The same authors showed the addition of transverse FRP composite wrap to previously damaged glulam beams restored their strength capacity and stiffness, arrested crack development, and altered the failure mode (Lacroix & Doudak 2018b). Most recently, Lacroix and Doudak (2020) showed bidirectional FRPs applied to glulam subjected to dynamic blast bending loads resulted in ductility ratios ranging from 2.3 – 3.6. Their proposed two-step approach to predict the resistance curves of the FRP reinforced beams was found satisfactory to the test data gathered. Although that material model can predict up to peak resistance, it is unable to effectively model the post-peak resistance due to a gap in the modelling of compressive behaviour of wood when wrapped with FRP (i.e., confined behaviour).

This only covers a handful of examples of FRP as flexural reinforcement for wood structures, but the common finding of shifting the failure mode from tensile splintering to compressive yielding is particularly noteworthy. As several authors have shown, transverse FRP wrap around the critical beam sections is not only critical to prevent premature debonding failure of the FRP at the point of wood tensile failure but can also provide further benefits from the reinforcement on the compression side behaviour.

2.4.2 FRP Reinforcement of Concrete Columns

FRP composites are widely used as transverse confinement for reinforced concrete in compression. The impact of FRP transverse confinement on concrete has been studied extensively (Mirmiran & Shahawy,

1997, Teng et al., 2002, Ozbakkaloglu and Vincent, 2013, etc.). This body of research may provide some insight as to factors that could impact the effect of transverse FRP on wood material.

Mander (1988) developed a stress-strain model for concrete under uniaxial compressive loads confined by transverse reinforcement as in the case of confining steel in hoops. Figure 2.7 provides a visualization of Mander's model and the effect of confinement on concrete compressive strength generally.

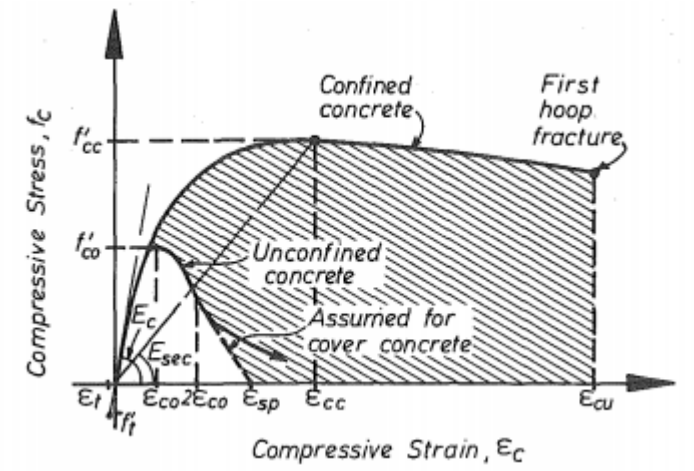

Figure 2.7: Mander Confined Concrete Model (1988)

*Reproduced from the Journal of Structural Engineering 114(8) Page 1807

The strength of concrete confined by FRP is modelled as a relationship to the confining pressure of the FRP, even as simply as adding to the unconfined strength the confinement pressure multiplied by an empirical factor. Confinement pressure in the FRP is developed due to the lateral dilation of the concrete under vertical strain described by the material's Poisson ratio.

There are a wide variety of models proposed, as a simple example Lam and Teng (2003) proposed for the strength of circular concrete columns passively confined in full-height FRP wrap a model given by Equation 2.7 as:

$$\frac{f'_{cc}}{f'_{co}} = 1 + 3.3\frac{f_l}{f'_{co}}, f_l = \frac{2E_f\varepsilon_{fe}t}{D} \qquad 2.7$$

where f'_{cc} is the confined concrete compressive strength, f'_{co} is the unconfined strength, f_l is the effective confinement pressure, E_f is the elastic modulus of the FRP, t is the FRP's nominal thickness, D is the diameter of the column section, and ε_{fe} is the actual rupture strain of FRP in the hoop direction. Figure 2.8 shows a graphical representation of the model for FRP confinement proposed by the authors versus unconfined concrete as modelled in Eurocode (EN 1992-1-1, 2004).

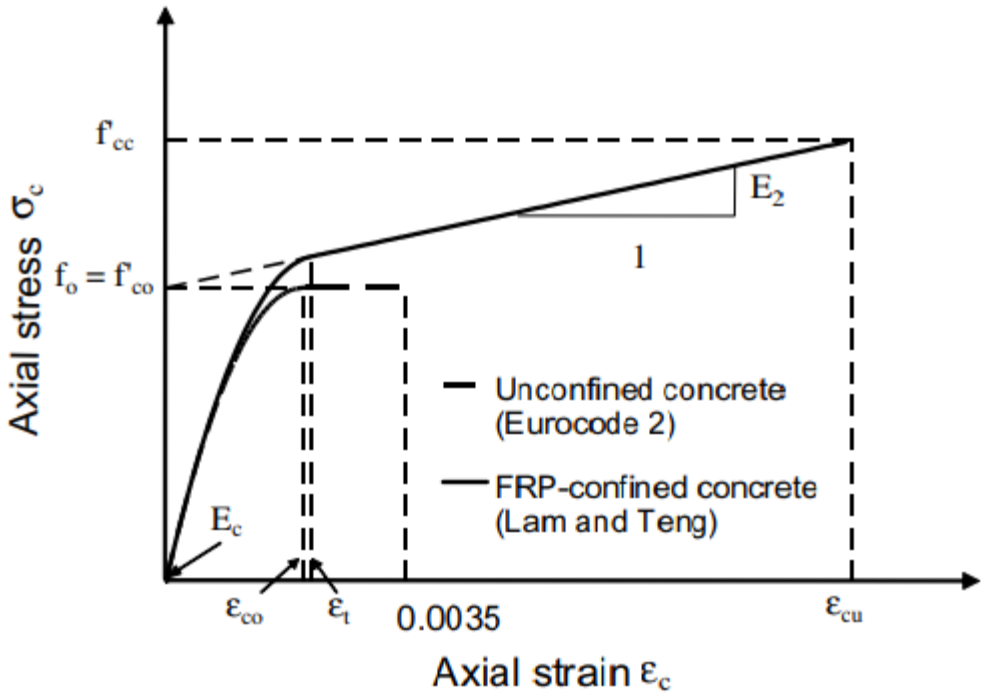

Figure 2.8: Axial Stress-Strain Curve for FRP Confined Concrete (Lam & Teng 2003)

*Reproduced from Journal of Reinforced Plastics and Composites Vol. 22 No. 13 Page 1173

As a linear elastic and brittle material in tension, the confining pressure of the FRP increases up to a maximum capacity where catastrophic failure (i.e., fibre rupture) occurs. For some applications, the FRP composite is pre-stressed in tension to provide active confinement pressure before compressive loads are applied to the concrete. However, wood material does not experience this dilation effect under compression. The principal means of wood material to deform is fundamentally different due to its orthotropic fibrous nature as compared to the isotropic matrix of concrete. Therefore the existing work in concrete can provide a guide to the general effects that might be seen (e.g., strength and stiffness improvement, a greater degree of FRP engagement after underlying material failure, mitigation of transverse strain and consequent failure), but is unlikely to reflect the actual mechanical changes in altering wood failure behaviour and stress-strain relationship.

It has been shown that there is a significant effect on confinement effectiveness by changing the cross-sectional shape. Whereas in a round cross-section the effects of the wrap and confining stresses are uniform, a square cross-section creates stress concentrations. Mirmiran et al. (1998) demonstrated that the confinement of square cross-sections was less effective than circular cross-sections for concrete. As the hoop strength of the FRP or the ratio of the corner radius to width of the column increased so did the relative confinement effect by Equations 2.8 & 2.9:

$$MCR = \left(\frac{2R}{D}\right)\frac{f_r}{f'_{co}} \quad 2.8$$

$$f_r = \frac{2f_j t_j}{D} \quad 2.9$$

where MCR is the modified confinement ratio, R is the corner radius, f_r is the confinement pressure, f_j is the hoop strength of the tube and t_j is the thickness of the tube. The expression f_r/f'_{co} would represent the circular column confinement pressure given equivalent diameter.

Since this reinforcement ratio phenomenon is as a consequence of specimen geometry rather than material, and some lateral strains are expected in wood, it is reasonable to assume that a sharp-cornered square wood cross-section would receive little to no benefit from transverse FRP wrap. Thus, some degree of corner rounding is required to mitigate stress concentrations for the wood specimens in this study.

2.4.3 Compressive Behaviour of FRP Reinforced Wood

Bazan's model of compressive behaviour was modified by Buchanan (1990) particularly for the purposes of flexural behaviour, and this bilinear model is often referenced in design and research (Plevris & Triantafillou, 1992, Song et al., 2007, Lacroix & Doudak, 2018b & 2018c). This bilinear falling branch type of model is also the only one presented in this study without an apparent steady state stress for plastic behaviour. Song et al. (2007) tested small rectangular specimens without knots or defects (clear wood) in uniaxial compression while controlling for moisture content and specific gravity. Their findings showed that failure mode and shape of the stress-strain relationship were closely connected. Song et al. (2007) stated that the failure modes which involved splitting parallel to the grain were most common; the author of this thesis observed the stress-strain curves of that failure mode most closely represent Bazan's (1980) model. Shearing and crushing modes were rare in the results of Song et al. (2007) and are most closely represented in shape by Glos' (1978) and Malhotra's (1970) models, respectively. André et al. (2014) cut small clear wood specimens from logs and glulam beam lamellae to test in parallel-to-grain compression; their findings are represented best by Malhotra and Glos's models only. However, it is well established by Barret and Lau (1994) that clear wood is not representative of the behaviour of full-size sawn lumber due to the presence of knots, cross-grain, and shrinkage or swelling cracks.

Available research on the effects of transverse FRP reinforcement for parallel-to-grain compression behaviour of full-size specimens is significantly sparser than the vast amount available for FRP as flexural reinforcement. For heavy timber piles under compression, FRP wrap was shown to significantly improve peak strength and ductility (Kim & Andrawes, 2016) and be an effective method

of restoring flexural and compressive strength through retrofit of damaged sections (Emerson, 2004, Caiza et al., 2012). Zhang et al. (2012) reinforced longitudinally cracked columns with bands of FRP wrap and found that the column capacity could be effectively restored. Dong et al. (2015) tested square columns (150 mm × 150 mm × 500 mm, width × thickness × length) of pine reinforced with aramid, carbon, and basalt FRP stirrups, and found that maximum strength was increased. Hieduschke & Haller (2010) engineered hollow circular wood column sections and showed that even minor FRP wrap reinforcement helped prevent buckling and brittle failure behaviour, as well as improving the compression strength. Chidiac (2003), Najm et al. (2007), and Song et al. (2010) investigated FRP wrap on small clear wood cylinders and had common findings of improvements to peak strength, ductility, and strength retention for large strain. Song et al. (2010), Dong et al. (2015) and Kim & Andrawes (2016) results showed that while the improvements to properties increased with greater quantities of FRP, the increase was not proportional to the increase in quantity. Conversely André et al. (2013) reinforced small clear wood specimens of square and dog-boned shapes with CFRP sheets to form a composite section parallel-to-grain and compressive loads rather than as transverse external wrap, which was shown to improve stiffness, strength, and post-peak steady-state stress linearly with reinforcement ratio.

Although several authors have investigated the general topic, a systematic approach in investigating the effects of fabric orientation, reinforcement quantity in terms of thickness, and other critical parameters has yet to be undertaken.

2.5 Summary

Wood structural elements often require retrofitting in existing wood structures to meet modern requirements, and to satisfy the demands of future design work in general. One method to strengthen wood structures is by reinforcement with FRP composites, which can be applied externally to both existing or new structures.

FRP composites are a lightweight, high strength, versatile and easily applied material comprised of a polymer matrix with embedded load-carrying fibres. In construction glass fibres are most commonly employed; they have greater ultimate strength than steel but lower stiffness and generally lower properties compared to other possible fibres. Fibres embedded in the polymer matrix can be interwoven or laminated to create fabric composite materials with multiple principal strength orientations.

In flexure, wood elements experience tension parallel-to-grain and compression parallel-to-grain, with tension side failure most common for wood elements containing defects. In tension, wood is linear elastic and experiences a sudden brittle failure, while in compression the behaviour is non-linear with residual capacity after maximum strength. Several models exist for the behaviour of unreinforced wood

under compression parallel-to-grain beyond the plastic transition point, with the most commonly accepted and applied being the bilinear falling branch model from Buchanan (1990). FRP has been found to effectively reinforce flexural behaviour when applied as tensile reinforcement, including the significant result of shifting failure from tension to compression controlled. Simple tensile reinforcement with FRP has an apparent upper limit of reinforcement ratio beyond which improvements are minimal. Several researchers documented that abrupt tensile failure and premature debonding failure were possible if the tensile reinforcement wasn't well anchored. These catastrophic or premature failure modes could be prevented by some degree of transverse FRP composite as a bidirectional fabric or with a transverse wrap layer for anchorage. Transverse wrap had added benefits improving horizontal shear strength and compressive behaviour. The ability to model the behaviour of flexural wood elements reinforced with transverse wrap is limited, however, by a lack of understanding in the behaviour of the compression lamellae confined by the FRP.

Although some research does exist on transverse FRP applied to wood compression elements, the approach has not been systematic. Existing research is primarily dividable into research on large-size timber piles being retrofitted (Emerson 2004, Kim & Andrawes 2016, etc.) or small samples that aren't representative of full-scale structural elements (Chidiaq 2003, Najm et al 2007, Song et al 2010, etc.). Furthermore, research has not typically been organized with respect to general parameters that affect the capacity of FRP composites including fibre orientation and composite thickness as for reinforced concrete. Although a greater field of research exists for the application of FRP as transverse confinement for reinforced concrete elements in compression, the results of those investigations must be reconfirmed as applied to wood material.

Therefore this study has been undertaken to provide initial findings that may help guide understanding compressive behaviour of representative wood material when reinforced with transverse FRP. Commonly available local lumber grade and GFRP composite products are employed, with some variation in the composite properties and number of layers applied to broaden the possible findings.

CHAPTER 3
Experimental Program

3.1 General

This section describes the creation, preparation, and testing of six unreinforced specimens and thirty GFRP reinforced column specimens subjected to axial compression loading. A detailed description of the methodologies and procedures employed throughout the research program is presented.

3.2 Description of Unreinforced Material

The species of Spruce-Pine-Fir (SPF) and grade of No. 2 or better were selected for the wood material based on local availability. The emphasis of the research program is to investigate the effects of GFRP composite wrap on the compressive behaviour of structural-size timber with natural defects. The cross-section size ordered was therefore 140 mm × 140 mm, nearing the upper limit of both sawn-lumber sizes commonly available and therefore grain defects present. In some instances, the material lengths were missing small amounts of cross-section at the corners for portions of the length. The lumber was delivered in lengths of 2,438 mm and stored in a temperature and humidity-controlled environment. Figure 3.1 shows the material stored in the humidity chamber before being cut to the required specimen length for the experimental program.

Figure 3.1: Storage of Material Lengths as Delivered

3.2.2 Humidity Chamber

At time of delivery, the lumber had a moisture content of approximately 27%, which was very high in comparison to the typical moisture content representative of service conditions for wood structures. The target for surface moisture content was 13% at the time of the test. In order to create a controlled moisture loss over a longer period, Anchorseal® wax emulsion was applied to seal the exposed grain at the ends of the 2,438 mm lengths, and the raw lumber was kept in an enclosed humidity chamber on a drying rack. Due to the orthotropic nature of the material with respect to the organization and orientation of cells in growth rings, the loss of moisture causes a different relative dimensional change in the radial and tangential directions, leading to perimeter tensile stresses that cause cracks on the faces. The aim of slowing the rate of moisture loss in the wood to a longer period of time is to prevent rapid moisture loss at the outermost material compared to slower moisture loss at the innermost. However, ultimately the discrepancy between radial and tangential dimensional shrinkage will inevitably lead to perimeter stresses and create shrinkage cracks. Avoiding the presence of these cracks completely is not a goal of the study, as the presence of these cracks is representative of real wood in service which are seasoned from green and may experience fluctuations in the environment. Figure 3.2 shows the humidity chamber and the end-grain of a typical specimen with shrinkage cracks.

(a) Humidity Chamber

(b) Shrinkage Cracks Prior to Testing

Figure 3.2: Storage Chamber and Differential Shrinkage Splits of Specimens Prior to Test

3.2.3 Specimen Construction

From the original 2,438 mm lengths of lumber, specimens of 685 mm length were fashioned resulting in a maximum of three specimens per material length. The specimens were first cut using a mitre saw at a slightly longer length before a large circular saw was used to ensure the ends of the specimen were flat and parallel. The length of 685 mm was determined in accordance with the Standard Test Methods of *Static Tests of Lumber in Structural* Sizes (ASTM D198-14e1). According to the standard, the selected length should ensure that the governing failure mode is not buckling of the column, and it will not need intermittent or continuous lateral supports. To avoid bias in the test results arising from underlying differences in the material lengths, groups of specimens receiving identical reinforcement were sourced from separate material lengths.

Square corners of the cross-section would result in stress concentrations within the transverse GFRP wrap and cause premature rupture. Therefore, to prevent these stress concentrations, the corners of the square cross section were rounded with a plunger hand-router to a radius of 19 mm. Then to prevent the smooth finish of the router from adversely affecting the bond of the polymer matrix to the wood material, the rounded corner surfaces were roughened using an angle grinder with a wire brush head attachment, as shown in Figure 3.3. Specimens were returned to the humidity chamber after being shaped until they could be wrapped in the appropriate GFRP for their test group.

(a) Rounding Cross-Section Corner with Router (b) Wire Brushing Rounded Corner to Roughen

Figure 3.3: Altering Specimen Corners to Mitigate FRP Stress Concentrations

3.3 GFRP Application

3.3.1 Summary of Reinforcement Configurations

The GFRP fabric and two-part thermoset epoxy resin were sourced from Simpson Strongtie®. Three fabric types were used; uniaxial fabric CSS-CUGF27 (U) and two bidirectional fabrics, one with fibres at 0° and 90° degrees CSS-BGF018 (B), and one with fibres at ±45° CSS-CBGF424 (X). For each fabric, five specimens were wrapped with a single layer and five specimens with three layers for a total of thirty reinforced specimens among six groups. The epoxy employed was CSS-ES epoxy primer and saturant. Table 3.1 provides an overview of the test matrix.

Table 3.1: Experimental Group Summary

Specimen Group	Group Label	FRP Retrofit Configuration
Control	C	No retrofit
Unidirectional 1-layer	U	1-layer Unidirectional wrap 90°
Unidirectional 3-layer	U_3	3-layer Unidirectional wrap 90°
Bidirectional perpendicular 1-layer	B	1-Layer Bidirectional wrap 0° & 90°
Bidirectional perpendicular 3-layer	B_3	3-Layer Bidirectional wrap 0° & 90°
Bidirectional 45° 1-layer	X	1-Layer Bidirectional wrap ±45°
Bidirectional 45° 3-layer	X_3	3-Layer Bidirectional wrap ±45°

As indicated in Table 3.1, fabric U is applied such that the fibres are at 90° relative to the load and wood grain, fabric B such that the fibres are at both 0° and 90° to the load, and fabric X is applied such that the fibres are oriented at ±45° to the load. The dimensions of the GFRP fabric for an individual layer were 610 mm × 635 mm (length × width). GFRP wrap was applied to allow for a 50mm overlap and 25mm clear distance from each end for handling, curing, and preventing direct load of the

composite in testing. For groups U_3, B_3, and X_3, specimens were wrapped with three sheets of fabric such that each layer's overlap joint was offset one face from the layer above. Orientation of the fabric was identical for all three layers. Curing of wrapped specimens occurred at room temperature over a period of at least 48 hours prior to testing. Figure 3.4 visualizes the orientation of the fabric fibres with respect to the specimen axis.

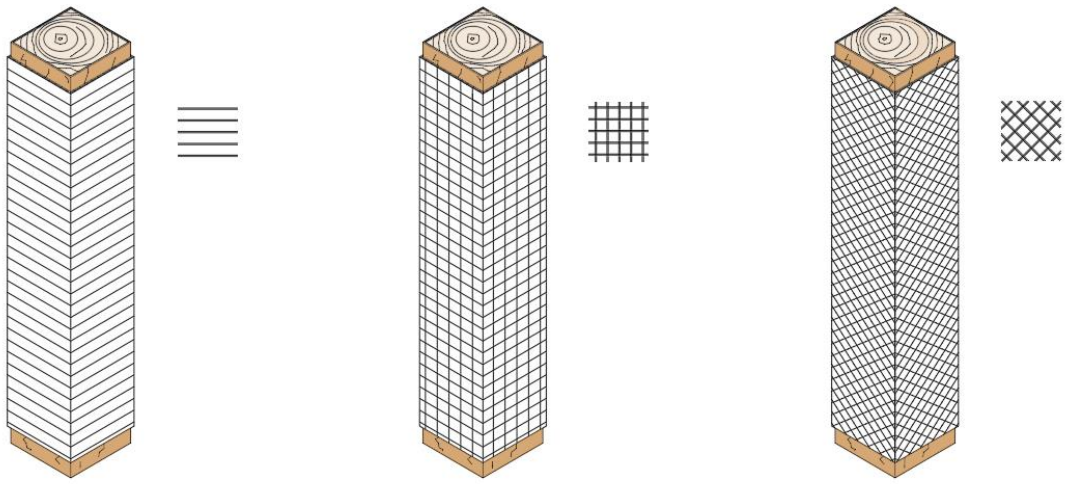

(a) U & U_3 (90°) (b) B & B_3 (0° & 90°) (c) X & X_3 (±45°)

Figure 3.4: Orientation of Fabric on Specimens in Groups U (left), B (middle) and X (right)

3.3.2 GFRP Composite Properties

Table 3.2 summarizes the properties of the cured GFRP composite. The properties are for the principal orientation of the fibres. The epoxy employed had a neat tensile strength of 36 MPa.

Table 3.2: Manufacturer Design Values of Cured Two-part Epoxy Matrix and Fabrics

Fabric Label (orientation)	Fabric Dry Weight (g/m^2)	Fabric Layer Thickness (mm)	Composite Tensile Strength (MPa)	Composite Modulus of Elasticity (GPa)	Composite Rupture Strain (mm/mm)
U (90°)	915	1.3	390	23	0.017
B (0°/90°)	611	0.66	310	17	0.018
X (±45°)	814	0.86	261	19	0.014

It is important to observe in Table 3.2 the variation in fabric layer thickness, composite tensile strength, modulus, and rupture strain among the fabrics. In this study, fabrics were sourced based on local common use and availability. Sourcing fabrics of equivalent properties with variable orientation is not feasible nor representative of industry. It would also have been exceptionally difficult to cut

equivalently sized sheets of a given fabric at varying orientations in order to use a standard material with variable orientation and would have required working on specimens of lesser size.

3.3.3 Wrapping Procedure

The two-part epoxy resin was measured to a 2:1 volume ratio and mixed using an electric mixer for a period of five minutes. The surface of the specimen on all sides was impregnated with the epoxy resin mixture using paint rollers to apply a thin even sheet. The GFRP sheets were first laid flat and impregnated with the epoxy resin on both sides using paint rollers and rib rollers to ensure good epoxy penetration between the fibres (Fig. 3.5a). The edge of the saturated fabric was fastened to the specimen with wide wood staples (Fig. 3.5b) and wrapped around the specimen hand tight (Fig. 3.5c) before the ribbed rollers were used to remove any air bubbles and ensure bonding between the materials (Fig. 3.5d). Specimens were checked during the first hours of curing to ensure slack was not developing before the polymer matrix set hard.

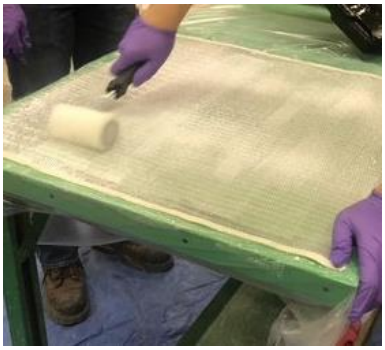

(a) Saturating Surfaces with 2-Part Epoxy

(b) Affixing FRP Edge with Wide Staples

(c) Wrapping Fabric Over Prepared Specimen

(d) Eliminating Air Pockets or Slack with Ribbed Roller

Figure 3.5: Application of Epoxy and GFRP Fabrics

3.4 Test Setup

Compressive tests were performed according to ASTM standard D198-14e1 (ASTM, 2014) using a 1,500 kN universal test machine (UTM). The tests were strain-controlled at a constant displacement

rate of 1.25 mm/min, with vertical displacement recorded through the use of two linear variable displacement transducers (LVDTs). The majority of specimens were loaded to high strain levels exceeding 0.07 mm/mm strain except when specimens became unstable. Figure 3.6 shows the test frame used and a test setup with the aforementioned sensors in place.

(a) UTM Test Frame (b) Specimen and LVDTs setup for test

Figure 3.6: UTM Frame and Test Setup Within

Immediately prior to testing, pin-probe moisture meter readings were taken from the end-grain of the specimen and visual observations made about the specifics of the wood material including presence and location of defects if any. Tests were recorded through the use of stationary time-lapse video, and photography from various locations, in addition to the numerical results captured by the UTM control console.

After terminating the test, damage to the specimen was recorded with observations and photography before the FRP wrap was removed via angle grinder cuts and pry-bars. Damage of the wood material below the FRP wrap was again observed and photographed before the specimen was rip-cut parallel to the grain to expose internal damage patterns. At this time pin-probe moisture readings were repeated in several internal locations to ensure rapid drying of the end-grain did not skew the understanding of moisture levels at time of the test. Finally, small clear samples were cut from the undamaged portions of the specimens in order to measure oven dry material density in accordance with ASTM D2395 (ASTM 2017) and ASTM D442 (ASTM 2016) standard Method B. Although the sensors and sample masses extracted would allow reporting to a tenth of a percentage point, since a comprehensive oven calibration was not performed, results are rounded to a whole percent. It was found that the average moisture content across all tested specimens was 14% which would be representative of standard service conditions, and the average oven dry density was 375 kg/m^3 with a coefficient of variation

(COV) of 0.11 which is typical for the species. Figure 3.7 shows the temperature-controlled oven used for drying the small block specimens along with a typical arrangement of specimens being dried.

(a) Drying Oven (b) Typical Sample Arrangement in Oven

Figure 3.7: Oven Dry Density Equipment

CHAPTER 4
Experimental Results

4.1 General

The experimental results from the axial compressive tests on the six unreinforced and thirty GFRP reinforced specimens are presented in this chapter. This includes the observed failure modes of unreinforced and reinforced specimens along with the effects of GFRP on the axial compressive stress-strain behaviour such as peak strength, ultimate strength, stiffness, and ductility.

The tests on the control and reinforced specimens were carried out to high levels of deformations when possible and stopped whenever complete failure of the specimen was attained, or when limits of the recording equipment were reached. Therefore, it was possible for multiple failure modes to be classified at different times during the test. For consistency, failure modes are classified based on a combination of internal damage observations from post-test dissection and the macroscopic failure mode first observed during testing. Furthermore, in order to facilitate the stress-strain comparisons all graphs presented in this chapter are presented up to a strain of 0.04 mm/mm. The complete stress-strain curves and failure modes are presented in greater detail for each unreinforced and reinforced test in Appendix A and B, respectively.

The test setup employed sampled data at extremely high rates, then presented an average of the samples taken at a rate of 8Hz or greater (typically 10Hz). The final data presented in plots within this chapter has been down sampled to approximately a rate of 1Hz to peak strength and 0.1 Hz thereafter due to the great length of test required to reach significant deformation at standard loading rate. The markers present in the plot curves serve only to differentiate the specimens visually and are in no way an indication of recorded points. In order to establish any average curves for a group of specimens, linear interpolation to standard strain increments was employed. The plots are not smoothed other than by any effects of said down sampling and linear interpolation for these purposes.

4.2 Control Specimens

4.2.1 Stress-Strain Behaviour

The stress-strain curves for all six control specimens can be seen in Figure 4.1 up to 0.04 mm/mm strain along with the average curve for the group. All control specimens are observed as linear elastic to peak strength followed by a rapid strength degradation which generally attains a plateau. Due to rapid strength degradation and instability in the frame, specimens C–5 and C–6 were deemed to have attained

ultimate failure at significantly lower strain. Though specimen C-1 did not reach 0.04 mm/mm, its strength curve was of similar shape as C-2 through C-4. The complete plots of each specimen are found in Appendix A.

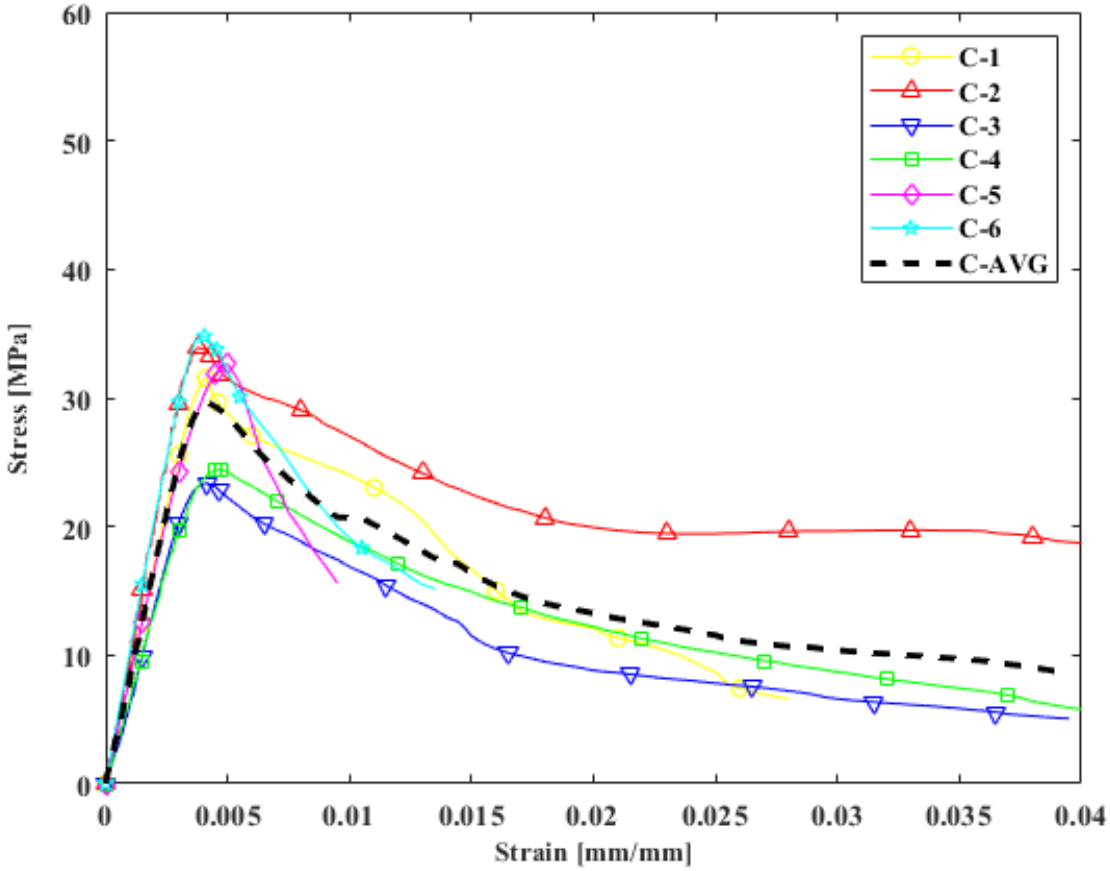

Figure 4.1: Average and Individual Stress-Strain Curves of Control Group

Table 4.1 summarizes the stress-strain curves presented in Figure 4.1 where only key parameters are presented along with their average, standard deviation, and coefficient of variation. The yield point is defined as the maximum or peak stress resisted by the specimen (σ_y) and the corresponding yield strain (ε_y) whereas the point denoting the end of the test (i.e., not shown in Fig. 4.1) is defined by the ultimate stress (σ_{ult}) and ultimate strain (ε_{ult}). As seen in Table 4.1 and Appendix A, there is a high variation in the ultimate strain of each specimen. Thus, it was decided to compare the levels of stress at a strain level of 0.04 mm/mm ($\sigma_{\varepsilon_{0.04}}$) as several control and reinforced specimens had reached an apparent plateau of strength by that point. Finally, the modulus of elasticity (*MOE*) was calculated as the slope of the initial linear portion of the stress-strain curve (i.e., prior to σ_y).

Table 4.1: Control Specimens Test Results

Specimen	σ_y [a] [MPa]	$\epsilon_y \times 10^{-3}$ [b] [mm/mm]	$\sigma_{\varepsilon_{0.04}}$ [c] [MPa]	σ_{ult} [d] [MPa]	$\epsilon_{ult} \times 10^{-2}$ [e] [mm/mm]	MOE [f] [MPa]
C-1	31.6	4.06	N/A	6.6	2.82	8660
C-2	34.0	3.78	18.8	11.5	7.23	10180
C-3	23.4	4.06	5.1	5.1	4.04	7220
C-4	24.5	4.68	5.8	4.2	4.78	6470
C-5	32.7	5.09	N/A	14.3	0.98	8250
C-6	34.8	4.06	N/A	13.9	1.38	10040
Average	*30.2*	*4.29*	*9.9*	*9.3*	*3.54*	*8470*
Std. Dev.	*4.5*	*0.45*	*6.3*	*4.1*	*2.13*	*1360*
COV	*0.15*	*0.10*	*0.64*	*0.44*	*0.60*	*0.16*

a – the maximum stress achieved per specimen

b –the strain at the maximum stress value

c – the stress recorded at 0.04 mm/mm strain

d – ultimate stress, the stress when the test was ended

e – ultimate strain, the strain when the test was ended

f – Modulus of Elasticity, the slope in the initial linear elastic region

4.2.2 Failure Modes

Figure 4.2 shows the failed control specimens after testing along with a view of the cross-section dissected longitudinally. As it can be seen in Figures 4.2a to 4.2f, a variety of failure modes were observed in the control specimens including splitting (Figs. 4.2a), crushing (Figs. 4.2b and 4.2e), and wedge splitting (Figs. 4.2c, 4.2d, and 4.2f), representative of full-scale size wood containing defects. In all six control specimens, the presence of defects within or immediately adjacent to the initial failure location was observed; the wedge splitting failures in particular universally involved a defect located centrally on the angled rupture plane. It can be seen from specimen C–5 in Figure 4.2e, where failure took place near the loaded end, that the arrangement and size of defects within the volume appear to be the controlling factors for failure location. Generally, damage in the form of wood fibre crushing was relatively localized to the rupture plane whereas longitudinal cracks and splits spanned between the loaded ends or from loaded end(s) to the rupture plane.

(a) Specimen C-1 (Splitting) (b) Specimen C-2 (Crushing)

(c) Specimen C-3 (Wedge Splitting) (d) Specimen C-4 (Wedge Splitting)

(e) Specimen C-5 (Crushing at the end) (f) Specimen C-6 (Wedge Splitting)

Figure 4.2: Post-Test Damage and Failure Modes of Control Specimens

Specimen C–2 demonstrated the optimal behaviour after peak strength, retaining significant strength for a much larger range of strains as can be seen in Figure 4.1 and Table 4.1. The large internal split seen in Figure 4.2b in the dissected view for specimen C–2 is representative of the final damage state,

but up to the strain of 0.04 mm/mm plotted in Figure 4.1, the failure was only seen to be crushing. Additional data and failure progression photos of specimen C–2 can be found in Appendix A.

Specimens C–5 and C–6 visually show less damage than other specimens in the same group due to tests being ended at relatively lower deformations. More specifically, the tests were stopped due to instability caused by significant crushing near the loaded end in the case of C–5 (Fig. 4.2e) and longitudinal splitting creating separation of the cross-section in C–6 (Fig. 4.2f) which resulted in especially rapid strength degradation. Both specimens were considered completely failed by the point of test termination.

Figures 4.3a to 4.3e shows a representative progression of the observed damage in specimen C–3. Figure 4.3a shows the specimen prior to the test where it can be seen that there are several knots on the surface. By examining the dissected view in Figure 4.2c, one such knot can be seen centrally in the critically damaged section. Failure initiated at mid-height planar with this defect, in the form of fibre crushing (Fig. 4.3b) which evolved to a wedge-split in the lower half of the specimen (Fig. 4.3c) that is further amplified with increasing axial deformations (Fig. 4.3d). The final deformed shape is shown in Figure 4.3e. Additional information regarding the individual failure progression and failure mode classification for the control specimens can be found in Appendix A.

(a) Prior to Test (b) Initial Crushing (c) Wedge-Splitting (d) Damage Amplification (e) End of Test

Figure 4.3: Representative Failure Progression of Control Group – Specimen C-3

4.3 Reinforced Specimens

4.3.1 Stress-Strain Behaviour

Thirty reinforced specimens reinforced with a single layer or three layers of unidirectional (U), 0-90º bidirectional (B), or ±45º bidirectional (X) GFRP fabrics were tested in axial compressive tests. The stress-strain curves for all six groups can be seen in Figures 4.4a to 4.4f up to 0.04 mm/mm strain, along

with the average curve of the control group initially introduced in Figure 4.1. In general, it can be seen that the addition of GFRP wraps contributes to an overall improvement in the behaviour of the reinforced specimens in comparison to the average of the control group through the enhancement of peak strength, stiffness, and the level of sustained post-peak stress. The complete stress-strain curves of all reinforced specimens can be found in Appendix B.

The summary of the test results for all thirty reinforced specimens is presented in Table 4.2 along with the average, standard deviation, and coefficient of variation for all six groups. Similarly to the control specimens, only the key parameters defining the stress-strain curve of the reinforced specimens are presented in Table 4.2, which includes: maximum or peak stress resisted by the specimen (σ_y), corresponding strain(ε_y), stress at a strain of 0.04 mm/mm ($\sigma_{\varepsilon_{0.04}}$), ultimate stress ($\sigma_{ult}$), ultimate strain ($\varepsilon_{ult}$), and modulus of elasticity (MOE).

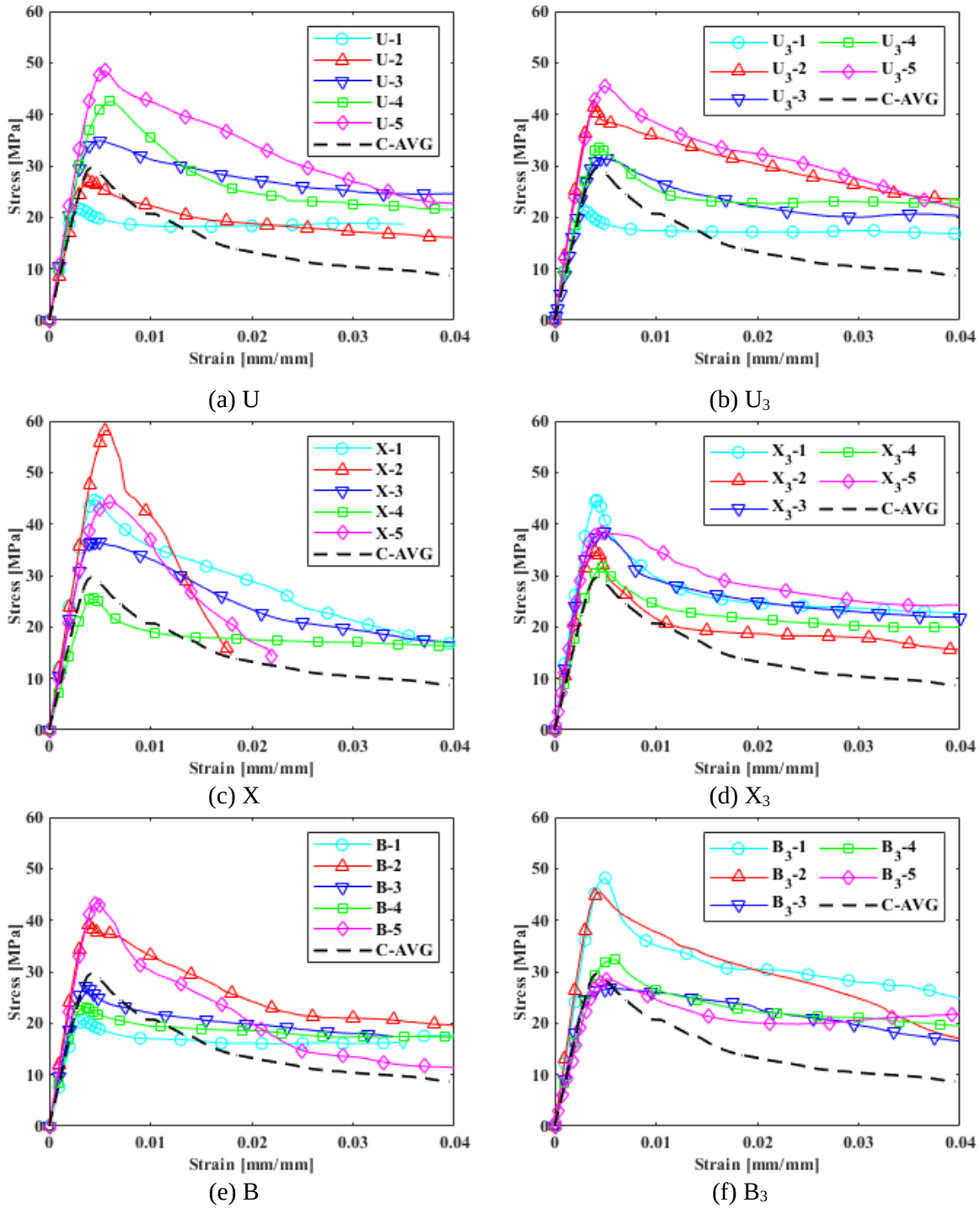

Figure 4.4: Stress-Strain Curves of GFRP Reinforced Specimens vs. Control Group Average

Table 4.2: Summary of Test Results for Reinforced Specimens

Specimen	σ_y [a] [MPa]	$\epsilon_y \times 10^{-3}$ [b] [mm/mm]	$\sigma_{\varepsilon_{0.04}}$ [c] [MPa]	σ_{ult} [d] [MPa]	$\epsilon_{ult} \times 10^{-2}$ [e] [mm/mm]	MOE [f] [MPa]
U–1	21.6	2.97	N/A	16.8	3.53	9570
U–2	26.9	3.86	15.9	11.4	5.99	8350
U–3	34.9	5.18	24.6	22.8	7.45	10040
U–4	42.6	6.03	21.5	20.0	6.25	9940
U–5	48.5	5.48	22.7	20.2	6.27	11110
Average	*34.9*	*4.70*	*21.2*	*18.2*	*5.90*	*9800*
Std. Dev.	*9.9*	*1.12*	*3.2*	*3.9*	*1.29*	*890*
COV	*0.28*	*0.24*	*0.15*	*0.21*	*0.22*	*0.09*
U_3–1	21.3	2.87	16.8	17.4	6.00	9450
U_3–2	41.5	3.88	23.4	22.2	6.32	12560
U_3–3	31.3	5.15	20.3	20.0	4.29	8830
U_3–4	33.5	4.44	22.7	17.8	6.42	9220
U_3–5	45.4	4.95	21.8	17.7	5.04	11760
Average	34.6	4.26	21.0	19.0	5.61	10360
Std. Dev.	8.4	0.82	2.3	1.8	0.82	1500
COV	0.27	0.22	0.12	0.11	0.16	0.16
X–1	44.6	4.45	16.7	15.2	4.57	11850
X–2	58.6	5.89	N/A	12.7	1.82	11830
X–3	36.5	4.21	17	13.3	6.02	10460
X–4	25.5	4.38	16.2	15.4	7.38	7060
X–5	44.2	6.13	N/A	14.2	2.21	10290
Average	41.9	4.71	16.6	14.2	4.40	10300
Std. Dev.	10.9	0.82	0.3	1.0	2.14	1750
COV	0.26	0.17	0.02	0.07	0.48	0.17
X_3–1	44.7	4.15	22.7	21.3	6.28	12830
X_3–2	34.6	4.02	15.5	12.4	5.57	10390
X_3–3	38.5	4.90	21.9	21.5	6.62	10860
X_3–4	31.7	4.71	20.0	19.2	6.66	8360
X_3–5	38.3	4.43	24.3	24.4	7.15	10910
Average	37.6	4.68	22.1	19.8	6.45	10670
Std. Dev.	4.4	0.33	3.0	4.0	0.52	1430
COV	0.12	0.07	0.14	0.20	0.08	0.13
B–1	20.7	3.41	17.6	18.3	6.82	7520
B–2	39.1	3.91	19.5	13.7	5.50	11900
B–3	27.0	3.64	N/A	17.4	3.45	9600
B–4	23.1	3.58	17.2	14.4	6.04	8410
B–5	43.3	4.62	11.3	8.0	6.51	11030
Average	30.6	3.95	14.3	14.4	5.66	9680
Std. Dev.	9.0	0.43	3.1	3.6	1.19	1610
COV	0.29	0.11	0.22	0.25	0.21	0.17
B_3–1	48.2	5.06	24.7	20.1	4.79	11820
B_3–2	45.4	4.35	20.2	5.8	6.03	12850
B_3–3	26.8	5.58	16.4	13.4	5.66	9040
B_3–4	32.4	5.81	19.5	16.4	6.66	8220
B_3–5	28.5	5.31	21.7	20.7	5.04	7400
Average	36.3	5.57	19.2	15.3	5.64	9870
Std. Dev.	8.8	0.51	2.7	5.4	0.67	2110
COV	0.24	0.09	0.14	0.35	0.12	0.21

a – the maximum stress achieved per specimen

b –the strain at the maximum stress value

c – the stress recorded at 0.04 mm/mm strain

d – ultimate stress, the stress when the test was ended

e – ultimate strain, the strain when the test was ended

f – Modulus of Elasticity, the slope in the initial linear elastic region

4.3.2 Failure Modes

Representative failure modes of the GFRP reinforced specimens are shown in Figures 4.5a to 4.5d for U and U_3, 4.6a to 4.6d for X and X_3, and 4.7a to 4.7d for B and B_3. For each arrangement of reinforcement, two specimens are presented at the end of the test, after GFRP removal, and dissected along the specimen's longitudinal axis, in order to accurately demonstrate the effect of the GFRP wraps on the failure modes and damage. In general, the GFRP appears to localize the damage region to the plane of rupture and prevents propagation of longitudinal damage throughout the volume. The failure modes observed were primarily crushing, shearing, and the combined crushing and parallel-to-grain shear modes (Fig. 2.5). Generally, GFRP failure was observed to be located where the wood experienced severe damage. GFRP failure was less common among specimens with three layers of wrap reinforcement.

Figures 4.5a to 4.5d show specimens in the U and U_3 groups after test completion, with FRP removed, and dissected to display internal damage. As seen in those figures, unidirectional GFRP tends to fail in parallel with the wood failure plane. Specimen U_3–2 (Fig. 4.5d), which experienced a higher angle shear failure in comparison to the other three specimens shown, had significantly less actual glass fibre rupture. The specimens with greater fibre rupture (i.e., Specimens U–3 and U_3–1, Fig. 4.5b and 4.5c, respectively) have a larger apparent lateral expansion at the plane of rupture than the other specimens shown. Specimens U–1 (Fig. 4.5a) and U_3–1 (Fig. 4.5c) show similar local wood crushing as control specimens C–3 (Fig. 4.2c) and C–5 (Fig. 4.2e), with the notable difference that any signs of a longitudinal split failure propagation are minimized.

(a) U – 1 (b) U – 3 (c) U_3 – 1 (d) U_3 – 2

Figure 4.5: U & U_3 Representative Specimens Post-Test, FRP Removed, Dissected

In the case of the bidirectional group X, Figures 4.6a to 4.6d show how the three-layer group X_3 has more intact FRP at the end of the test than single-layer group X, and in general is more intact than the unidirectional reinforced specimens in Figures 4.5a to 4.5d. From Figures 4.6a and 4.6c, it can be observed that the presence of severe defects is still a controlling factor in the failure behaviour and damage patterns of the reinforced specimens as it was in the control specimens. Specimens X–1 and

X_3–3 show how knots, voids, and grain pattern flaws create a path of weakness for the failure plane to form on and follow. However, the presence of the reinforcement has limited some paths of failure due to the large knot in X–1, and the longitudinal void and weak grain angle in X_3–3. As a consequence, the vast majority of the damage is still captured in the fibre crushing behaviour at the plane or planes of rupture and not in longitudinal splits or parallel-to-grain shear slippage. Conversely, specimens X–4 (Fig. 4.6b) and X_3–5 (Fig. 4.6d) have exceptionally clear wood material without any obvious defects in the dissected failure region. These specimens displayed low angle crushing planes that are highly localized and regular.

(a) X – 1 (b) X – 4 (c) X_3 – 3 (d) X_3 – 5

Figure 4.6: X & X_3 Representative Specimens Post-Test, FRP Removed, Dissected

Figures 4.7a to 4.7d show specimens in the B and B_3 groups where it can be observed once more that three-layer reinforcement allows for greater ability of the FRP composite to remain globally intact even at high strains. Specimens B–2 (Fig. 4.7a) and B–4 (Fig. 4.7b) as shown have ideal crushing behaviour but with a larger lateral bulging and corresponding greater fibre rupture at the point of localized damage, though some fibres oriented parallel to the load are still intact spanning over the plane of rupture.

Specimen B_3–2 (Fig. 4.7c) has a clear grain angle flaw where a cross-grain defect acted as a driving wedge and created a potential path for a longitudinal split, but the FRP arrested the crack growth. Instead, the adjacent fibre crushing behaviour allowed for a rotation effect in the plane of the image, to the point that a second crushing plane, rather than further propagation of the weak longitudinal split, developed near the loaded top end. Specimen B_3–4 (Fig. 4.7d) experienced a crushing failure near the end of the specimen; which appears to be a consequence of a large knot visible in the FRP removed view. This is similar to specimen C–5 (Fig. 4.2e); however, unlike specimen C–5 the crushing plane was captured within the end of the FRP wrap until very large strain. As in other wrapped specimens, damage remained tightly localized. It can be seen from the post-test picture that in this instance the FRP wrap itself was in contact with the loading platen, which occurred at approximately half the ultimate strain of the specimen (i.e., 0.035 mm/mm). At this time the wood failure and initial FRP rupture failure had already begun.

(a) B – 2 (b) B – 4 (c) B_3 – 2 (d) B_3 – 4

Figure 4.7: B & B_3 Representative Specimens Post-Test, FRP Removed, Dissected

CHAPTER 5
Discussion

5.1 General

A total of six control and thirty GFRP reinforced specimens were tested under axial compressive tests. The experimental program investigated the effects of the GFRP fabric orientation and number of reinforcement layers provided on the compressive behaviour of 140 mm x 140 mm x 685 mm SPF No. 2 or better columns. The following sections discuss the observations and findings from the experimental program.

5.2 Compressive Behaviour of Control Specimens

5.2.1 Stress-Strain Behaviour

The overarching aim of this study was to investigate the effects of transverse GFRP reinforcement on the compressive behaviour of timber specimens representative of what is used in structural applications (i.e., containing defects such as knots vs. clear wood which is free of defects). Since the material behaviour is of primary interest, the specimens were loaded well past the point at which failure would be considered attained by typical loading conditions or design standards. For example, the equivalent energy elastic-plastic curve (EEEP), which was originally developed for steel and concrete systems, considers that the deformation at failure is defined as 80% of peak load. The EEEP method has since been adopted by the *Standards Test Methods for Cyclic (Reversed) Load Test for Shear Resistance of Vertical Elements of the Lateral Force Resisting Systems for Buildings* (ASTM E2126, 2011) for wood shear walls. Generally speaking, compressive coupons used as input to moment-curvature analysis consider coupons to have failed when 80% of peak strength has been reached (Lacroix 2017). This is in part because wood is a brittle material in tension, and as such compression failure in moment-curvature analyses rarely govern. However, prior research on flexural behaviour has shown significantly higher compression strain can be attained when reinforced with FRP. For example, Lacroix and Doudak (2020) investigated the behaviour of GFRP reinforced glulam beams under blast loading and recorded wood compressive strains as high as 0.022 mm/mm. It was thus critical to investigate the behaviour of the control specimens to the highest deformation levels possible with the test frame capabilities and global instabilities of the specimens.

As it can be seen in Figure 5.1, the control specimens were loaded well past the point of 80% of peak stress in order to understand how the control specimens would behave over the same range of strains that the reinforced specimens could be subjected to.

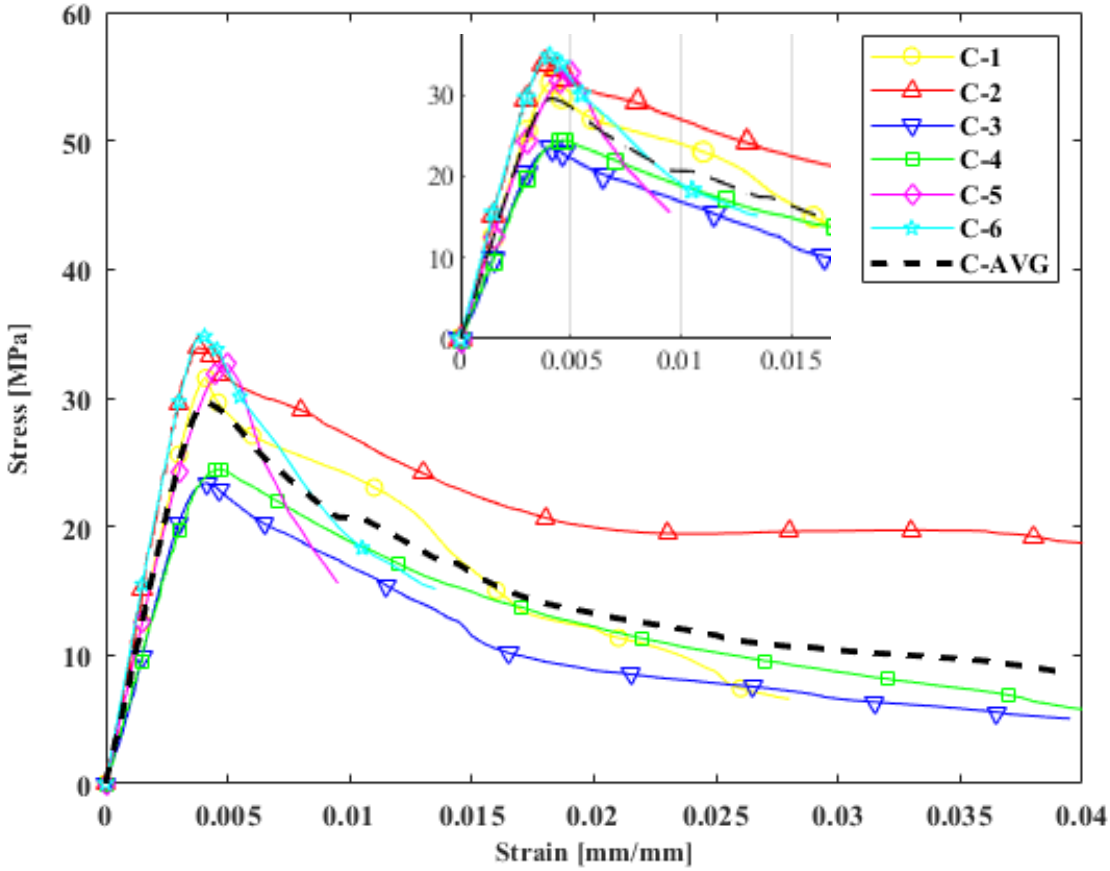

Figure 5.1: Control Group Stress-Strain Behaviour and Low-Strain Snapshot

Figure 5.1 shows the compressive stress-strain curve for all six specimens including the average of the group. At first glance, it can be observed that the global stress-strain behaviour of the control specimens appears to differ from the bilinear curve proposed by Buchanan (1990) as well as to what is used in the *Standards Test Methods for Establishing Characteristic Values for Reinforced Glued Laminated Timber (Glulam) Beams Using Mechanics-Based Models* (ASTM D7199, 2020) to predict the moment-curvature relationship of glulam beams reinforced with simple tension GFRP. However, a closer examination of the behaviour up to 0.015 mm/mm does appear bilinear as in Buchanan's model (i.e., Fig. 2.4d). The idealized bilinear curve proposed by Buchanan (1990) appears to be applicable to the early stages (i.e., $\varepsilon \leq 0.015$ mm/mm), and when pushing the material to its limit, a bilinear model is no longer sufficient to describe the global behaviour. To describe the behaviour up to 0.04 mm/mm stain, Glos' model (i.e., Fig. 2.4c) may be the best of the models discussed in this paper. In general, the

most severe loss of strength is seen from peak stress to approximately the 0.015 mm/mm strain mark, after which rate of strength loss becomes lower.

In Figure 5.1 it can be seen that multiple specimens appear to be converging to a low strength (~5MPa) plateau, while specimen C–2 is seen to show a significantly higher post-peak sustained stress (~18MPa) plateau up to 0.04 mm/mm. Specimen C–2 was remarkably defect-free compared to other control specimens (Fig. 4.2b), and experienced pure crushing failure type up to strains of 0.04 mm/mm, the only control specimen to do so. Generally, it could be said the failure of C–2 was not significantly influenced by the presence of defects unlike other control specimens.

Two of the six tests had to be stopped prior to the 0.015 mm/mm mark due to global instabilities in the specimen. Specimen C–5 developed an angled crushing plane near the loaded end due to a significant defect (Fig. 4.2e) which resulted in severe strength loss and the specimen becoming unstable at very low strain. The observed variability of behaviour among the specimens is typical of unreinforced wood which is attributable to the natural defects. It is functionally impossible to consistently predict the failure mode, failure location, or strength of individual pieces, particularly when the severity of defects may not be externally visible. The full stress-strain behaviour and more details on the failure behaviour of control specimens are found in Appendix A.

5.2.2 Failure Modes

The observed failure modes of control specimens were consistent with those observed in wood under axial compressive loading. Since the specimens were loaded well past their initial failure point, Figures 4.2a to 4.2f can give the appearance that the wood specimens were significantly ductile based on the final state of damage. To illustrate the point that the observed final damage state occurs after significant strain and strength losses, Figures 5.2a to 5.2d show specimen C–4 at peak strength (initial failure), 80% of peak strength, 0.015 mm/mm strain (60% of peak strength), and at the end of the test.

(a) Initial failure (b) 80% peak strength (c) 0.015 mm/mm (d) Final damage state

Figure 5.2: C–4 Damage Progression

The failures in the control specimens were observed to follow the path of least resistance. Although crushing is initially observed in some specimens, eventually longitudinal splitting occurs. Since the specimens were loaded until they could no longer safely sustain more deformations, the level of crushing seen in Figures 4.2a to 4.2f can appear more pronounced when compared to what would be considered a failure in terms of design.

5.3 Effects of GFRP Reinforcement

To simplify comparisons, the average stress-strain parameters for each experimental group investigated in this study are presented summarily in Table 5.1 along with their standard deviation and COV.

Table 5.1: Summary of Stress-strain Parameters from Tests Results

Key Parameters		Experimental Groups						
		C	**U**	**U_3**	**X**	**X_3**	**B**	**B_3**
σ_y [a] **[MPa]**	Average	30.2	34.9	34.6	41.9	37.6	30.6	36.3
	Std. Dev	4.5	9.9	8.4	10.9	4.4	9.0	8.8
	COV	0.15	0.28	0.27	0.26	0.12	0.29	0.24
$\epsilon_y \times 10^{-3}$ [b] **[mm/mm]**	Average	4.29	4.70	4.26	4.71	4.68	3.95	5.57
	Std. Dev	0.45	1.12	0.82	0.82	0.33	0.43	0.51
	COV	0.10	0.24	0.22	0.17	0.07	0.11	0.09
$\sigma_{\epsilon_{0.04}}$ [c] **[MPa]**	Average	9.9	21.2	21.0	16.6	22.1	14.3	19.2
	Std. Dev	6.3	3.2	2.3	0.3	3.0	3.1	2.7
	COV	0.64	0.15	0.12	0.02	0.14	0.22	0.14
σ_{ult} [d] **[MPa]**	Average	9.3	18.2	19.0	14.2	19.8	14.4	15.3
	Std. Dev	4.1	3.9	1.8	1.0	4.0	3.6	5.4
	COV	0.44	0.21	0.11	0.07	0.20	0.25	0.35
$\epsilon_{ult} \times 10^{-2}$ [e] **[mm/mm]**	Average	3.54	5.90	5.61	4.40	6.45	5.66	5.64
	Std. Dev	2.13	1.29	.82	2.14	0.52	1.19	0.67
	COV	0.60	0.22	0.16	0.48	0.08	0.21	0.12
MOE [f] **[MPa]**	Average	8470	9800	10360	10300	10670	9680	9870
	Std. Dev	1360	890	1500	1750	1430	1610	2110
	COV	0.16	0.09	0.16	0.17	0.13	0.17	0.21

a – the maximum stress achieved per specimen
b –the strain at the maximum stress value
c – the stress recorded at 0.04 mm/mm strain
d – ultimate stress, the stress when the test was ended
e – ultimate strain, the strain when the test was ended
f – Modulus of Elasticity, the slope in the initial linear elastic region

Compared to the control group, the average peak stress was 1.01 – 1.39 times greater and the MOE was 1.14–1.26 times greater among reinforced groups. Increases up to a factor of 1.3 were also observed for strain corresponding to peak stress amongst reinforced groups when compared to the control group. At 0.04 mm/mm strain, the strength of the reinforced specimens was 1.44 – 2.23 times compared to the control group; and in addition a significantly greater number of reinforced specimens were able to retain strength at high strain. At 0.04 mm/mm strain, reinforced specimens retained up to 61% of their respective peak capacity, compared to just 33% in the control specimens. Furthermore, reinforced specimens typically showed minimal strength degradation beyond 0.04 mm/mm strain to end of the test as seen in Table 5.1. The average end of test strain amongst reinforced specimens ranged between 0.044 and 0.064 mm/mm while the ultimate stress ranged from 80% to 90% of the stress at 0.04 mm/mm strain.

The overall effects of the GFRP reinforcement on the stress-strain curves can be seen in Figure 5.3 where the behaviour of all reinforced specimens is compared to the average of the control group. In

particular the post-peak descending branch of the reinforced specimens is generally observed to be less pronounced or level off earlier and more significantly than the average of the control specimens, leading to the higher plateau value at high strains.

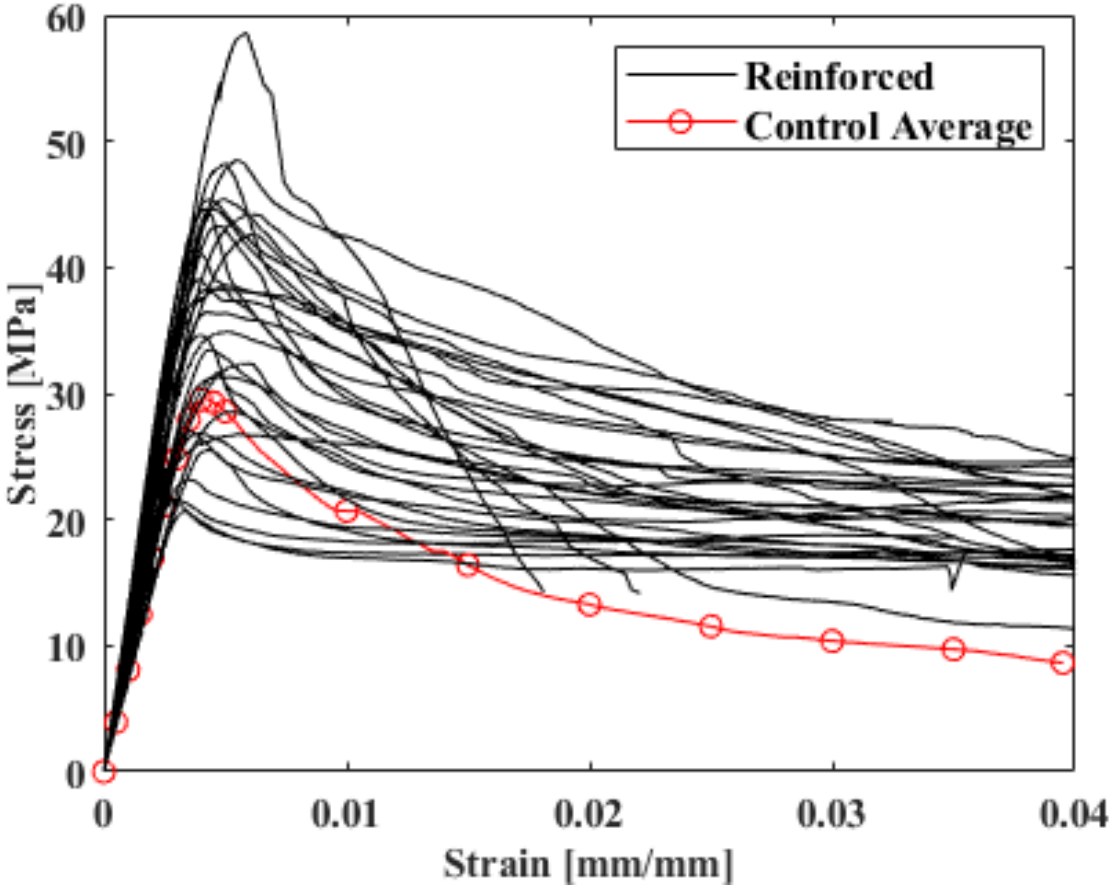

Figure 5.3: All GFRP Reinforced Specimens Compared to Average of the Control Group

Figure 5.4 shows the average of each reinforced group in comparison to the average of the control group. It can be seen that all reinforcement configurations tested appear to exhibit some amount of improved behaviour compared to the average of the control group. The effect of adding GFRP is significantly more pronounced in the post-peak region, especially when comparing the strengths retained at high strains. The complete curves for the reinforced specimens are available in Appendix B.

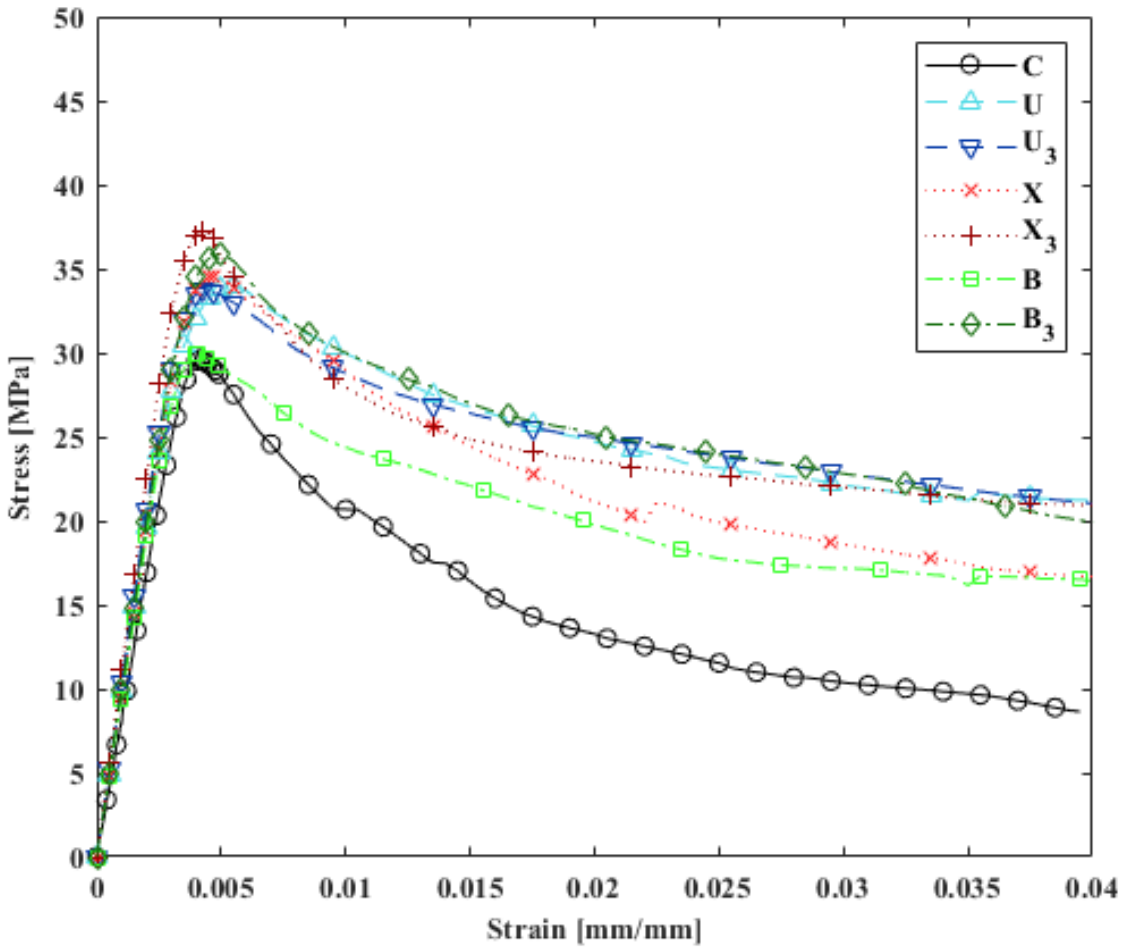

Figure 5.4: Average Stress-strain Curves for Control and Reinforced Groups

Despite the wide range of peak strengths and stiffnesses amongst all reinforced specimens as shown in Figure 5.3, it is apparent in Figure 5.4 that all reinforced specimens converge to similar strength plateau with the exception of groups B and X. Stress-strain curves for reinforced specimens, but particularly when averaged into groups, are very similar in shape to the model of the compressive behaviour developed by Glos (1978). Even if only considering the behaviour up to 0.015 mm/mm, where it was demonstrated the bilinear model of Buchanan (1990) was still applicable for the control group, reinforced groups show evidence of plateau behaviour at greater percentages of their peak strength.

It is noteworthy that groups U, U_3, X_3, and B_3, performed extremely similarly on average (Fig. 5.4). These groups had significantly different reinforcement arrangements with varying amounts and orientations of transverse fibre and fabric thickness among other properties identified in Table 3.2. This suggests that an upper limit to the behaviour of the wood material is the controlling variable, rather than the specifics of the reinforcement applied. The average curves of these groups which performed best is also very similar to the curve of specimen C–2, which was pointedly free of defects and the only control

specimen that experienced pure crushing failure type. Recalling the observation that reinforcement significantly localized damage, even when a major defect was present at the location of wood failure, it would be reasonable to suggest that the transverse reinforcement is mitigating the influence of defects from creating weaker load paths. Thus, the behaviour of reinforced specimens would resemble that of defect-free wood material.

It can be observed that single-layer bidirectional configurations (i.e., B and X) were slightly less effective on average in terms of post-peak sustained stress levels. Furthermore, single-layer 0–90° bidirectional fabric was the only reinforcement configuration that did not contribute to a peak strength improvement relative to the average of the control group. Single-layer bidirectional fabrics are the thinnest GFRP fabrics investigated with 0.66 mm and 0.86 mm thicknesses for B and X, respectively, and in addition a smaller fraction of that thickness is made up of transverse fibre fraction than unidirectional fabric in group U. Thus, it may be that this quantity of transverse reinforcement is simply not sufficient to effectively alter the behaviour by mitigating the influence of defects and lateral strains.

Since Table 5.1 suggests that on average there are increases in stress-strain parameters, t–Tests were conducted to verify if these increases are statistically significant. Due to the limited number of specimens per group, these tests only compare control specimens against all reinforced specimens. For post-peak behaviour, not enough data is available in the control group to do a reasonable statistical analysis for significance of the improvement to sustained stress. However, the visual differences in retained strength between the control and reinforced specimens are readily apparent in Figures 4.4a to 4.4f, Figure 5.3, and Figure 5.4. Similarly, differences in ultimate stress and strain values between Table 4.2 and 4.3, or as highlighted on average in Table 5.1, are also apparent.

Prior to conducting the t–Tests, an F–test was performed to assess differences in the variances in each sample population. The variances in the control and reinforced populations were not found to be significantly different for peak stress, corresponding strain, or MOE with probabilities of equal variances (i.e., F_{stat} or the ratio of the mean square differences for the two populations less than $f_{critical}$ the value of F_{stat} such that a confidence of non-equal values of 95 % is achieved) being 7.3 %, 10.1 %, and 44.4 %, respectively.

The confidence level for the two–tail t–Tests for two samples was chosen to be 95%. The null hypothesis (e.g., no difference between the mean of the two data sets) was rejected if the absolute value of t_{stat} (the ratio of the departure of the estimated value of a parameter from its hypothesized value to its standard error) was greater than the absolute value of t_{crit} (the value of t_{stat} such that a confidence of non-equal values of 95 % is achieved). The t–Tests are presented in Table 5.2 where bold numbers indicate that there is a significant difference between the two means.

Table 5.2: Comparisons of Properties by t–Test Assuming Equal Variances

Parameter	Comparison of Means – Control vs. Reinforced	
	t_{stat}	t_{crit}
σ_y	1.44	2.03
ε_y	0.78	2.03
MOE	**2.25**	**2.03**

Despite the increases observed in Table 5.1, the only statistically significant improvement is to modulus of elasticity, likely due to the more similar variances in the control and reinforced samples. In order to assess the significance of the improvement to peak strength more accurately, greater sample size is necessary. Similarly, a greater sample of unreinforced specimens achieving high strains is necessary to evaluate the impact of GFRP on mechanical properties in that strain range.

Therefore, in order to further quantify the improvements provided by the addition of the GFRP, integration of the area under the average stress-strain curves for each reinforcement configuration as well as the control group was conducted up to two key strains. Table 5.3 shows the area under the stress strain curve in MPa · mm/mm and the improvement factor relative to the control group up to 0.015 mm/mm strain and 0.04 mm/mm strain for each reinforcement configuration.

Table 5.3: Improvements to Average Energy Dissipation up to 0.04 mm/mm strain

Group	**Average Energy Dissipation and Improvement Factors**			
	$E_{0.015\ mm/mm}$ [a] $(MPa \cdot mm/mm)$	$\frac{E_i}{E_C}$ [b]	$E_{0.04\ mm/mm}$ [c] $(MPa \cdot mm/mm)$	$\frac{E_i}{E_c}$ [b]
C	0.308	-	0.588	-
U	0.409	1.33	0.974	1.66
U_3	0.403	1.31	0.978	1.66
B	0.350	1.14	0.794	1.35
B_3	0.417	1.36	0.990	1.68
X	0.400	1.30	0.879	1.50
X_3	0.410	1.33	0.961	1.64

a – Energy Dissipated by 0.015 mm/mm Strain

b – Ratio of Energy Dissipated by Group to Energy Dissipated by Control Group

c – Energy Dissipated by 0.04 mm/mm Strain

GFRP reinforced wood specimens on average were able to dissipate 1.35 – 1.68 times more energy by 0.04 mm/mm strain than control specimens even with only a single layer of GFRP. This improved compressive post-peak behaviour could provide significant benefits for flexural and combined compression–flexure members that are expected to experience compression–based failure. The improved post-peak behaviour will also provide significant benefits against extreme loads such as earthquakes or blast loading, where GFRP reinforced beam–columns can experience maximum

compressive strain values exceeding 0.02 mm/mm (Lacroix and Doudak, 2018b, Lacroix and Doudak, 2020).

In terms of the effect of transverse reinforcement on failure modes, the addition of GFRP wrapping eliminated splitting failure behaviour, and localized damage to the plane of initial failure regardless of reinforcement configurations. In the dissected specimens from reinforced groups shown in Figures 4.5a to 4.5d, 4.6a to 4.6d, and 4.7a to 4.7d, it can clearly be seen that local crushing of wood fibres is the predominant failure mechanism. Crushing of the wood fibres is obvious in the damaged region but there was no other visually discernible damage despite the presence of defects within the damaged region or elsewhere in the specimen. In the dissected view of reinforced specimens there were functionally no visible voids, cracks, or longitudinal splits as in the control group. Instead, the wood fibres crush, buckle, and fold over exclusively. Figures 5.5a to 5.5d shows the final damage states of representative control (Figs. 5.5a and 5.5b) and reinforced (Figs. 5.5c and 5.5d) specimens for comparison.

(a) C–3 (b) C–4 (c) U–3 (d) X_3–3

Figure 5.5: Final Damage States of Control Specimens vs. Reinforced Specimens

Recalling that the control specimens in general were not pushed to the most extreme strains as specimens in the reinforced group, the comparison of final damage states is made all the more impressive. Even when the crushing plane is highly localized and planar for control specimens as in Figure 5.5a, the ability of longitudinal splits to develop between the rupture plane and loaded end is readily apparent. Conversely, even reinforced specimens exhibiting a combined failure mode with longitudinal damage component as in Figure 5.5d, the propagation of the longitudinal damage is arrested by the presence of FRP composite reinforcement.

This correlation between the apparent failure mode or failure behaviour and the rate of strength loss and stress-strain behaviour post-peak provides insight into how FRP wrapping improves ductility and sustained post-peak strength. The effect cannot be described as passive confinement because wood does

not dilate like concrete under compression. However, the statistical significance of MOE improvements would suggest that some lateral forces and displacements are being restricted by the FRP even prior to peak strength developing. Furthermore, amongst reinforced specimens the rate of strength losses is frequently lower post peak than the control group as seen in Figure 5.3. This would indicate engagement of the transverse FRP is preventing some weak load paths from controlling the global failure at low strains as well as extreme strains.

Figures 5.6a to 5.6e show failure progression of specimen B–1, highlighting the key moments during testing of underlying wood rupture, FRP wrinkling in compression, initial transverse fibre rupture, and final damage state.

(a) Wood Rupture (b) Wrinkling (c) Fibre Rupture (d) Test Complete (e) Wood Damage

Figure 5.6: Representative Failure Progression of Reinforced Specimens – Specimen B–1

For the U & U_3 specimens (Figs. 4.5a to 4.5d), the composite rupture took place completely in the matrix between the transverse glass fibres with the glass fibres themselves eventually rupturing due to stress concentrations caused by bulging in the damaged region. In the case of the bidirectional fabric groups B & B_3 (Figs. 4.6a to 4.6d) and X & X_3 (Figs. 4.7a to 4.7d), although rupture of GFRP composite is observed, the crossed GFRP fibres in orthogonal directions helped hold the wrap together globally. Both wood material failure and FRP rupture initiated due to stress concentrations at corners (Fig. 5.6c), then propagated around the perimeter of the specimen. Therefore, the effect of the corner radius on failure modes, failure behaviour, and stress-strain behaviour of reinforced specimens and the transverse reinforcement itself need to be further investigated. Even beyond the point of fibre rupture the FRP above and below the ruptured area remains intact and tight and continues to provide resistance to lateral strain away from the weakened wood rupture plane. During this time, the plateau strength behaviour remains consistent regardless of local rupture, which suggests the critical location for transverse FRP is above and below the point of wood failure to restrict longitudinal crack formation and propagation.

A comparison of the failure progression damage states along with the approximate point in the stress-strain curves where they occur is presented in Figures 5.7 and 5.8 to directly show the effects of GFRP

on the total behaviour. Figure 5.7 shows the failure progression of C-4, it can be observed at peak strength and even by 80% strength post-peak minimal damage has taken place. As damage amplifies, it can be observed how longitudinal splits form or widen, until finally complete cracks from the point of initial failure to specimen end form. This failure was classified as a wedge-split type (Fig. 4.2d). Conversely Figure 5.8 shows the progression of X_3–5, where a higher peak and greater strain are observed, with significantly improved strength retention as discussed. As with control, a very small amount of visible damage has taken place by 80% of peak strength, but in the reinforced specimen the corresponding strain at 80% is equivalent to the strain of the control specimen at 60% of peak. The least strength observed in the reinforced specimen is 64% of the peak, which begins at ~0.035 mm/mm strain and persists up to 0.07 mm/mm. Furthermore, although the damage visibly amplifies from the 80% strength point to the 64% strength point, from 0.04 mm/mm to 0.07 mm/mm the damage increase is visibly negligible. This failure was classified as a crushing type.

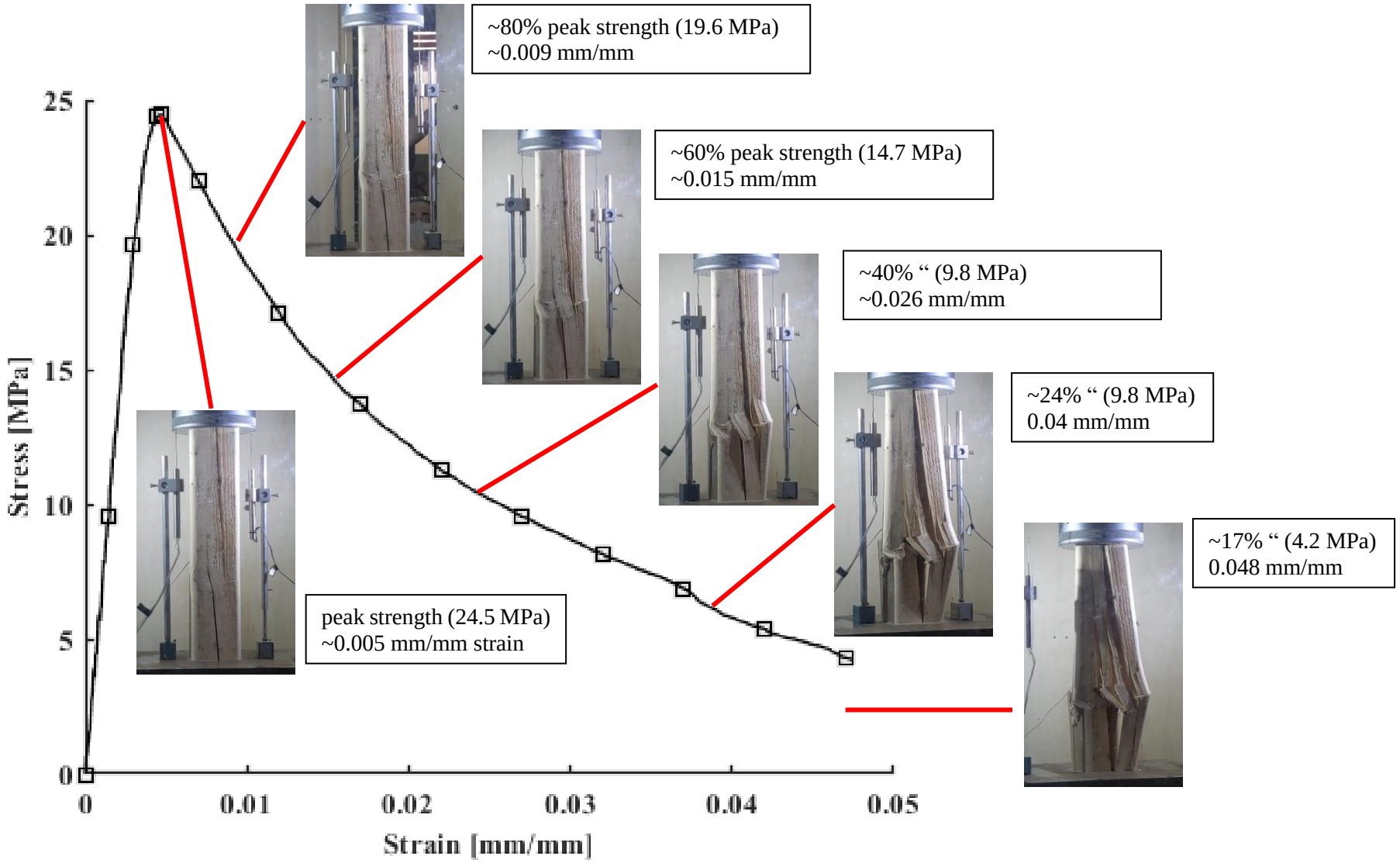

Figure 5.7: Detailed Failure Progression of C–4

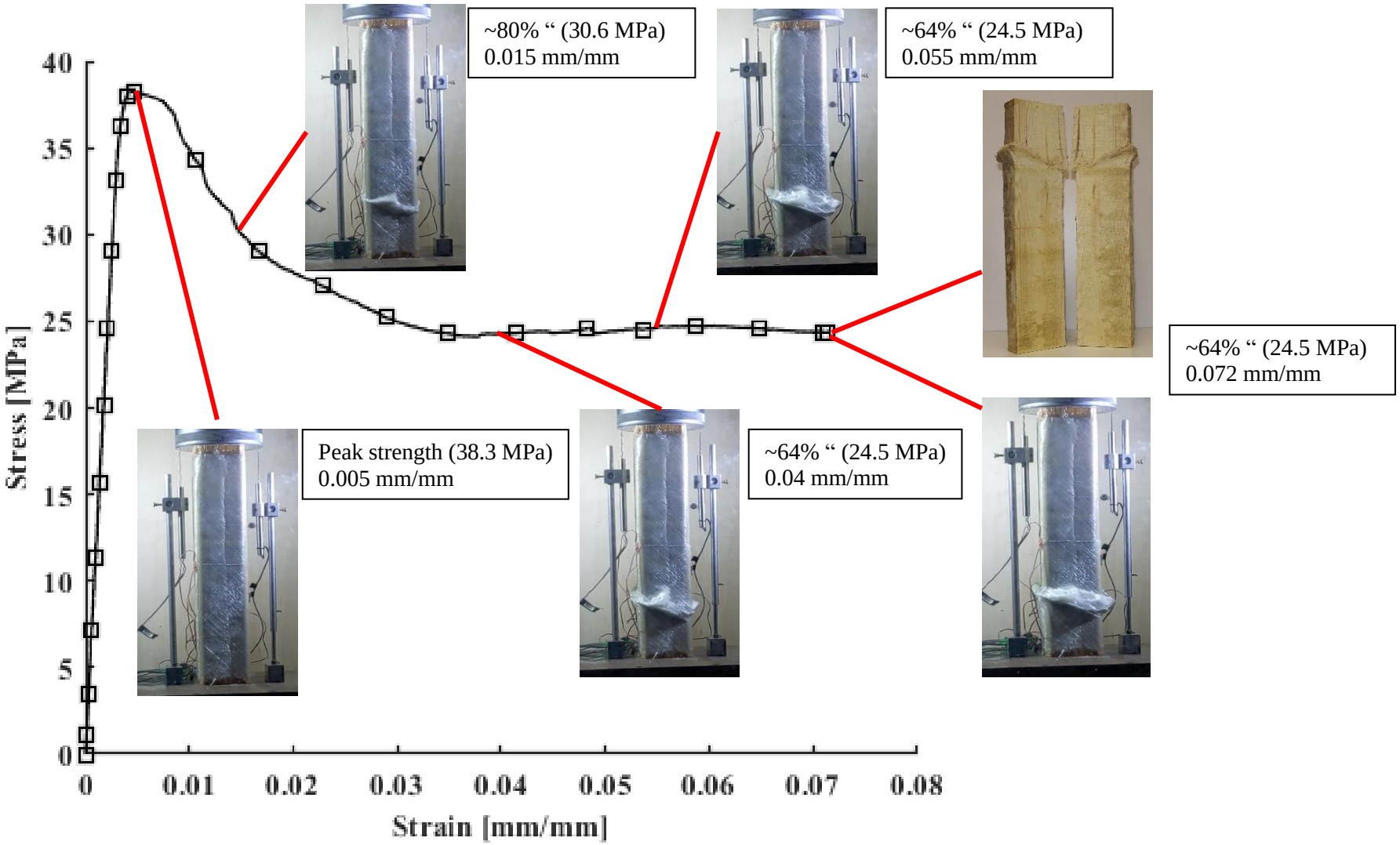

Figure 5.8: Detailed Failure Progression of X3–5

The plateau behaviour of reinforced specimens had fairly consistent stress values centered about roughly 20 MPa, even up to 0.04 mm/mm. 27 of 30 reinforced specimens conformed to this behaviour with consistency. The control group specimens averaged only approximately 10 MPa at this strain and behaviour was inconsistent. Specimens X–2, X–5, and B–5 were the outliers among reinforced specimens which did not develop plateau behaviour, and often had lower ultimate strains; Figures 5.9a to 5.9e show explanative damage states of these specimens.

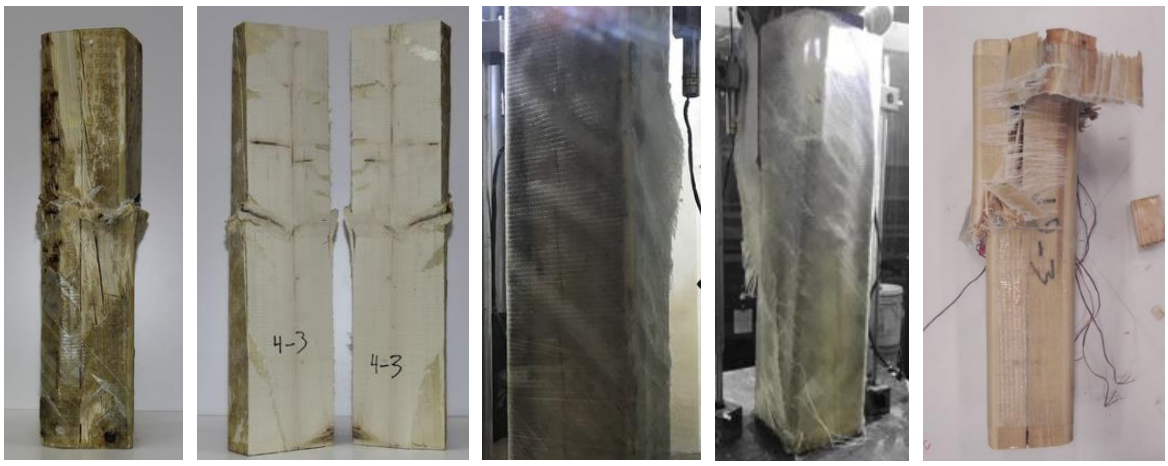

(a) X–2 (Post-Test) (b) X–2 (Dissected) (c) X–5 (Debonding) (d) X–5 (Post-Test) (e) B–5 (Post-Test)

Figure 5.9: Final Damage States of Specimens with Odd Behaviour: X–2, X–5, B–5

In the case of specimens X–5 and B–5, the odd behaviour is explicable as a non-standard failure of the FRP composite. Specimen X–5 experienced the bulk of its deformation on the same face as the overlap in the FRP composite, such that local debonding failed the overlap joint prematurely as pictured in Figures 5.9c and 5.9d. Specimen B–5 failed such that the FRP composite was able to rupture longitudinally from the wood rupture plane to the top of the specimen. Subsequently, the top half of the specimen acted as though unreinforced. The underlying wood was able to buckle and split at the top end grain, the final damage state as shown in Figure 5.9e. Specimen X–2 is remarkably defect-free compared to other specimens as seen in Figure 5.9b. Additionally, it had greater peak strength than all other specimens tested. Its failure mode and damage was not irregular compared to other specimens however. One notable observation is a significant degree of torsion between the loaded ends as visible in Figure 5.9a. It is likely that if tested to extreme strains, plateau behaviour would be observed as with other specimens; however at the point of test termination more than 75% of strength had been lost, remaining strength was only 12 MPa, and the strain was below 0.02 mm/mm. Furthermore, there was no indication prior to that point the rate of strength loss was lessening, thus the test was considered complete. It may be that due to a lack of defects, or

deformation in the form of torsion at the damaged area, there were less transverse forces and the FRP was not engaged at that point.

5.4 Summary

The experimental program consisting of thirty-six column specimens investigated the effects of GFRP fabric on the compressive behaviour of 140 mm × 140 mm × 685 mm SPF of grade No. 2. Reinforcement arrangements were varied by the fabric employed, particularly the orientation of fibres in said fabric, and the quantity of reinforcement layers provided (i.e. one or three layers).

Specimens were loaded to high strains relative to the point at which they would be considered failed from a design perspective in order to investigate the material behaviour. Up to strains of 0.015 mm/mm, the behaviour of control specimens is well represented by Bazan (1980), and Buchanan's (1990) commonly used bilinear falling branch model. When including higher strains, the descending stress-strain behaviour begins levelling off to plateau values more akin to the model proposed by Glos (1978).

There was an observed correlation between the failure mode, stress-strain behaviour, and presence of defects within the specimens. The defect-free control specimen acted with considerably greater post-peak residual capacity, and experienced crushing failure with minimal longitudinal splitting up to high strain. Reinforced specimens were found to behave similarly to this control specimen, with highly localized damage that excluded longitudinal splitting behaviour completely. The behaviour of specimens reinforced with a transverse wrap of GFRP is significantly closer to Glos's model than the bilinear falling branch, even if only considering fairly low strains or typical cut-offs for post-peak strength.

The initiation and propagation of cracks and ruptures, particularly longitudinally oriented ones, was observed to considerably lower strength during testing. The mitigation of splitting failure and prevention of damage propagation and amplification through the specimen volume allowed the wood material to maintain a relatively large strength plateau effectively indefinitely for the range of strains investigated. The notable exceptions were those reinforced specimens with premature or longitudinal GFRP, which did not attain a high strength plateau behaviour. The rate of post-peak strength loss immediately after maximum strength was frequently lower for reinforced specimens. Furthermore, regardless of the fabric orientation, fabric thickness, or peak stress value, the plateau strength observed was fairly constant. Even if the GFRP was ruptured at the location of local damage, it tended to remain intact above and below, and the plateau strength persisted. Thus, this plateau strength could be described as a property of the wood material when weak load paths through longitudinal splits are prevented by adjacent FRP.

The bidirectional fabrics, when applied as a single layer (i.e. Groups B and X), showed less strength retention at high strain and some inability to raise the peak strength and stiffness when compared to other groups. These arrangements of reinforcement were both thinnest and provided the lowest fraction of fibres acting transverse to the load orientation; thus it could be said that there is a transverse reinforcement ratio required to achieve the behaviour observed in other groups (I.e. U, U_3, X_3, and B_3). Conversely, despite tripling the thickness groups U and U_3, as well as X_3 and B_3 which would fall between the two, had near identical behaviour on average. This suggests the upper limit to the effectiveness of increasing reinforcement ratio of the transverse GFRP is based in the behaviour of the wood material. The simple conclusion is that the provision of transverse GFRP allows the wood material to behave as though defect-free, thus the limits of defect-free material are the limits of reinforced material with defects.

Peak stress, corresponding strain, and modulus of elasticity were all seen to improve to some degree with FRP wrapping. However, a t-Test showed that only the improvement to the elastic modulus was statistically significant to a 5% confidence level in this study. Statistical analyses were not possible for post-peak behaviour due to the lack of data from the control group but the improvements to retained strength at given strain (1.44 – 2.23 times control at 0.04 mm/mm) as well as the ultimate strain (1.24 – 1.67 times control) were clearly visible in figures and tables. When using the area under the curve as a measure of energy dissipated, the improvement from reinforcement was 1.35-1.68 times by 0.04 mm/mm strain, even for single-layer reinforcement. Therefore, these types of reinforcement clearly have benefits to designers that would not be captured by using the models for plain wood behaviour without update, although this would remain conservative.

CHAPTER 6
Conclusions

6.1 General

In the current study, a total of six control and thirty GFRP reinforced 140 mm × 140 mm × 685 mm SPF No. 2 columns were tested under parallel-to-grain compression. Three different reinforcing GFRP fabrics consisting of unidirectional at 90°, bidirectional at ±45°, and bidirectional at 0°/90° relative to the wood grain were investigated with either one or three layers applied. The experimental results including mechanical properties and failure modes were presented and discussed.

6.2 Conclusions

The following conclusions can be drawn from the current study:

- For the control group, the commonly used bilinear falling branch model established by Buchanan (1990) appears to be accurate in describing the stress-strain behaviour up to strains of 0.015 mm/mm. At higher strains (i.e., up to 0.04 mm/mm), behaviour might be better represented by Glos' (1978) model.
- Within the control group, failure was observed to follow the path of least resistance. Pure crushing failure up to 0.04 mm/mm strain was rare. Ultimately, the failure involved longitudinal cracks or splitting as strain levels increased throughout the entire specimen. Failure modes included splitting, crushing, and wedge splitting.
- In the reinforced groups, stress-strain curves are more representative of the model of the compressive behaviour developed by Glos (1978). The failure modes observed were crushing, shearing, and combined crushing & shearing. Generally, the behaviour of reinforced specimens is closer to the behaviour of defect-free material; experiencing lower strength losses post-peak, a high-strength plateau at great strains, slight improvement to peak strength and stiffness, and failure behaviour dominated by wood crushing.
- Factors of improvement to peak strength were as high as 1.39, corresponding strain increased up to 1.3 times, and for the modulus of elasticity improvement ranged from 1.14 to 1.26 times . Only the improvement to the modulus of elasticity was found statistically significant, in order to assess the significance of the improvement to peak strength a greater sample size is necessary.
- Considering post-peak behaviour, greater strength retention was observed at all strains investigated for reinforced specimens. By 0.04 mm/mm reinforced specimens retained 1.44 –

2.23 times the capacity of control specimens. This was a retention of 61% of the peak capacity compared to 33% amongst control specimens. The area under the stress-strain curve was 1.35 – 1.68 times greater by 0.04 mm/mm strain than control specimens, even with only a single layer of GFRP wrap. In order to investigate the statistical significance of these findings, a greater sample size of control specimens tested to high strains is necessary.

- Reinforcement ratio appears significant on the ability of the GFRP to alter behaviour. The reinforcement configurations providing the least transverse fibre area were less effective in raising post-peak strength and in the worst configuration ineffective in raising the peak strength and stiffness on average. Conversely, the variability in reinforcement provided in the other groups shows no variation in the stress-strain behaviour on average despite large differences in thickness and area of reinforcement provided.
- The location of rupture in the FRP reinforcement is coincident with the wood damage. Both material failures initiated due to stress concentrations at cross-section corners, then propagated. The presence of intact FRP composite immediately adjacent to and away from the wood damage appears to mitigate lateral strain and perpendicular to grain tension from propagating longitudinal failure through the volume of the specimen, localizing damage. This appears critical to achieving the plateau behaviour observed in the study.

6.3 Recommendations for Future Work

Based on the observations and results of this study presented in the previous chapters a number of areas have been identified as recommended future work, which includes:

- For the purposes of greater confidence and significant results in statistical analyses, a greater sample size should be investigated. In particular for unreinforced specimens, a greater quantity of data at high strains is necessary.
- Given the thinnest reinforcements provided were less satisfactory yet increases in thickness beyond group Us had minimal impact, it would be useful to determine the critical reinforcement ratio necessary to alter the behaviour to the apparent maximum observed.
- It could be investigated whether pre-stressing the transverse reinforcement such that a state of active confinement was developed has a greater effect on the wood behaviour, particularly whether it can more substantially improve peak performance and if at high strains the FRP can continue to achieve the behaviour observed in the study.
- Findings of the current study should be confirmed for additional wood species and grades. This also includes other wood products such as glulam, laminated veneer lumber, and cross-laminated timber.

- Despite precautions taken the rounded corners were still a point of stress concentration in both the cross-section and reinforcement; the influence of the ratio between corner radius and column size should be thoroughly examined for determining best radii for application of this reinforcement type.
- It is well established for plain wood structural elements that moisture plays a significant role, the influence of moisture in conjunction with the effects of GFRP reinforcement should be tested, particularly as it pertains to wet service condition design

Bibliography

André, A., Kliger, R., & Olsson, R. (2013). Compression failure mechanism in small-scale wood specimens reinforced with CFRP: An experimental study. *Construction and Building Materials*, *41*, 790–800. https://doi.org/https://doi.org/10.1016/j.conbuildmat.2012.12.038

André, A., Kliger, R., & Asp, L. E. (2014). Compression failure mechanism in small scale timber specimens. *Construction and Building Materials*, *50*, 130–139. https://doi.org/https://doi.org/10.1016/j.conbuildmat.2013.09.018

ACI Committee 440 (2017). Guide for the Design and Construction of Externally Bonded FRP Systems for Strengthening Concrete Structures. In ACI PRC-440.2-17. American Concrete Institute.

ASTM. (2011). Standard Practice for Establishing Clear Wood Strength Values. In *ASTM D2555-11* (p. 18). American Society for Testing and Materials.

ASTM. (2014). Static Tests of Lumber in Structural Sizes. In *ASTM D198* (p. 26). American Society for Testing and Materials. http://www.astm.org

ASTM D2395 - 17 Standard Test Methods for Density and Specific Gravity (Relative Density) of Wood and Wood-Based Materials. (n.d.). Retrieved December 31, 2020, from https://www.astm.org/Standards/D2395.htm

ASTM D442-16, Standard Test Methods for Direct Moisture content Measurement of Wood and Wood-Based Materials. ASTM International, West Conshohocken, PA, 2016. www.astm.org

ASTM E2126-11. (2011). Cyclic (Reversed) Load Test for Shear Resistance of Vertical Elements of the Lateral Force Resisting Systems for Buildings (p. 15). ASTM International.

ASTM. (2020). Standard Practice for Establishing Characteristic Values for Reinforced Glued Laminated Timber (Glulam) Beams Using Mechanics-Based Models. In *ASTM D7199-20*. American Society for Testing and Materials. https://doi.org/10.1520/D7199-07R12

ASTM. (2014). Standard Test Methods for Small Clear Specimens of Timber. In *ASTM D143-14* (p. 31). American Society for Testing and Materials.

Barrett, J. D., & Lau, W. (1994). *Canadian Lumber Properties*. Canadian Wood Council.

Bazan, I. M. M. (1980). *Ultimate bending strength of timber beams: Vol. Ph.D.* Nova Scotia Technical College.

Bjertnaes A., M., & Malo A., K. (2014). Wind-induced motions of "Treet" - A 14-storey timber residential building in Norway. In A. Salenikovich (Ed.), *World Conference on Timber Engineering* (p. 8).

Buchanan, H.A. (1984). Strength model and design methods for bending and axial load interaction in timber members. In *Civil Engineering: Vol. Ph.D.* The University of British Columbia.

Buchanan, H.A. (1990). Bending strength of lumber. *Journal of Structural Engineering*, *116*(5), 17. https://doi.org/http://dx.doi.org/10.1061/(ASCE)0733-9445(1990)116:5(1213)

Buchanan, H.A., & Fairweather H., R. (1993). Seismic design of glulam frame structures. *Bulletin of the New Zealand National Society for Earthquake Engineering*, *26*(4), 22.

Buell, T. W., & Saadatmanesh, H. (2005). Strengthening timber bridge beams using carbon fiber. *Journal of Structural Engineering*, *131*(1), 173–187. https://doi.org/doi:10.1061/(ASCE)0733-9445(2005)131:1(173)

Breyer E., D., Fridley J., K., Cobeen E., K., & Pollock G., D. (2007). *Design of Wood Structures-ASD/LFRD*. McGraw-Hill.

Caiza, Pablo. (2012). Flexure-Compression Testing of Bridge Timber Piles Retrofitted with Fiber Reinforced Polymers. Open Journal of Civil Engineering. 02. 115-124. 10.4236/ojce.2012.23017.

Chidiaq, R. (2003). *Axial Compression of Rounded Wood Poles with Carbon Fibers*. State University of New Jersey.

CSA. Design and Assessment of Building Subjected to Blast Loads. CAN/CSA Standard No. S850-12. CSA Group, Mississauga, Ontario. 2012.

CSA. (2019). Engineering design in wood. In *CSA O86*. Canadian Standards Association Group.

Custidio, J., Broughton, J., and Cruz, H. (2009). A review of factors influencing the durability of structural bonded timber joints. International Journal of Adhesives, 29:173-185.

Davids, W. G., Nagy, E., & Richie, M. C. (2008). Fatigue Behavior of Composite-Reinforced Glulam Bridge Girders. *Journal of Bridge Engineering*, *13*(2), 183–191. https://doi.org/10.1061/(ASCE)1084-0702(2008)13:2(183)

Dong, Chunxiao & Kwan, Albert & Ho, J.C.M.. (2015). Effects of confining stiffness and rupture strain on performance of FRP confined concrete. Engineering Structures. 97. 10.1016/j.engstruct.2015.03.037. Hieduschke & Haller 2010

Dorey, A. B., & Cheng, J. J. R. (1996). The behavior of GFRP glued laminated timber beams. In M. M. El-Badry (Ed.), *Adv. Comp. Mat. in Bridges and Struct. II* (pp. 787–794). The Canadian Society for Civil Engineering.

Emerson, R.N. (2004), In Situ Repair Technique for Decayed Timber Piles. ASCE Structures Congress 2004, Nashville, TN, USA.

Estrada, H. and Lee, L.S. (2014). FRP Composite Constituent Materials. In: Zoghi M (ed) The International Handbook of FRP Composites in Civil Engineering. CRC Press, New York, USA, p.32

Fitzer, E., Kleinholz, R., Tiesler, H., Stacey, M.H., et al. (2000) Fibers, 5. Synthetic Inorganic. In: Ullmann's Encyclopedia of Industrial Chemistry, Wiley-VCH Verlag GmbH & Co. KGaA, Weinheim.

Forest Products Laboratory. (2010). *Wood handbook - Wood as an engineering material* (R. J. Ross (ed.); Issue General Technical Report FPL-GTR-190,). Forest Products Laboratory, USDA Forest Service,.

Fox P., S. (1978). *Bending strength of a proposed Douglas-Fir 20f glulam stress grade* (Issue VP-X-175). Environment Canada, Canadian Forestry Service, Western Forest Products Laboratory,.

Gentile, C., Svecova, D., & Rizkalla H., S. (2002). Timber beams strengthened with GFRP bars: Development and applications. *Journal of Composites for Construction*, *6*(1), 10. https://doi.org/http://dx.doi.org/10.1061/(ASCE)1090-0268(2002)6:1(11)#sthash.phi4zCIr.dpuf

Glos, P. (1978). Reliability Theory for Timber Structures: Determination of Compression Strength Behaviour of Glulam Components from Interaction of Material Properties. *Heft 34*. Laboratorium fur den Konstrucktieven Ingenieurbau. Technical University of Munich.

Hernandez, R., Davalos F., J., Sonti, S. S., Kim, Y., & Moody C., R. (1997). *Strength and stiffness of reinforced yellow-poplar glued laminated beams* (Issue FPL-RP-554). U.S. Department of Agriculture, Forest Service, Forest Products Laboratory.

Johns, K. C., & Lacroix, S. (2000). Composite reinforcement of timber in bending. *Canadian Journal of Civil Engineering*, *27*(5), 899–906. https://doi.org/10.1139/l00-017

Kim, K. H. E., & Andrawes, B. (2016). Compression behavior of FRP strengthened bridge timber piles subjected to accelerated aging. *Construction and Building Materials*, *124*, 177–185. https://doi.org/10.1016/j.conbuildmat.2016.07.020

Lacroix, D. N. (2017). Investigating the Behaviour of Glulam Beams and Columns Subjected to Simulated Blast Loading. In Civil Engineering: Vol. Ph.D. University of Ottawa

Lacroix, D., & Doudak, G. (2018). FRP Reinforced Glulam Beams Under High Strain-Rates. *CSCE 2018 Annual Conference*.

Lacroix, D. N., & Doudak, G. (2018). Experimental and Analytical Investigation of FRP Retrofitted Glued-Laminated Beams Subjected to Simulated Blast Loading. *Journal of Structural Engineering*, *144*(7), 04018089. https://doi.org/10.1061/(ASCE)ST.1943-541X.0002084

Lacroix, D. N., & Doudak, G. (2018). Effects of High Strain Rates on the Response of Glulam Beams and Columns. Journal of Structural Engineering, 144(5), 04018029. https://doi.org/10.1061/(ASCE)ST.1943-541X.0002020

Lacroix, D., & Doudak, G. (2020). Towards enhancing the post-peak performance of glued-laminated timber beams using multi-directional fibre reinforced polymers. *Engineering Structures*, *215*, 110680. https://doi.org/10.1016/j.engstruct.2020.110680

Lam L, Teng JG. Design-Oriented Stress-Strain Model for FRP-Confined Concrete in Rectangular Columns. Journal of Reinforced Plastics and Composites. 2003;22(13):1149-1186. doi:10.1177/0731684403035429

Lee, J.-J., & Kim, G.-C. (2000). Study on the estimation of the strength properties of structural glued laminated timber I: determination of optimum MOE as input variable. *Journal of Wood Science*, *46*(2), 7. https://doi.org/10.1007/BF00777357

Lindyberg, R. F., & Dagher, H. J. (2012). ReLAM: Nonlinear Probabilistic Model for the Analysis of Reinforced Glulam Beams in Bending. *Journal of Structural Engineering*, *138*(6), 777–788. https://doi.org/doi:10.1061/(ASCE)ST.1943-541X.0000496

Lopez-Molina, A., & Doudak, G. (2019). Retrofit techniques for Cross-Laminated Timber (CLT) elements subjected to blast loads. Engineering Structures, 197, 109450. https://doi.org/10.1016/j.engstruct.2019.109450

Malhotra, S.K. and Mazur, S.J. Buckling Strength of Solid Timber Columns. *Transactions of Engineering Institute of Canada, Published in Engineering Journal, 13, No. A-4.*

Mallick, P.K. (1993) Fibre Reinforced Composites: Materials, Manufacturing and Design. 2nd Edition, Marcel Dekker Inc., New York, 74.

Mander, J. B., Priestley, M. J. N., & Park, R. (1988). Theoretical Stress‐Strain Model for Confined Concrete. *Journal of Structural Engineering*, *114*(8), 1804–1826. https://doi.org/doi:10.1061/(ASCE)0733-9445(1988)114:8(1804)

Mirmiran, A., & Shahawy, M. (1997). Behavior of concrete columns confined by fiber composites. Journal of structural engineering, 123(5), 583-590.

Moody C., R., Hernandez, R., Davalos F., J., & Sonti, S. S. (1983). *Yellow poplar glulam beam performance*. U.S. Department of Agriculture, Forest Service, Forest Products Laboratory.

Najm, H., Secaras, J., & Balaguru, P. (2007). Compression tests of circular timber column confined with carbon fibers using inorganic matrix. *Journal of Materials in Civil Engineering2*, *19*(2), 198–204.

Neely, S.T. (1898). Relation of Compression-Endwise to Breaking Load of Beam. *Progress in Timber Physics, USDA Division of Forestry*. Circular No. 18, 13-17.

Ozbakkaloglu, T., Lim, J. C., & Vincent, T. (2013). FRP-confined concrete in circular sections: Review and assessment of stress–strain models. *Engineering Structures*, *49*, 1068–1088. https://doi.org/https://doi.org/10.1016/j.engstruct.2012.06.010

Plevris, N., & Triantafillou C., T. (1992). FRP-Reinforced wood as structural Material. *Journal of Materials in Civil Engineering*, *4*(3), 18. https://doi.org/doi:10.1061/(ASCE)0899-1561(1992)4:3(300)

Plevris, N., & Triantafillou C., T. (1995). Creep behavior of FRP-Reinforced wood members. *Journal of Structural Engineering*, *121*(2), 13. https://doi.org/doi:10.1061/(ASCE)0733-9445(1995)121:2(174)

Raftery, G. M., & Harte, A. M. (2013). Nonlinear numerical modelling of FRP reinforced glued laminated timber. *Composites Part B: Engineering*, *52*, 40–50. https://doi.org/http://dx.doi.org/10.1016/j.compositesb.2013.03.038

Samaan, M., Mirmiran, A., & Shahawy, M. (1998). Model of Concrete Confined by Fiber Composites. *Journal of Structural Engineering*, *124*(9), 1025–1031. https://doi.org/10.1061/(asce)0733-9445(1998)124:9(1025)

Song, J.K., Kim, S.Y., and Oh, S.W. (2007) The Compressive Stress-Strain Relationship of Timber. In SB07 Seoul: *Proceedings of the International Conference on Sustainable Building Asia, p. 977-982*

Song, X., Tang, H., Zhang, W., & Gu, X. (2010). Compressive stress strain relationship of wood confined with fiber composite sheets. *Advanced Materials Research*, *133–134*, 1207–1211. https://doi.org/10.4028/www.scientific.net/AMR.133-134.1207

Sonti, S. S., GangaRao, H. V. S., & Superfesky, M. C. (1996). Rehabilitation and strengthening of glulam stringers for bridge superstructures. In H. Saadatmanesh & M. R. Ehsani (Eds.), *First International Conference on Composites in Infrastructures*. University of Arizona.

Teng, J. G., Chen, J. F., Smith, S. T., & Lam, L. (2002). FRP: strengthened RC structures, John Wiley and Sons, Chichester, U.K., *in press* (p. 266).

Xiong, P. (1985). Modelling strength and stiffness of glued-laminated timber using machine stress rated lumber. In *Forestry: Vol. M.A.Sc.* The University of British Columbia.

Yan, L.B., Chouw, N. and Yuan, X.W. (2012) Improving the mechanical properties of natural fiber fabric reinforced epoxy composites by alkali treatment. Journal of Reinforced Plastics and Composites, 31:425-437.

Yang, H., Liu, W., Lu, W., Zhu, S., & Geng, Q. (2016). Flexural behavior of FRP and steel reinforced glulam beams: Experimental and theoretical evaluation. *Construction and Building Materials*, *106*, 550–563. https://doi.org/http://dx.doi.org/10.1016/j.conbuildmat.2015.12.135

Zhang W, Song X, Gu X, Tang H. Compressive Behavior of Longitudinally Cracked Timber Columns retrofitted using FRP Sheets. Journal of Structural Engineering, ASCE. 2012;138(1);90-98

APPENDIX A

Detailed Results for Control Specimens

Specimen Name: C-1

Stress-Strain Curve and Group Average:

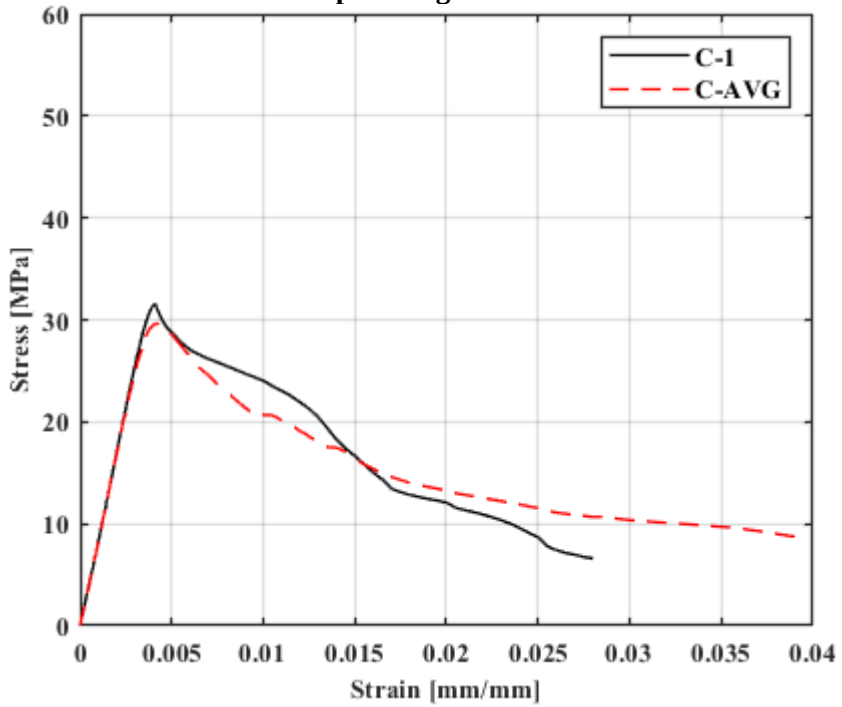

Progression of Failure and Final Damage State:


i) Prior to Test


ii) Failure Initiates


iii) Failure Propagates


iv) Damage Increases


v) Final Damage

vi) Dissected

Notes:

First observed failures were at or near knots located in the corners. Failure propagation converted local fibre crushing planar with knots to longitudinal splits parallel with knots. Separate crushing planes developed on opposing faces and seemed to connect via pre-existing shrinkage cracks. Post-test and dissection views showed that the shrinkage crack connection and a collection of small but tightly spaced knots or absorbed branches allowed total splitting between the loaded ends, therefore a splitting type of failure.

Figure A1: Detailed Information for Control Specimen C-1

Specimen Name: C-2

Stress-Strain Curve and Group Average:

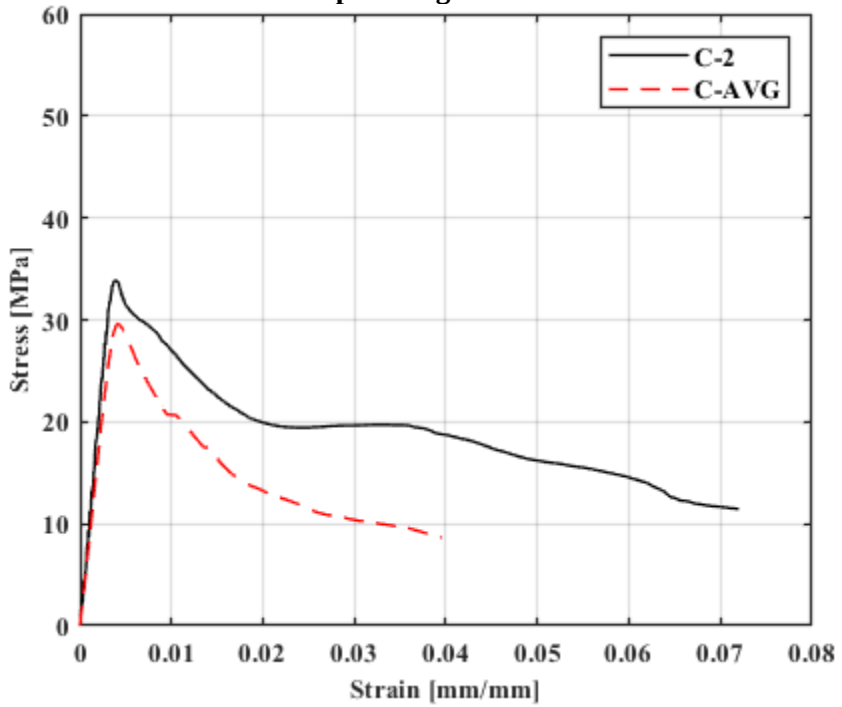

Progression of Failure and Final Damage State:

i) Prior to Test

ii) Crushing Initiates

iii) Crushing Intensifies

iv) Damage Front

v) Damage Side

vi) Dissected

Notes:

Some material missing on corners thus not rounded. The crushing plane was coincident with the greatest volume of planar knots. Failure first observed at separate corners and connecting on faces. Longitudinal crack formation was coincident with more rapid strength loss periods. As corner material began splitting off and eventually the central longitudinal crack widened the plateau behaviour was lost. Only at the highest strains did the large central split begin significantly widening as the top section split completely and rotated.

Figure A2: Detailed Information for Control Specimen C-2

Specimen Name: C-3

Stress-Strain Curve and Group Average:

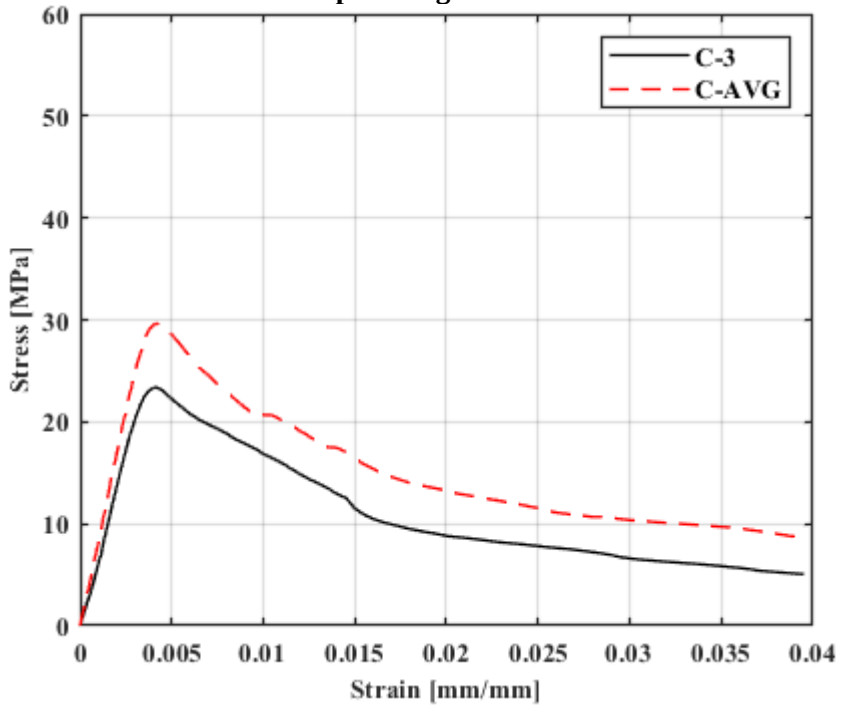

Progression of Failure and Final Damage State:

i) Prior to Test

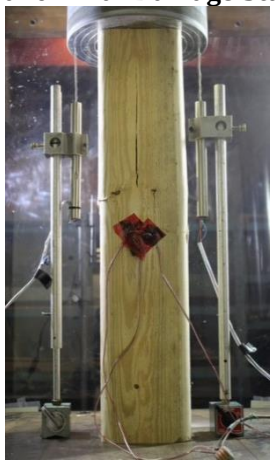

ii) Wedge Initiates

iii) Failure Propagation

iv) Damage Intensifies

v) Final Damage Side

vi) Dissected

Notes:

A planar arrangement of knots was correctly predicted to control failure behaviour. Even by 0.011 mm/mm strain a longitudinal crack had formed at the corner and widened significantly by 0.016 mm/mm. After the longitudinal splits spanned from rupture plane to end, the majority of strength losses had taken place, losses were lower thereafter.

Figure A3: Detailed Information for Control Specimen C-3

Specimen Name: C-4

Stress-Strain Curve and Group Average:

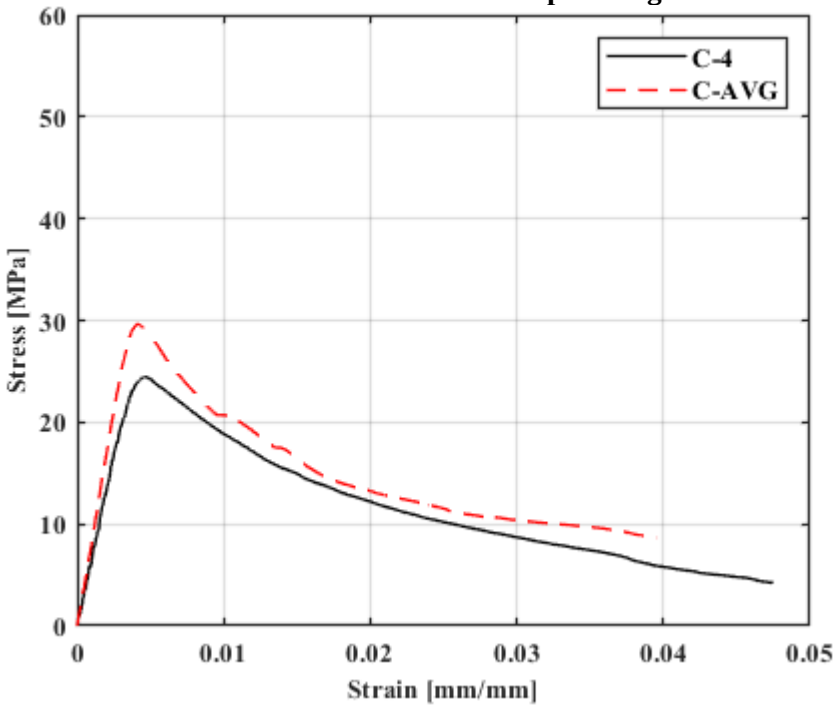

Progression of Failure and Final Damage State:

i) Prior to Test

ii) Initial Crushing

iii) Splits Widen

iv) Damage Intensifies

v) Side View Damage

vi) Dissected

Notes:

Significant torsion was observed. The specimen appeared to fail by splitting in multiple directions, in one orientation the wedge-split seen in the left of the dissected view and in the orthogonal orientation the right side of the dissected view buckled away and split off the left side, resulting in a total section loss of almost ¼ at the corner as seen in iv) at right. Splitting-dominant failure behaviour was apparent immediately and propagated to end of test.

Figure A4: Detailed Information for Control Specimen C-4

Specimen Name: C-5

Stress-Strain Curve and Group Average:

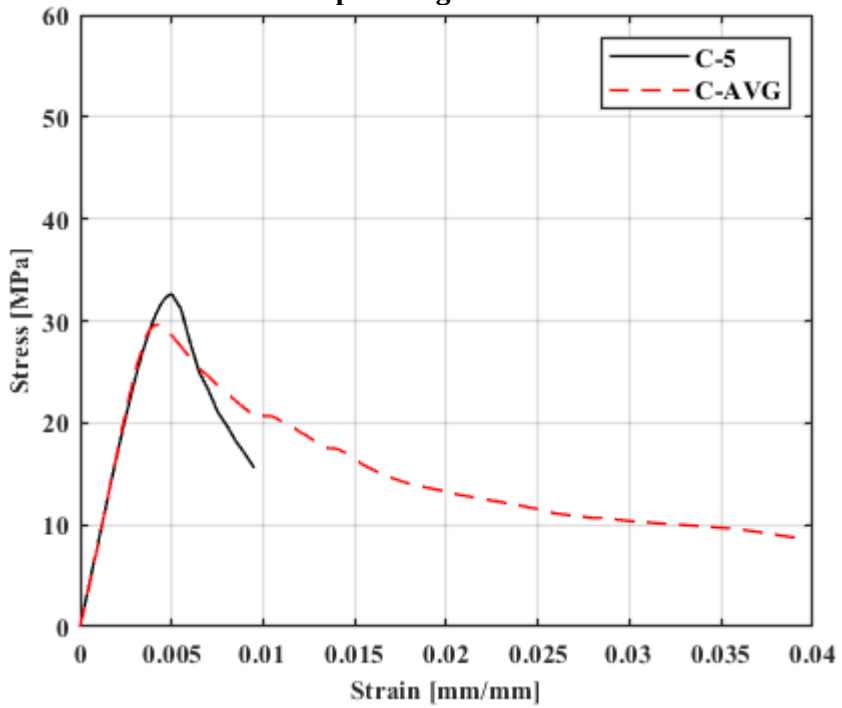

Progression of Failure and Final Damage State:

i) Prior to Test

ii) Face Splitting Off

iii) Splits Forming

iv) Final Damage

v) End Grain Damage

vi) Dissected

Notes:

The immediate initial failure was as a crushing plane very near the top loaded endgrain, as a consequence of multiple knots. Shortly after crushing had initiated, multiple longitudinal splits propagated away from the loaded end down the specimen several centimetres. On the extreme faces portions of the perimeter were seen buckling away and appeared to be disconnected by splits. The damage is most visible in the failed end-grain showing complete cross-section splits from the pith to the extreme faces as shown in v). Deemed unstable.

Figure A5: Detailed Information for Control Specimen C-5

Specimen Name: C-6

Stress-Strain Curve and Group Average:

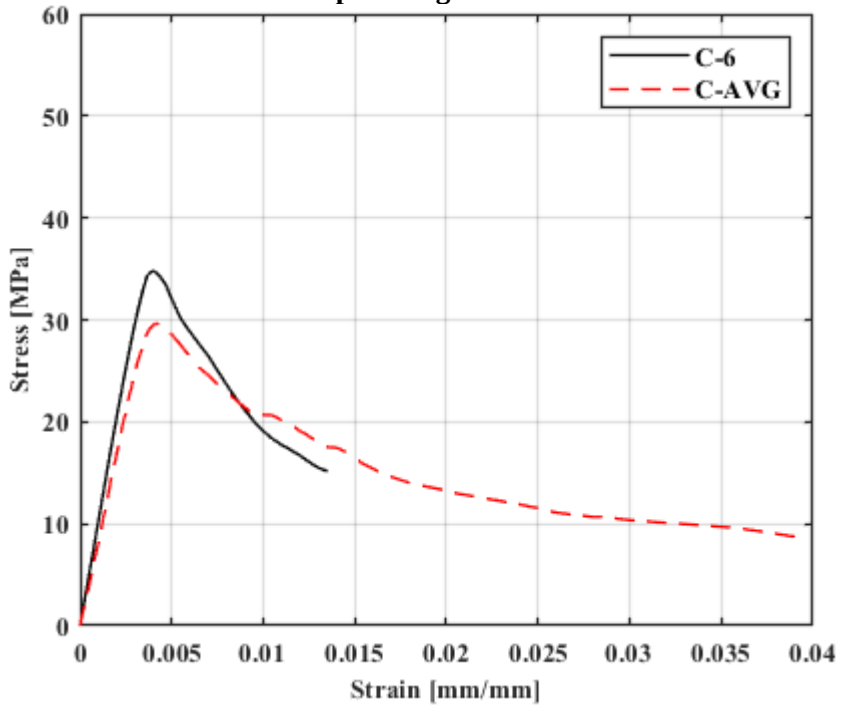

Progression of Failure and Final Damage State:


i) Prior to Test


ii) Initial Crushing


iii) Failure Redirection


iv) Front View Damage


v) Side View Damage


vi) Dissected

Notes:

It would be impossible to predict from external inspection whether failure would be planar with one or the other collection of knots; ultimately longitudinal splits were seen to pass through knots in both planar groups by end of test as shown in iv) and v). The crushing plane failure was dramatically reoriented by the knot on the front face as shown in ii) and iii). A section of the split material began slipping and buckling as cracks spanned from rupture to loaded end.

Figure A6: Detailed Information for Control Specimen C-6

APPENDIX B

Detailed Results for Reinforced Specimen

Specimen Name: U–1

Stress-Strain Curve:

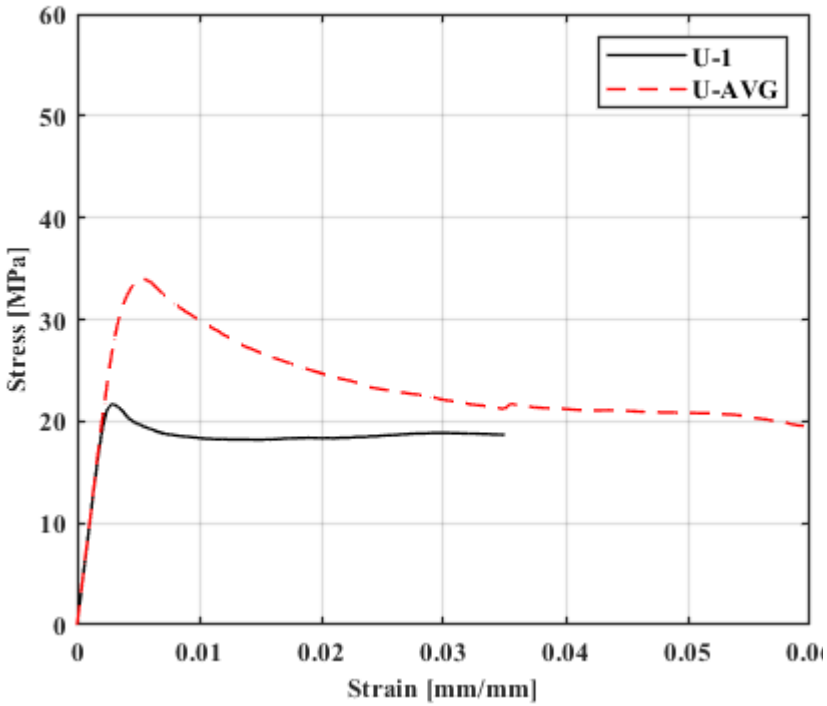

Progression of Failure and Final Damage:

i) Prior to Test

ii) Wood Crushing

iii) Damage Propagation

iv) Final Damage

v) FRP Removed

vi) Dissected

Notes:

One of the first tested, test ended prematurely as behaviour had become constant and extreme strains were not yet identified. Crushing plane extremely flat, the presence of the central knot initiates a longitudinal split as seen in the dissected view; similar to control wedge split Failures, but the crack has been arrested by FRP. Similarly lateral displacements are visibly very small for the extreme buckling fibres or shear slippage of the plane.

Figure B1: Detailed Information for Reinforced Specimen U-1

Specimen Name: U–2

Stress-Strain Curve:

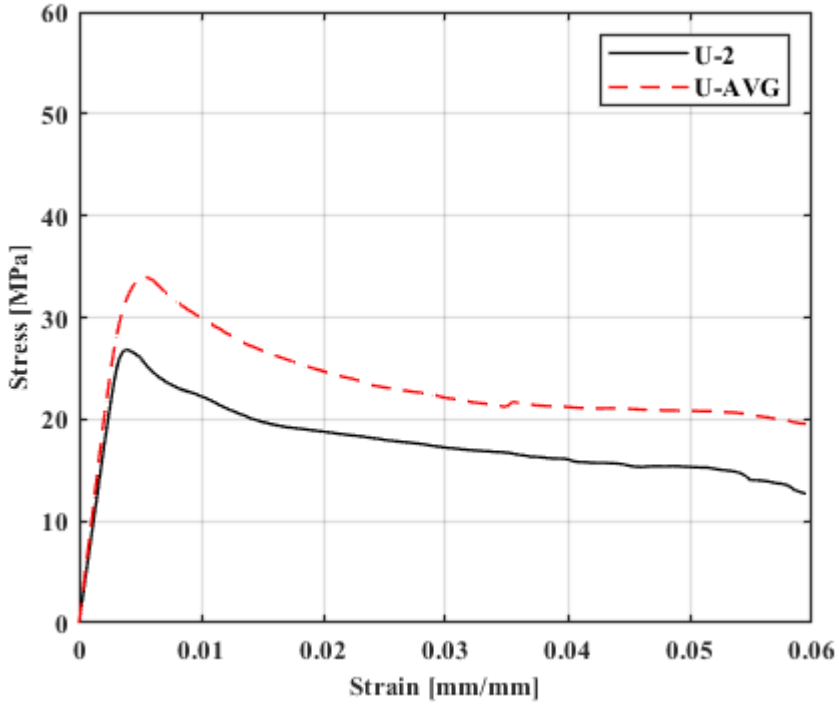

Progression of Failure and Final Damage:

i) Prior to Test

ii) Wood Rupture, Fibre Wrinkling

iii) Propagation, Fibre Rupture

iv) Final Damage

v) FRP Removed

vi) Dissected

Notes:

Externally, Failure plane is adjacent or tangential to a large knot, appears similar to combined crushing and parallel shear. In dissected view, a grain weakness along the pith is apparent within the angled shearing plane. Fibres ruptured only very near the end of the test, prior to which only wrinkling and debonding was seen. Major fibre rupture correlates to the small downturn of stress-strain behaviour seen between 0.05 and 0.06 mm/mm.

Figure B2: Detailed Information for Reinforced Specimen U–2

Specimen Name: U–3

Stress-Strain Curve:

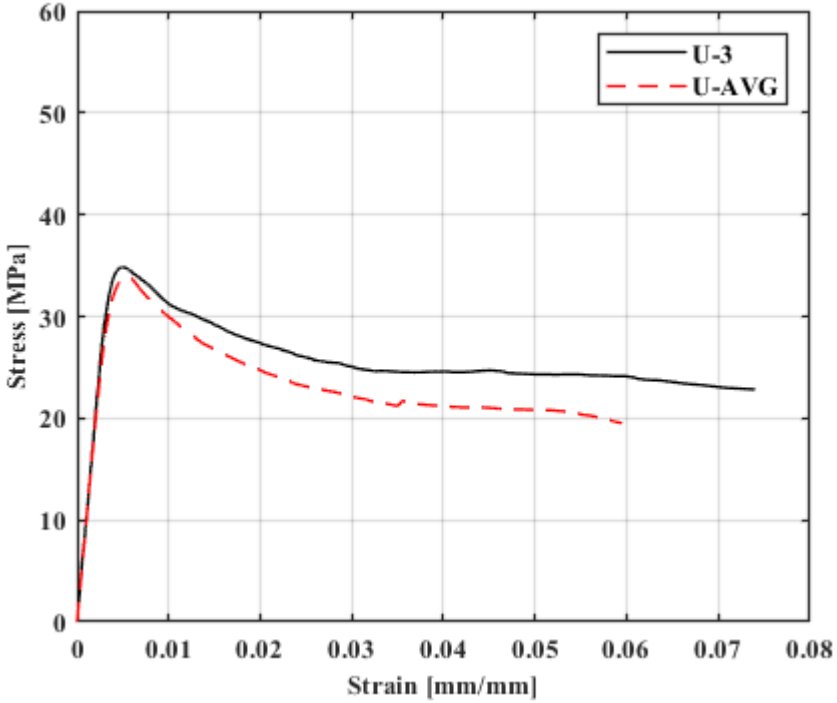

Progression of Failure and Final Damage:

i) Prior to Test

ii) Wood Rupture

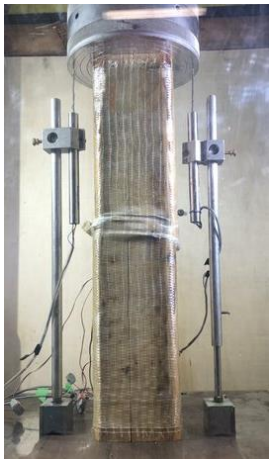

iii) Fibre Rupture

iv) Final Damage

v) FRP Removed

vi) Dissected

Notes:

The specimen ends were not perfectly coplanar, resulting in an initial small gap at loaded end, which was eliminated prior to test start. Visibly, multiple crushing points developed near one another at collections of knots. Fibre rupture followed shortly after, fibre rupture at the rupture plane took place at ~0.025 mm/mm strain. Relatively flat pure crushing plane.

Figure B3: Detailed Information for Reinforced Specimen U–3

Specimen Name: U–4

Stress-Strain Curve:

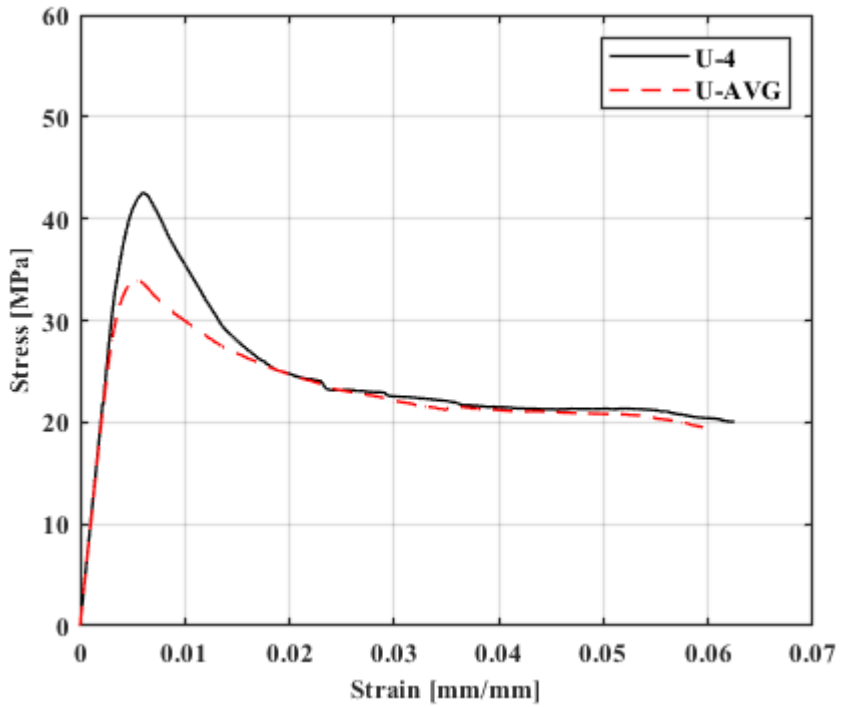

Notes:

Progression of Failure and Final Damage:

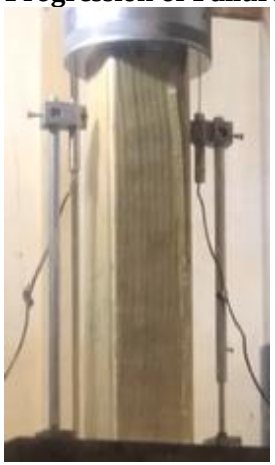

i) Prior to Test

ii) Wood Failure

iii) Failure Progression

iv) Final Damage

v) FRP Removed

vi) Dissected

Figure B4: Detailed Information for Reinforced Specimen U–4

Specimen Name: U–5

Stress-Strain Curve:

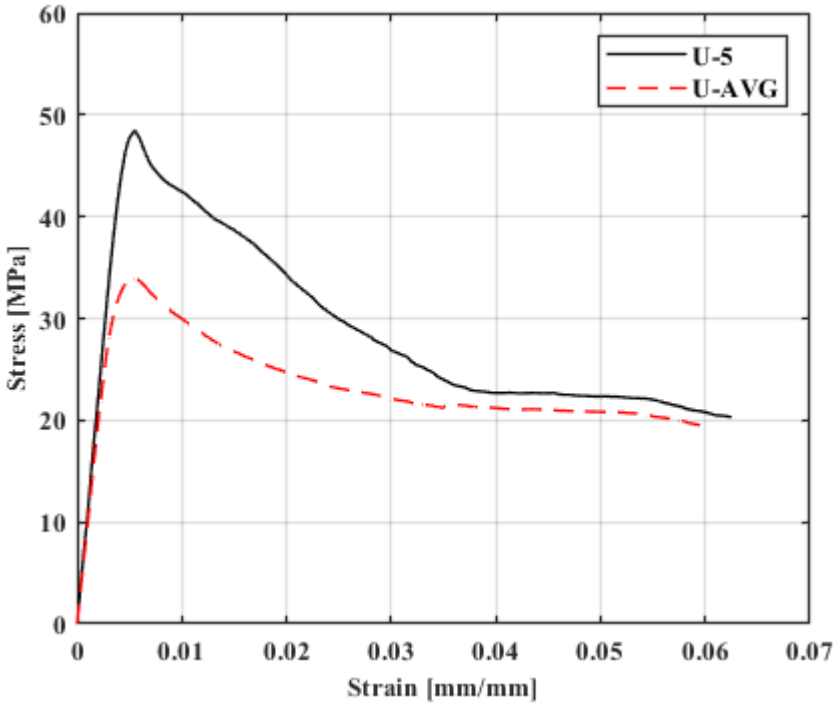

Progression of Failure and Final Damage:

i) Prior to Test

ii) Initial Crushing

iii) Failure Propagation

iv) Final Damage

v) FRP Removed

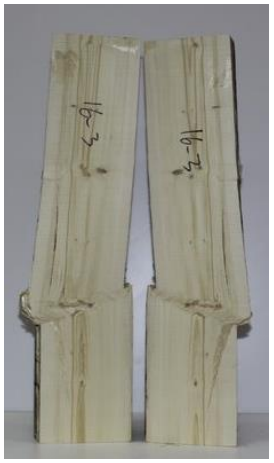

vi) Dissected

Notes:

Fibre rupture in the hoop orientation occurred at ~ 0.04 mm/mm strain. The slanted crushing plane developed coincident with some cross-grain effects visible in the dissected view. As the intact sections slid past one another following the slant, they rotated in the plane of the dissected grain and in torsion between the ends. Effectively the continuous deformation was lopsided densification and twisting of the crushed fibre plane.

Figure B5: Detailed Information for Reinforced Specimen U–5

Specimen Name: U_3–1

Stress-Strain Curve:

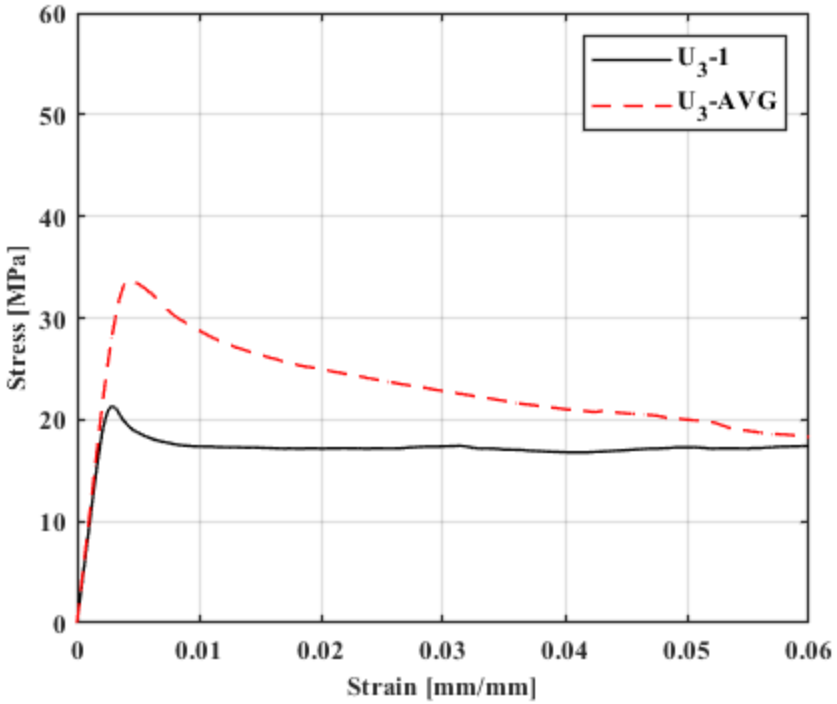

Progression of Failure and Final Damage:

i) Prior to Test

ii) Fibre Wrinkling

iii) Fibre Rupture

iv) Final Damage

v) FRP Removed

vi) Dissected

Notes:

Very straightforward specimen, low strength is likely a function of the weak cross-section with central defect in line with the pith. Following immediate failure, plateau stress lasted until end of test without any indication of further behaviour. Dissected view demonstrates the progressive buckling angle from pith to extreme faces of crushed fibres. Fibre rupture did not take place until very high vertical strain, behaviour was identical after fibre rupture.

Figure B6: Detailed Information for Reinforced Specimen U_3–1

Specimen Name: U_3–2

Stress-Strain Curve:

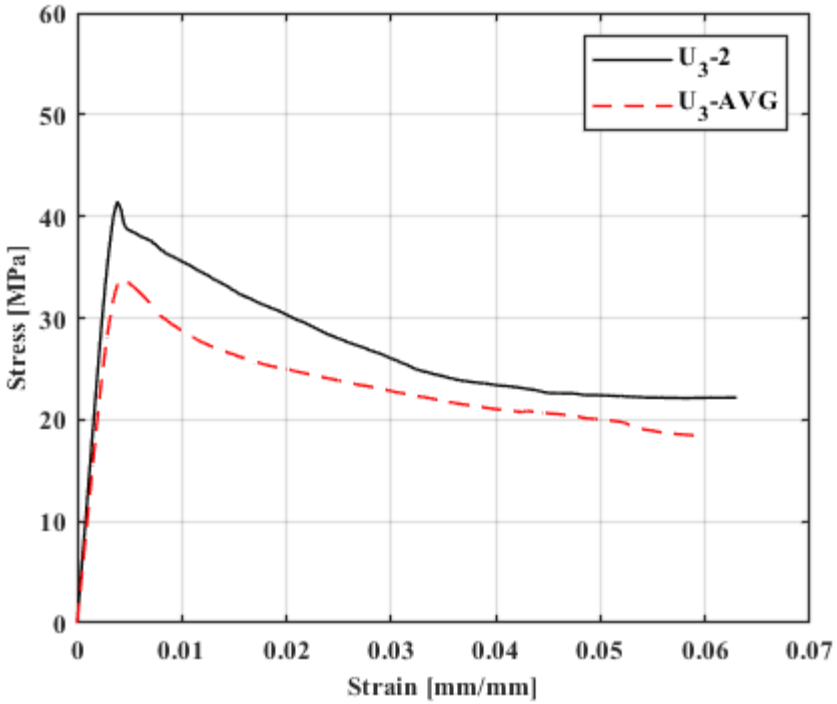

Notes:

Combined crushing and parallel-to-grain shear failure; the crushing behaviour appears to be coincident with an angled knot defect in the dissected view, while externally large knots are placed on the angled rupture plane in the side view. The parallel-to-grain shear portion of failure can be seen in the dissected view and is very short. Fibre rupture was not evident in final damage state.

Progression of Failure and Final Damage:

i) Prior to Test

ii) Fibre Wrinkling

iii) Final Damage 1

iv) Final Damage 2

v) FRP Removed

vi) Dissected

Figure B7: Detailed Information for Reinforced Specimen U_3–2

Specimen Name: U_3–3

Stress-Strain Curve:

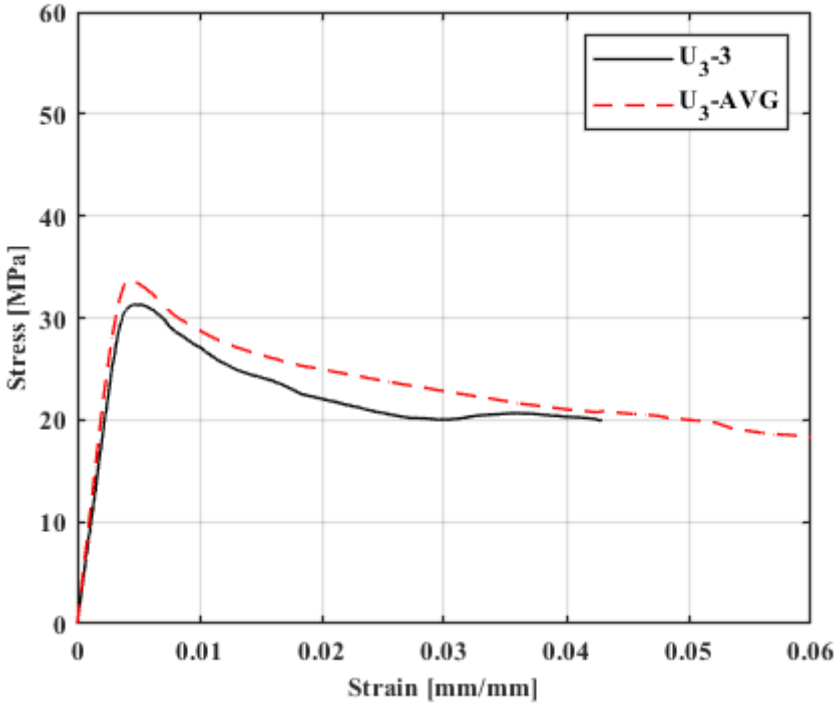

Notes:

Oval-shaped defects oriented perpendicular to grain apparently controlled failure very near the bottom loaded end. As a result, the vertical strain took place in the 25 mm clear distance from the end to the start of FRP wrap. Up to 0.03 mm/mm, test was proceeding normally, at 0.03 mm/mm the FRP was in contact with the platen, resulting in a brief apparent increase in strength. Test was ended shortly afterward. Crushing type failure.

Progression of Failure and Final Damage:

i) Prior to Test

ii)

iii)

iv) Final Damage

v) FRP Removed (flipped)

vi) Dissected

Figure B8: Detailed Information for Reinforced Specimen U_3–3

Specimen Name: U_3–4

Stress-Strain Curve:

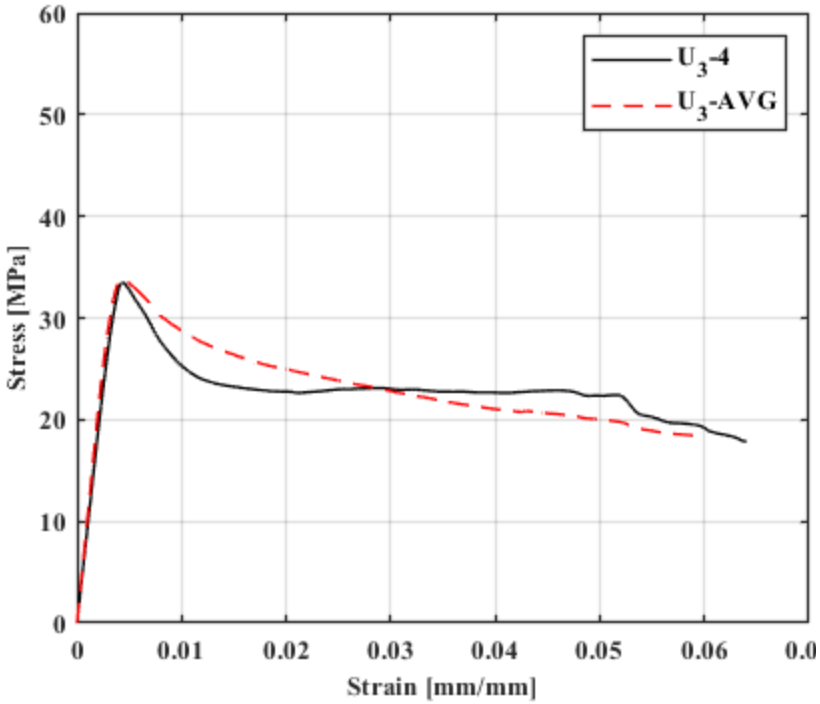

Notes:

The stress-strain and top row of photos presented correlate, following reaching the limits of LVDTs, the specimen was pushed further to ultimate strains of 0.25 mm/m. It was observed from 0.05 mm/mm onward the strength fell sporadically, ultimate strength 5 MPa. This stress-strain data is not pertinent to the study at hand, but picture of the final damage state is presented at right. Shearing failure.

Progression of Failure and Final Damage:

i) Prior to Test

ii) Crushing Initiation

iii) Fibre Rupture

iv) Final Damage at 0.065 mm/mm

v) Extremely High Strain Damage

vi) FRP Removed 0.25 mm/mm Strain Damage

Figure B9: Detailed Information for Reinforced Specimen U_3–4

Specimen Name: U_3–5

Stress-Strain Curve:

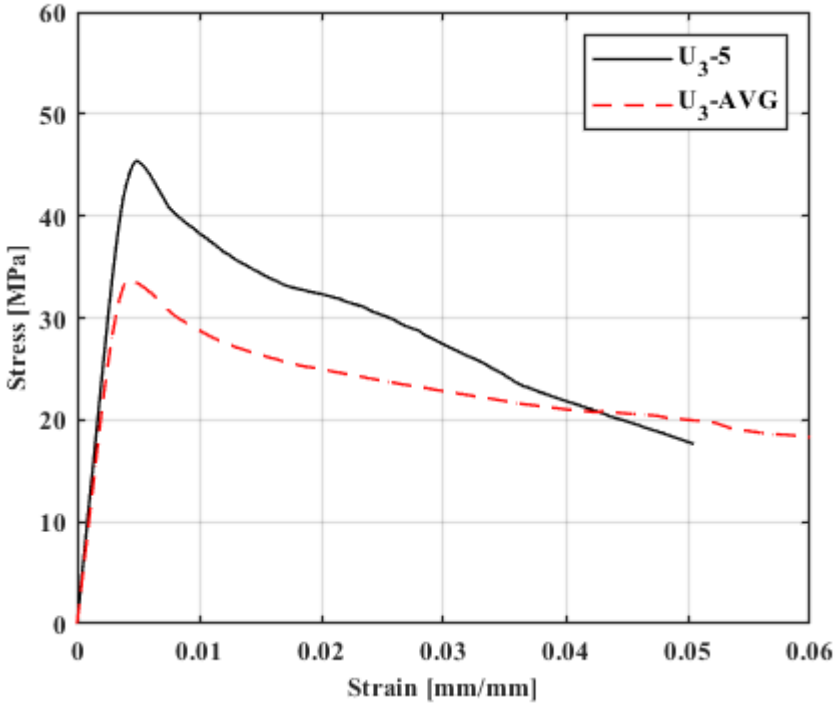

Progression of Failure and Final Damage:

i) Prior to Test

ii) Crushing Planes

iii) 0.05 mm/mm strain

iv) Final Damage at 0.13 mm/mm strain

v) FRP Removed

vi) Dissected

Notes:

As with U_3–4, pushed to extreme strains reaching ultimate of 0.13 mm/mm end behaviour had plateau of ultimate strength of 5 MPa. Data beyond what LVDTs recorded is not shown above, but final damage states are provided at right. Multiple crushing planes formed allowing for global kinking. In essence a crushing failure mode, however the global behaviour may not be well classified by any of the established types in ASTM.

Figure B10: Detailed Information for Reinforced Specimen U_3–5

Specimen Name: X–1

Stress-Strain Curve:

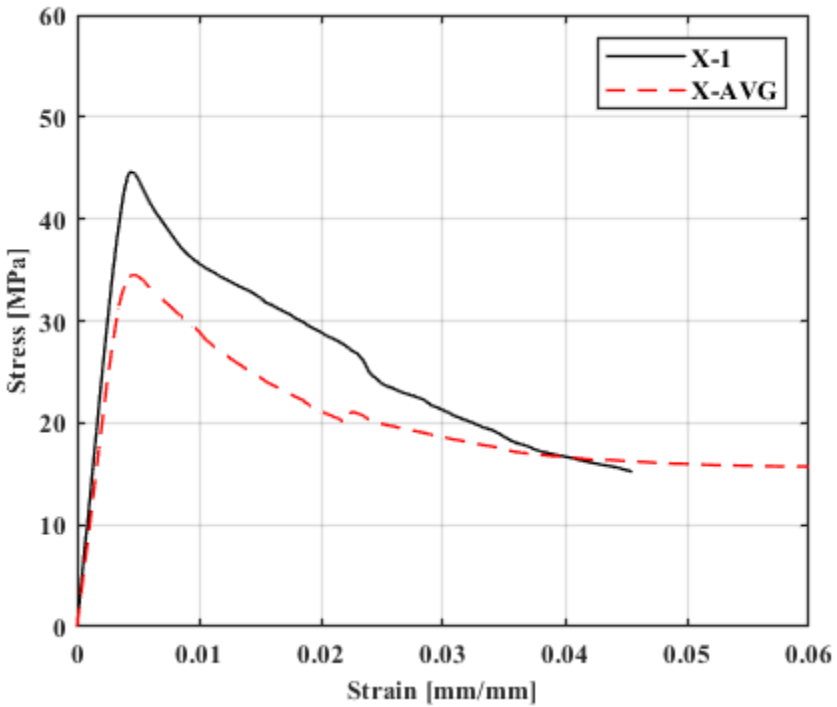

Notes:

Multiple crushing planes developed in separate locations, each in line with defects as seen in unwrapped view. Secondary crushing plane near loaded end was less affected by present FRP. Fibre ruptures were partly contained or mitigated by the orthogonal fabric layer.

Progression of Failure and Final Damage:

i) Prior to Test

ii) Initial Crushing

iii) Failure Propagation

iv) Final Damage

v) FRP Removed

vi) Dissected

Figure B11: Detailed Information for Reinforced Specimen X–1

Specimen Name: X–2

Stress-Strain Curve:

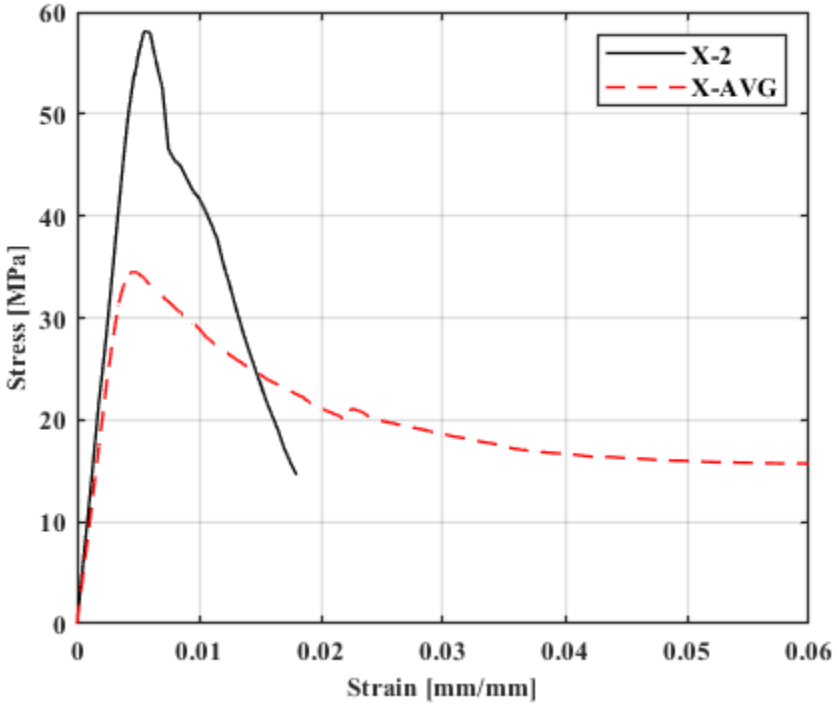

Progression of Failure and Final Damage:

i) Prior to Test

ii) Crushing Initiates

iii)

iv) Final Damage

v) FRP Removed

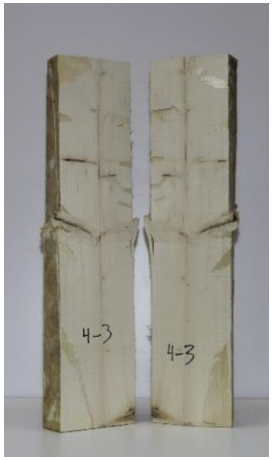

vi) Dissected

Notes:

Specimen had extremely high strength, likely a function of consistent grain and central pith. However, specimen showed no strength retention and extremely low ductility. Fairly significant torsion between the specimen ends as seen in FRP removed view, possibly the deformation behaviour involved very little buckling/bulging but more exclusively rotation on the crushing plane such that intact FRP away from rupture wasn't critical.

Figure B12: Detailed Information for Reinforced Specimen X–2

Specimen Name: X–3

Stress-Strain Curve:

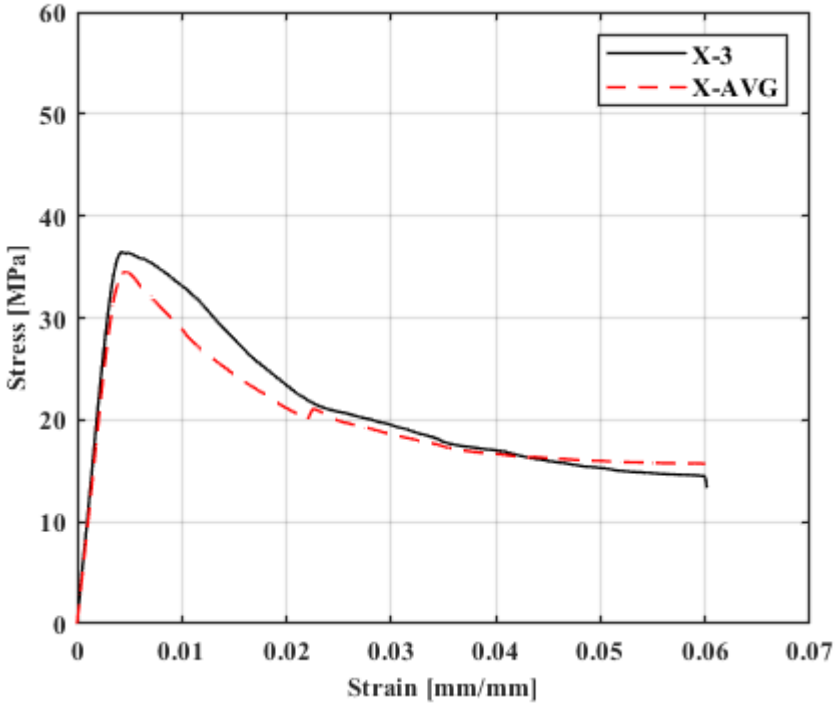

Notes:

Ultimately classified as a crushing failure; a shear failure mode is arguable except for the wedge-shaped section seen in the dissected view.

Progression of Failure and Final Damage:

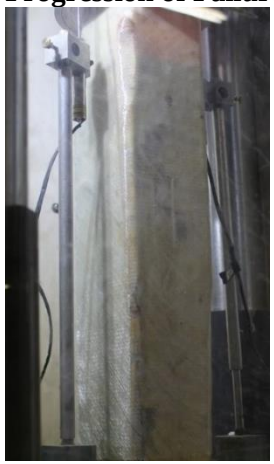

i) Prior to Test

ii) Initial Failure

iii) Damage Amplification

iv) Final Damage

v) FRP Removed

vi) Dissected

Figure B13: Detailed Information for Reinforced Specimen X–3

Specimen Name: X–4

Stress-Strain Curve:

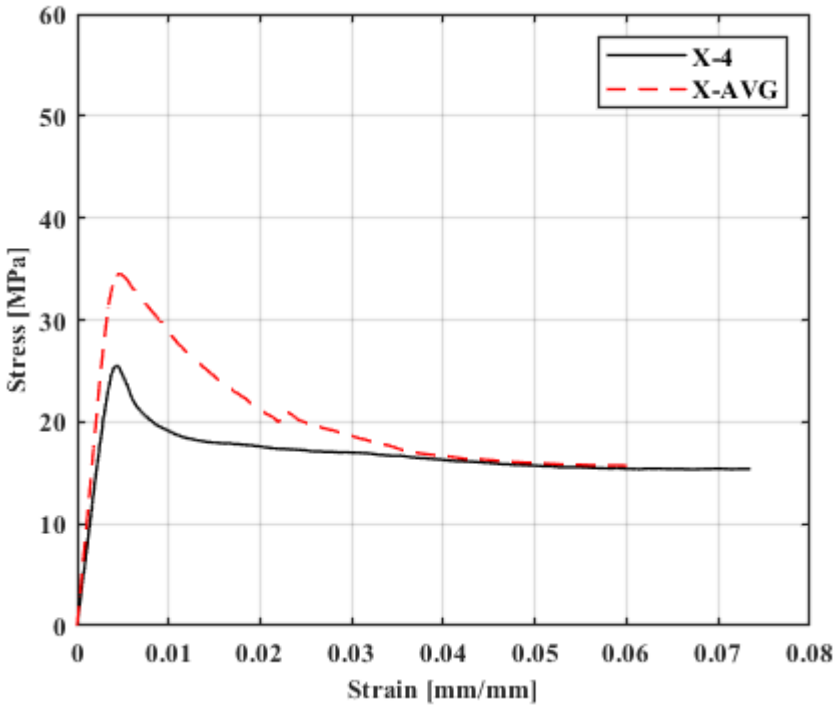

Progression of Failure and Final Damage:

i) Prior to Test

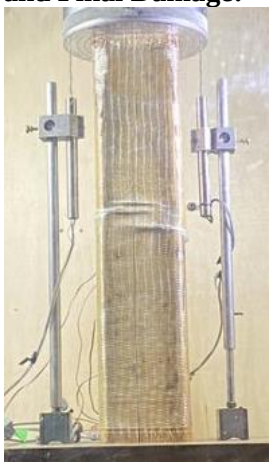

ii) Failure Initiates

iii) Fibre Rupture

iv) Final Damage

v) FRP Removed

vi) Dissected

Notes:

Figure B14: Detailed Information for Reinforced Specimen X–4

Specimen Name: X–5

Stress-Strain Curve:

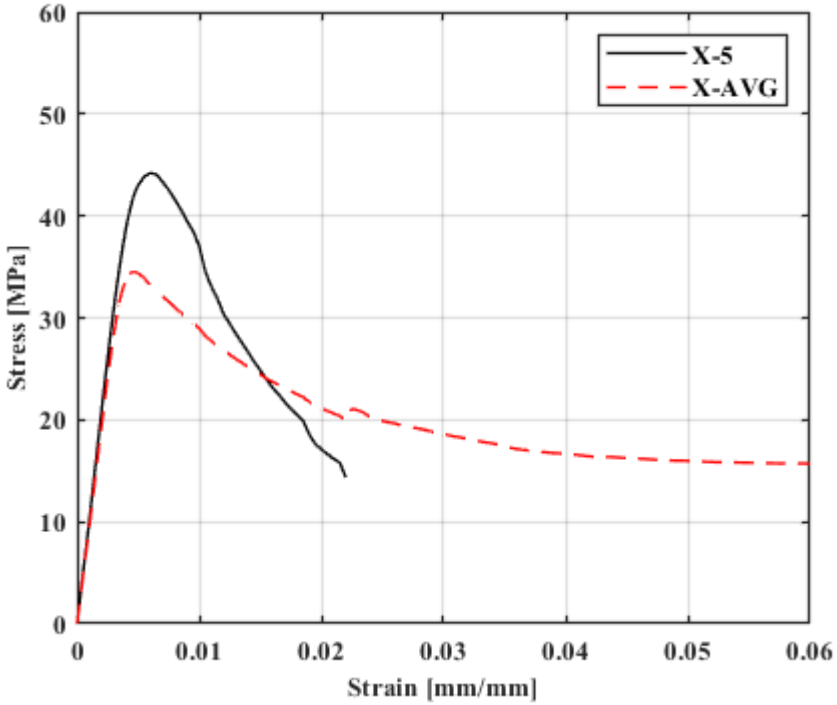

Progression of Failure and Final Damage:

i) Prior to Test

ii)

iii)

iv) Final Damage

v) FRP Removed

vi) Dissected

Notes:

Figure B15: Detailed Information for Reinforced Specimen X–5

Specimen Name: X_3–1

Stress-Strain Curve:

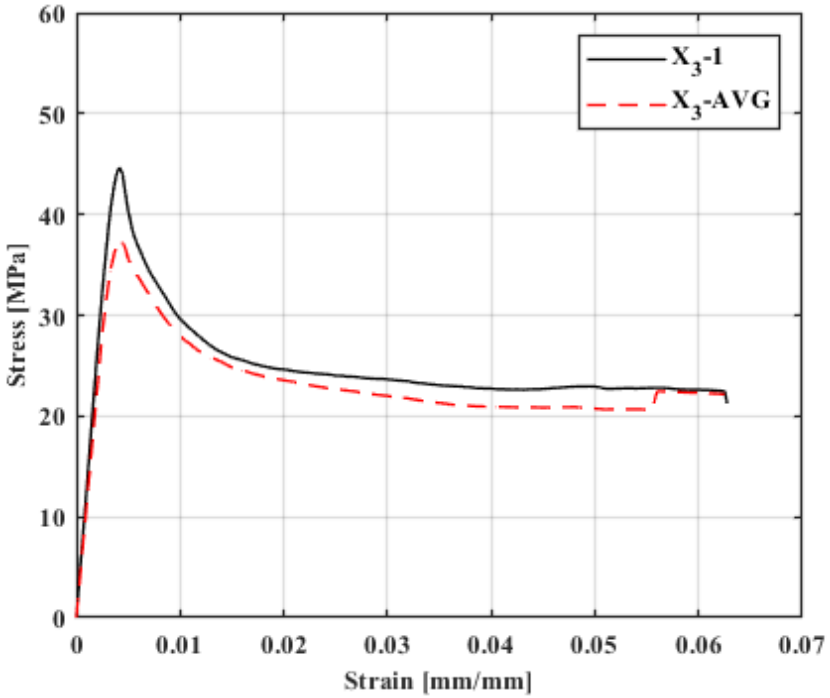

Notes:

Progression of Failure and Final Damage:

i) Prior to Test

ii) Failure Initiates

iii) Failure Propagates

iv) Final Damage

v) FRP Removed

vi) Dissected

Figure B16: Detailed Information for Reinforced Specimen X_3–1

Specimen Name: X_3–2

Stress-Strain Curve:

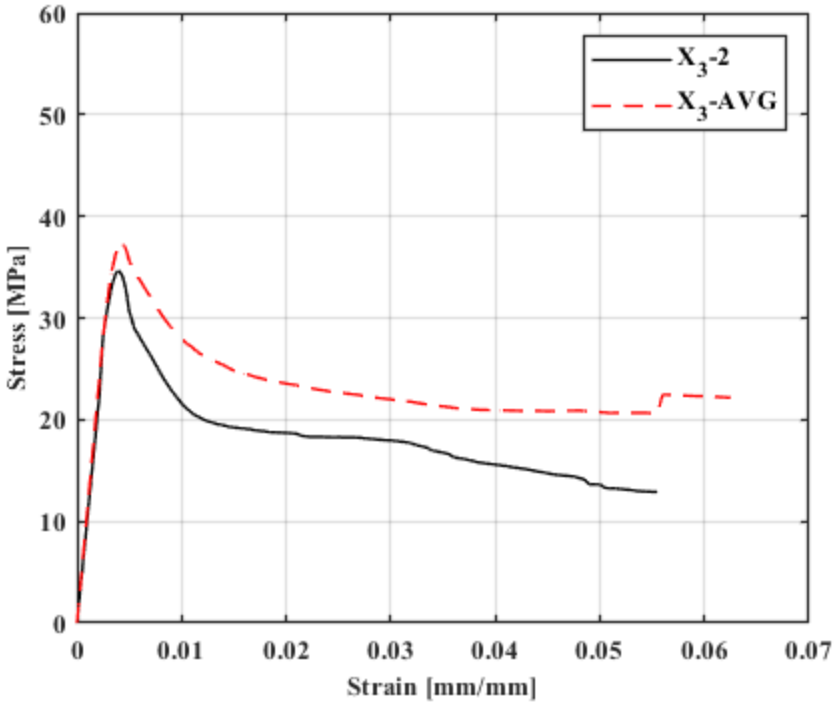

Progression of Failure and Final Damage:

i) FRP Removed

ii) Dissected

Notes:

Photo documentation of this specimen during testing procedures has been lost. Failure was at the bottom end-grain by crushing, leading to eventual fibre rollover at higher strain.

Figure B17: Detailed Information for Reinforced Specimen X_3–2

Specimen Name: X_3–3

Stress-Strain Curve:

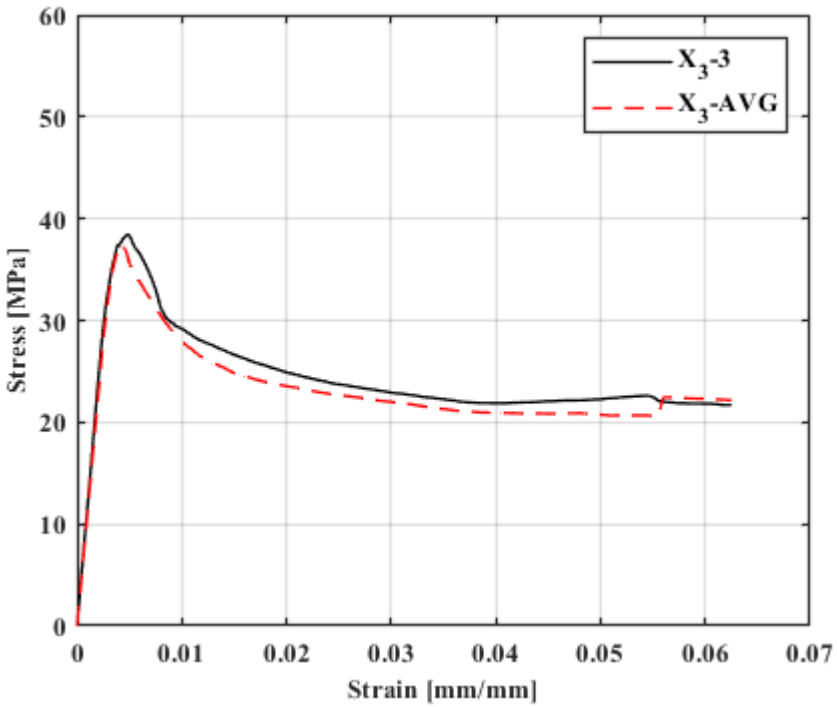

Progression of Failure and Final Damage:

i) Prior to Test

ii) Crushing Plane

iii) Failure Propagation

iv) Final Damage

v) FRP Removed

vi) Dissected

Notes:

Several large defects were present in the material; initially failure was controlled at mid-height by force redirection about a knot. Further into the test a second crushing plane developed as a consequence of the parallel-to-grain shear possible within the cross-section due to a weak grain arrangement. FRP did not rupture by end of test. Failure mode of combined crushing and parallel-to-grain shear.

Figure B18: Detailed Information for Reinforced Specimen X_3–3

Specimen Name: X_3–4

Stress-Strain Curve:

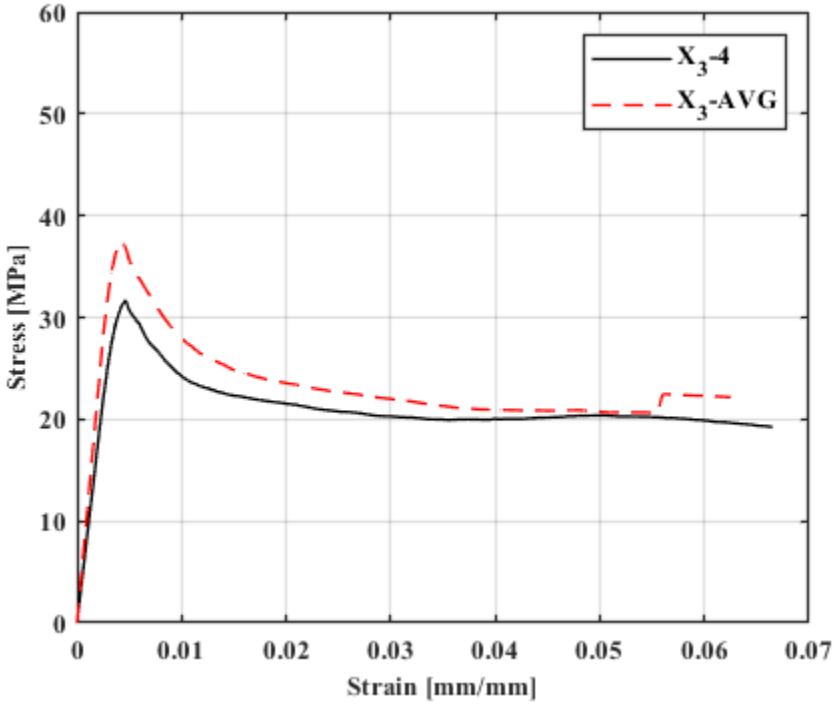

Notes:

Progression of Failure and Final Damage:

i) Prior to Test

ii) Crushing Initiates

iii)

iv) Final Damage

v) FRP Removed

vi) Dissected

Figure B19: Detailed Information for Reinforced Specimen X_3–4

Specimen Name: X_3–5

Stress-Strain Curve:

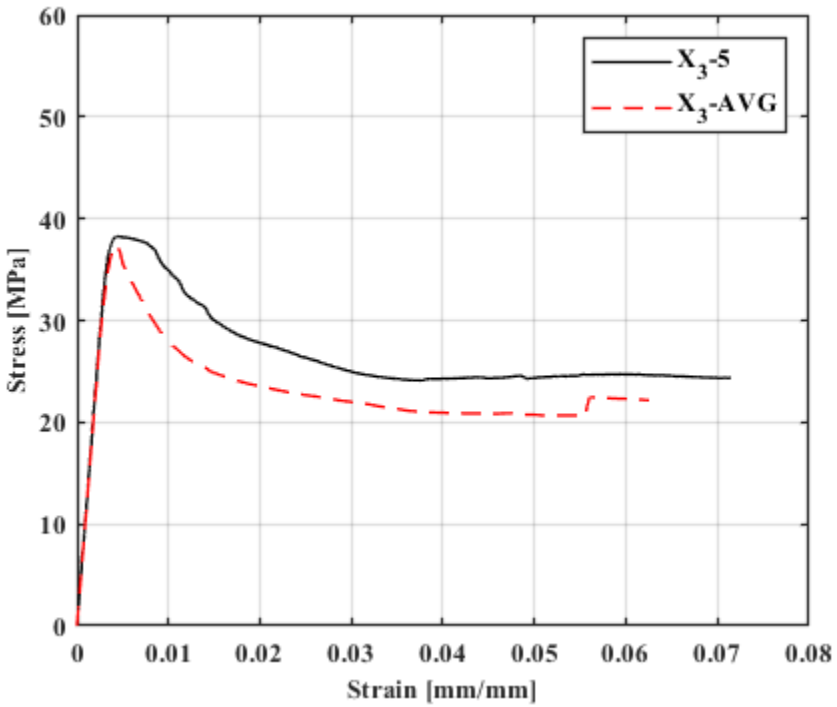

Progression of Failure and Final Damage:

i) Prior to Test

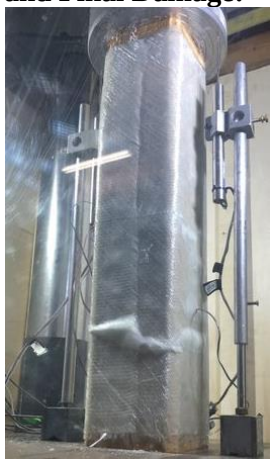

ii) Failure Initiation

iii) Damage Amplification

iv) Final Damage

v) FRP Removed

vi) Dissected

Notes:

Figure B20: Detailed Information for Reinforced Specimen X_3–5

Specimen Name: B–1

Stress-Strain Curve:

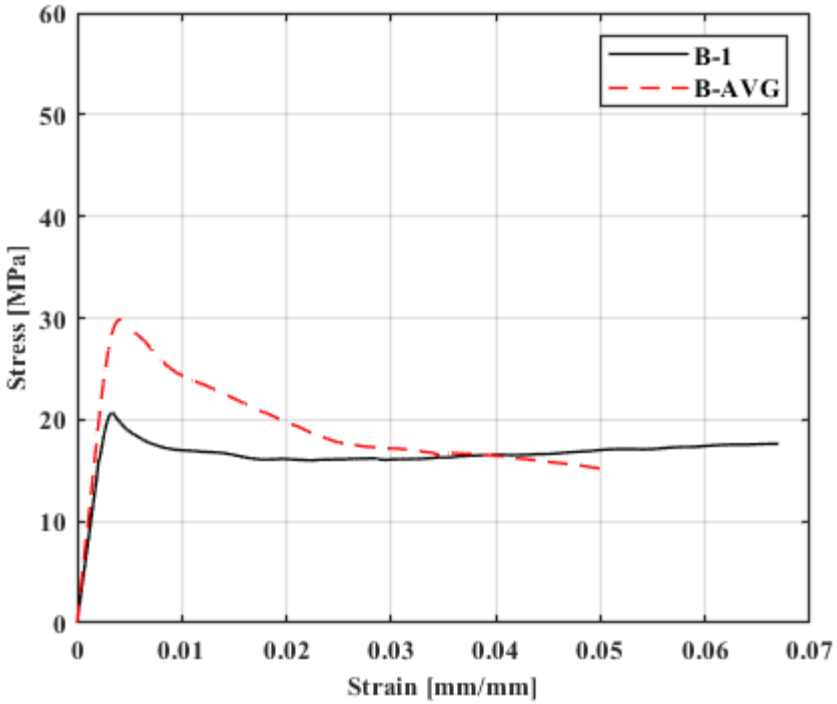

Notes:

Progression of Failure and Final Damage:

i) Prior to Test

ii) Failure Plane

iii) Fibre Rupture

iv) Final Damage

v) FRP Removed

vi) Dissected

Figure B21: Detailed Information for Reinforced Specimen B–1

Specimen Name: B–2

Stress-Strain Curve:

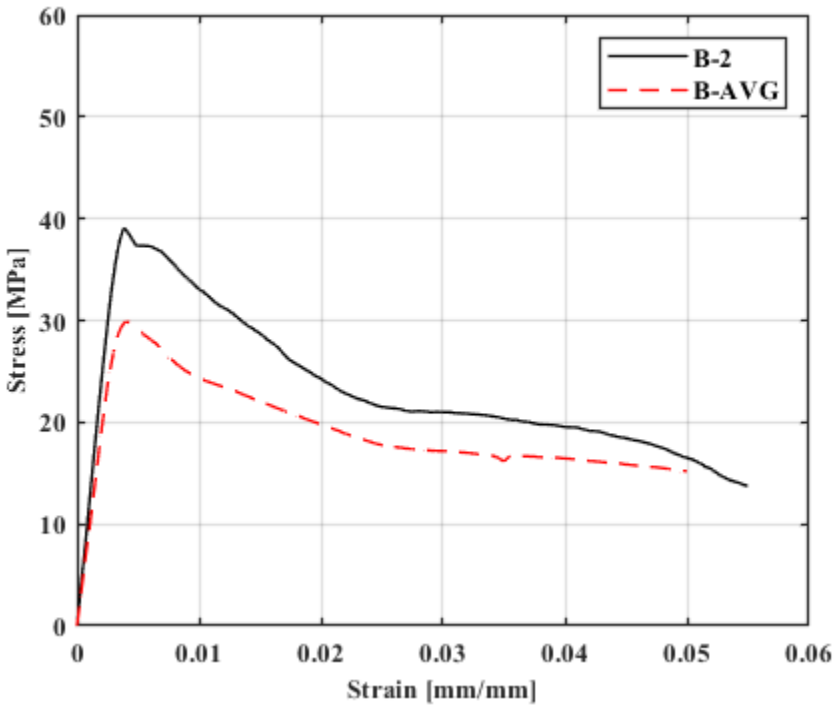

Progression of Failure and Final Damage:

i) Prior to Test

ii) Failure Initiation

iii) Fibre Rupture

iv) Final Damage

v) FRP Removed

vi) Dissected

Notes:

Figure B22: Detailed Information for Reinforced Specimen B–2

Specimen Name: B–3

Stress-Strain Curve:

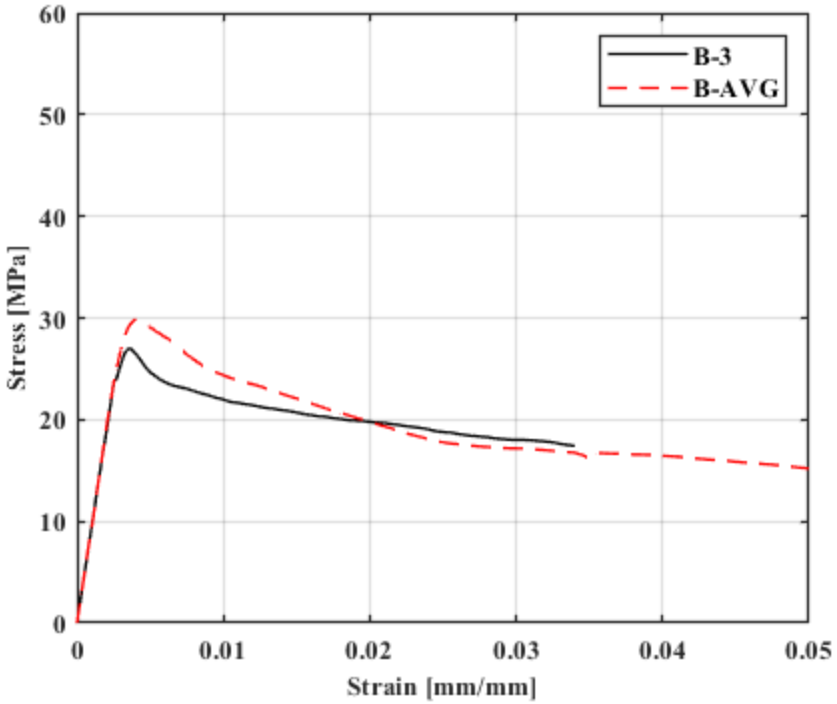

Progression of Failure and Final Damage:

i) Prior to Test

ii)

iii)

iv) Final Damage

v) FRP Removed

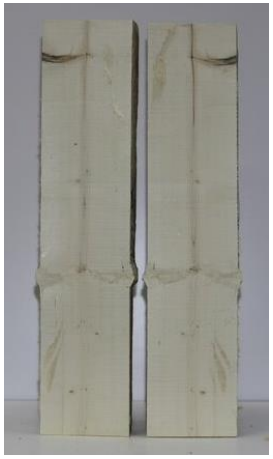

vi) Dissected

Notes:

Figure B23: Detailed Information for Reinforced Specimen B–3

Specimen Name: B–4

Stress-Strain Curve:

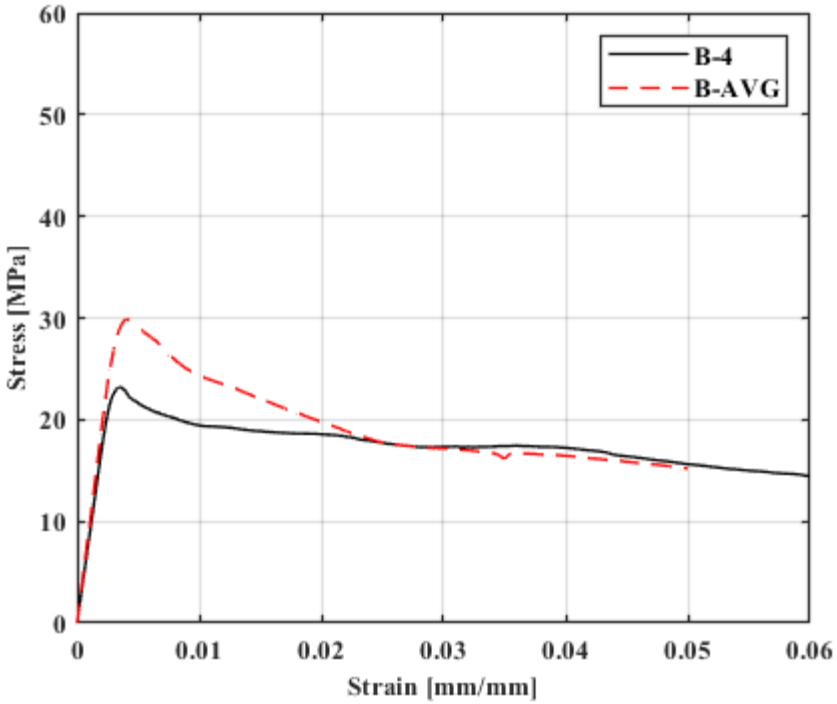

Notes:

Progression of Failure and Final Damage:

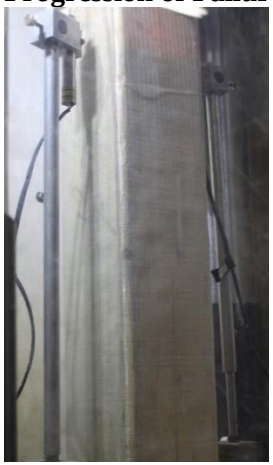

i) Prior to Test

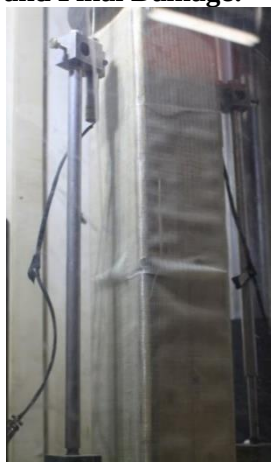

ii) Wood Failure

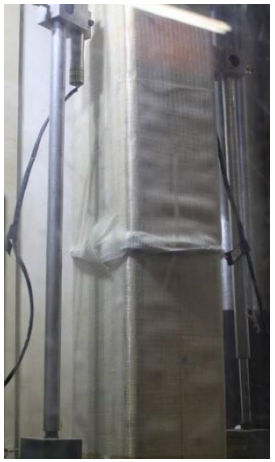

iii) FRP Failure

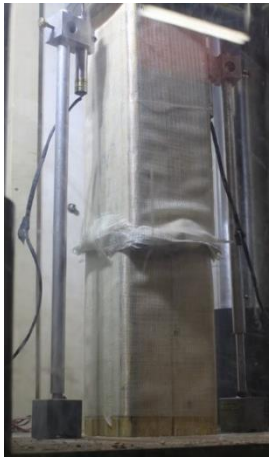

iv) Final Damage

v) FRP Removed

vi) Dissected

Figure B24: Detailed Information for Reinforced Specimen B–4

Specimen Name: B–5

Stress-Strain Curve:

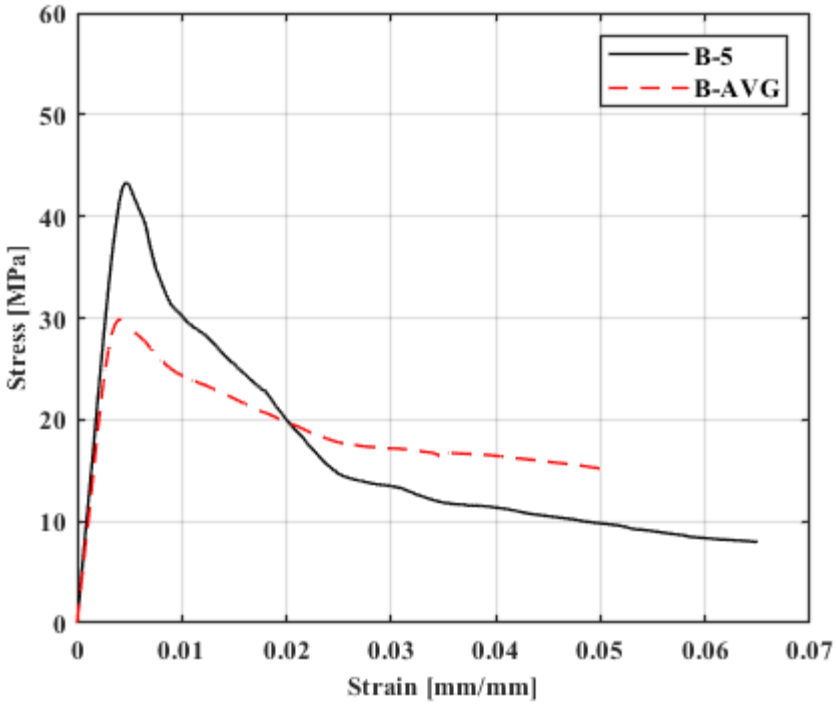

Notes:

Progression of Failure and Final Damage:

i) Prior to Test

ii) Failure Initiation

iii) Damage Amplification

iv) Final Damage

v) FRP Removed

vi) Dissected

Figure B25: Detailed Information for Reinforced Specimen B–5

Specimen Name: B_3–1

Stress-Strain Curve:

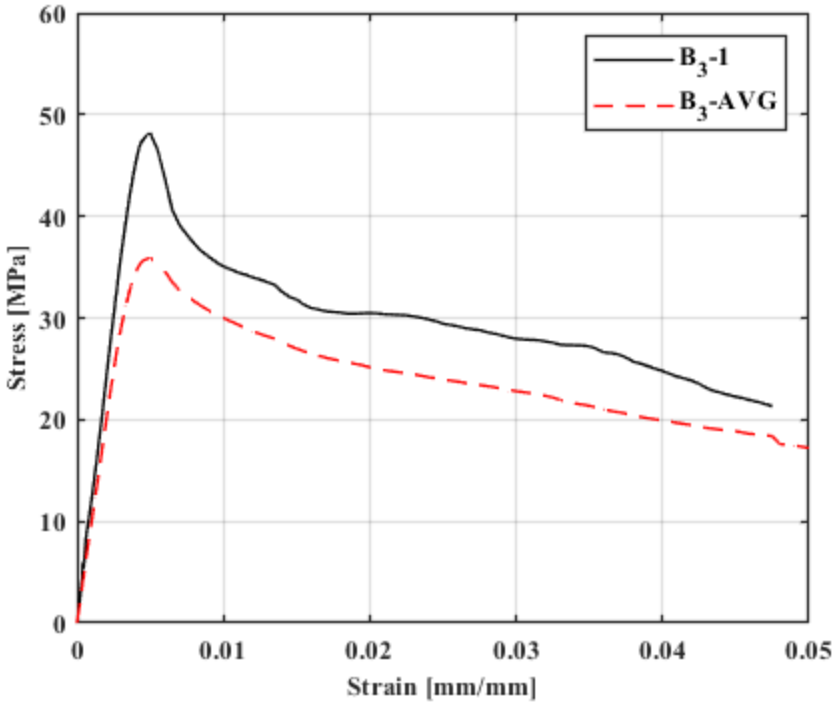

Notes:

Progression of Failure and Final Damage:

i) Prior to Test

ii) Fibre Rupture

iii) Damage Amplification

iv) Final Damage

v) FRP Removed

vi) Dissected

Figure B26: Detailed Information for Reinforced Specimen B_3–1

Specimen Name: B_3–2

Stress-Strain Curve:

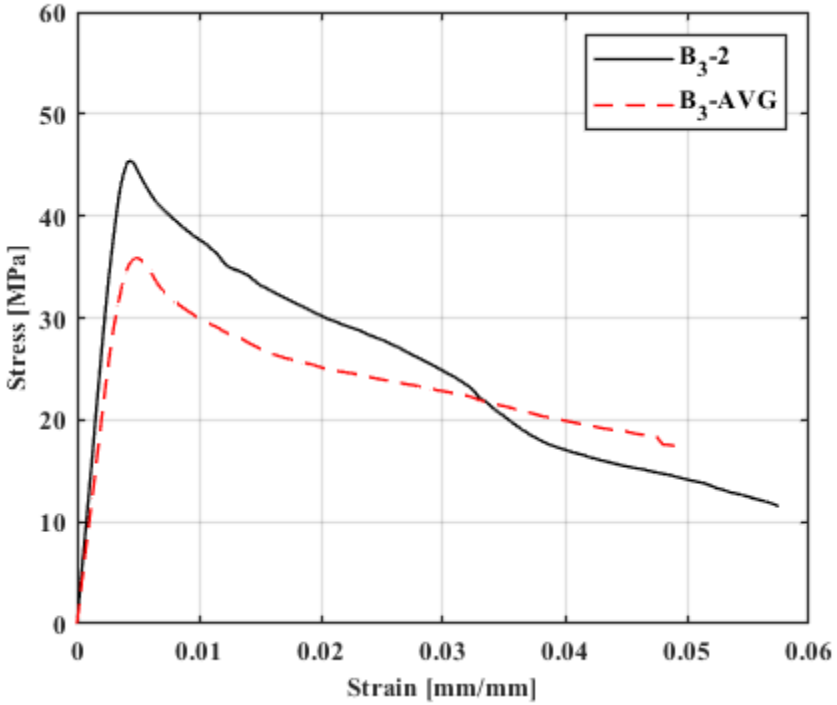

Progression of Failure and Final Damage:

i) Prior to Test

ii) Crushing Initiates

iii) Mid Test

iv) Final Damage

v) FRP Removed

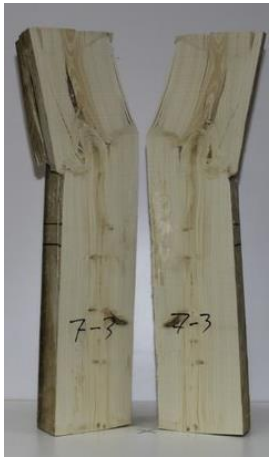

vi) Dissected

Notes:

Figure B27: Detailed Information for Reinforced Specimen B_3–2

Specimen Name: B_3–3

Stress-Strain Curve:

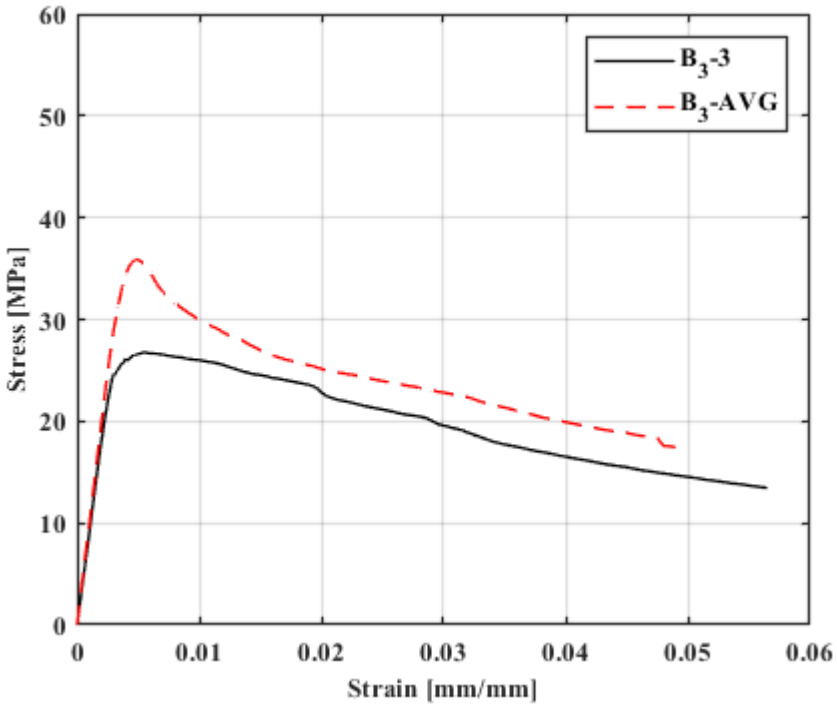

Progression of Failure and Final Damage:

i) Prior to Test

ii)

iii)

iv) Final Damage

v) FRP Removed

vi) Dissected

Notes:

Figure B28: Detailed Information for Reinforced Specimen B_3–3

Specimen Name: B_3–4

Stress-Strain Curve:

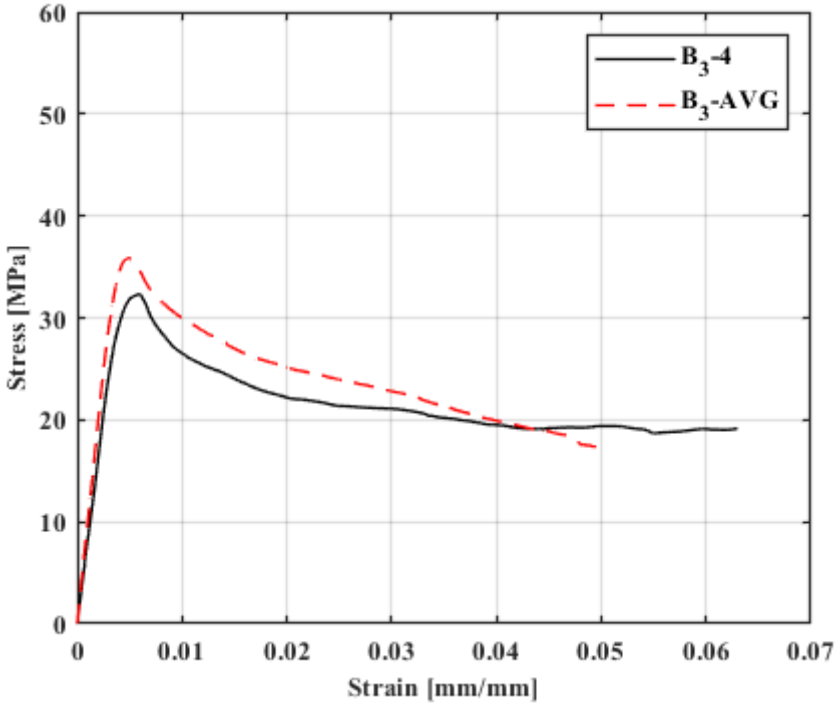

Progression of Failure and Final Damage:

i) Prior to Test

ii)

iii)

iv) Final Damage

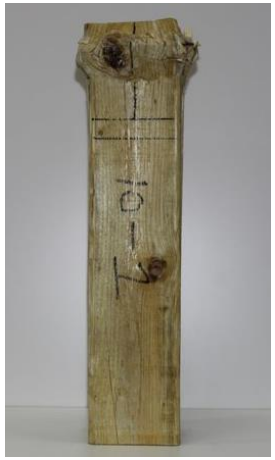

v) FRP Removed

vi) Dissected

Notes:

Figure B29: Detailed Information for Reinforced Specimen B_3–4

Specimen Name: B_3–5

Stress-Strain Curve:

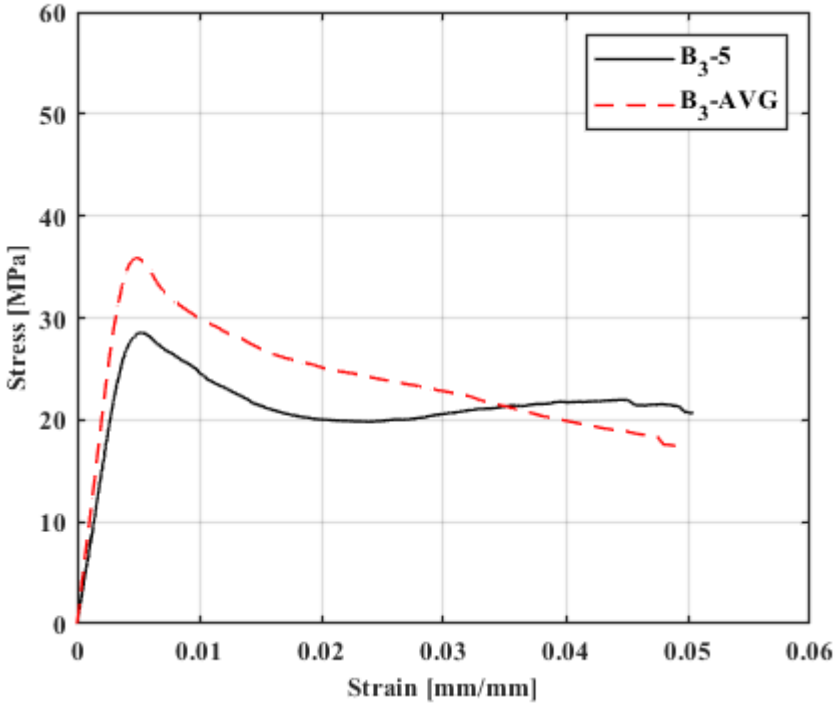

Notes:

Progression of Failure and Final Damage:

i) Prior to Test

ii)

iii)

iv) Final Damage

v) FRP Removed

vi) Dissected

Figure B30: Detailed Information for Reinforced Specimen B_3–5